

COMPUTATIONAL FLUID DYNAMIC  
SIMULATION OF  
ABRASIVE WATERJET NOZZLE EROSION



NAQIB HAKIM BIN KAMARUDIN

اونيورسيتي مليسيا قهغ

UNIVERSITI MALAYSIA PAHANG

MASTER OF SCIENCE

UNIVERSITI MALAYSIA PAHANG

## UNIVERSITI MALAYSIA PAHANG

### DECLARATION OF THESIS AND COPYRIGHT

Author's Full Name : NAQIB HAKIM BIN KAMARUDIN

Date of Birth : 2<sup>ND</sup> MAY 1988

Title : COMPUTATIONAL FLUID DYNAMIC SIMULATION  
OF ABRASIVE WATERJET NOZZLE EROSION

Academic Session : SEM II 2019/2020

I declare that this thesis is classified as:

- CONFIDENTIAL (Contains confidential information under the Official Secret Act 1997)\*
- RESTRICTED (Contains restricted information as specified by the organization where research was done)\*
- OPEN ACCESS I agree that my thesis to be published as online open access (Full Text)

I acknowledge that Universiti Malaysia Pahang reserves the following rights:

1. The Thesis is the Property of Universiti Malaysia Pahang
2. The Library of Universiti Malaysia Pahang has the right to make copies of the thesis for the purpose of research only.
3. The Library has the right to make copies of the thesis for academic exchange.

Certified by:

\_\_\_\_\_  
(Student's Signature)

\_\_\_\_\_  
(Supervisor's Signature)

880502-10-5071

Dr. Mohd Azmir Mohd Azhari

\_\_\_\_\_  
New IC/Passport Number

\_\_\_\_\_  
Name of Supervisor

Date:

Date:

NOTE : \* If the thesis is CONFIDENTIAL or RESTRICTED, please attach a thesis declaration letter.

## SUPERVISOR'S DECLARATION

I hereby declare that I have checked this thesis and in our opinion, this thesis is adequate in terms of scope and quality for the award of the degree of Master of Science.

---

(Supervisor's Signature)

Full Name : DR MOHD AZMIR MOHD AZHARI

Position : SENIOR LECTURER

Date :



UMP

اونيورسيتي ملايسيا قهغ

UNIVERSITI MALAYSIA PAHANG



## STUDENT'S DECLARATION

I hereby declare that the work in this thesis is based on my original work except for quotations and citations which have been duly acknowledged. I also declare that it has not been previously or concurrently submitted for any other degree at Universiti Malaysia Pahang or any other institutions.

---

(Student's Signature)

Full Name : NAQIB HAKIM BIN KAMARUDIN

ID Number : MMF 15003

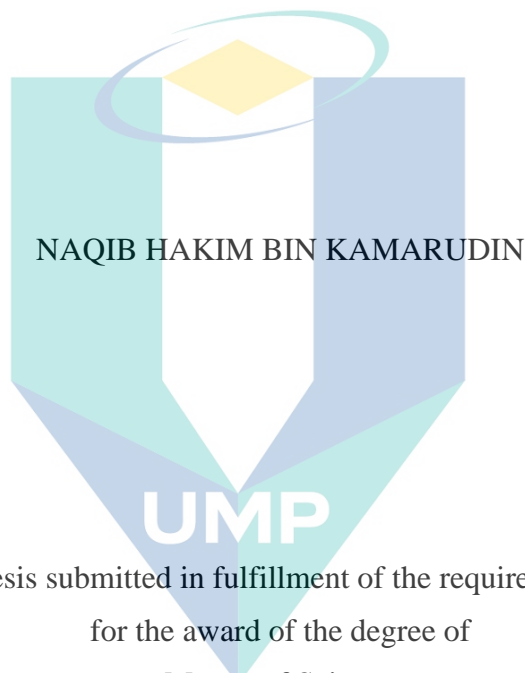
Date :

UMP

اونيورسيتي ملايسيا قهغ

UNIVERSITI MALAYSIA PAHANG

COMPUTATIONAL FLUID DYNAMIC SIMULATION  
OF  
ABRASIVE WATERJET NOZZLE EROSION



Thesis submitted in fulfillment of the requirements  
for the award of the degree of  
Master of Science

اونيورسيتي ملايسيا قهغ

UNIVERSITI MALAYSIA PAHANG

Faculty of Manufacturing and Mechatronics Engineering Technology

UNIVERSITI MALAYSIA PAHANG

SEPTEMBER 2020

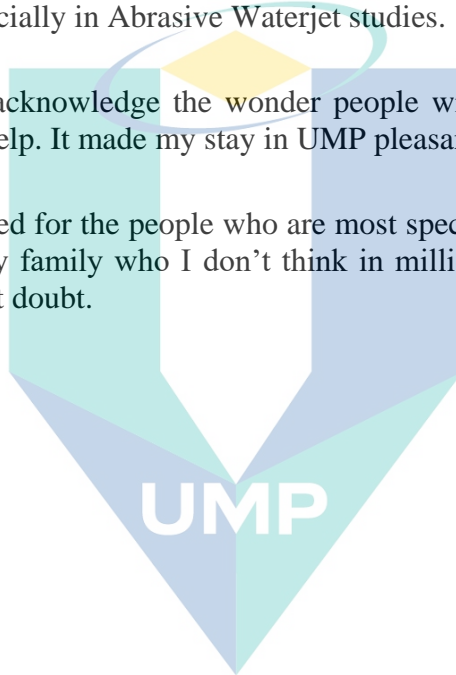
## ACKNOWLEDGEMENTS

Firstly, the author would like to express gratitude to the Most Gracious and The Most Merciful (Ar-Rahman and Ar-Rahim). Thanks to the creator for giving me the opportunity in indulging on knowledge, most friendly environment and wonderful people to study and work with along my time in finishing my Masters studies.

The author would like to express my sincerest appreciation to my supervisor, Dr. Mohd. Azmir Bin Mohd Azhari. Who provided me with his ideas, invaluable guidance, encouragement and the research opportunity that was very rewarding. He always impressed me with his outstanding professional conduct and his strong conviction in engineering field especially in Abrasive Waterjet studies.

I would like to also acknowledge the wonder people within my life who are always there when I needed help. It made my stay in UMP pleasant and unforgettable.

The last one is allocated for the people who are most special to me. Of course, it would be my parents and my family who I don't think in million years I can return of what they gave me. Without doubt.



اونيورسيتي مليسيا قهغ

UNIVERSITI MALAYSIA PAHANG

## ABSTRAK

Nozel Mesin Waterjet adalah komponen yang paling kritikal dan mempengaruhi keseluruhan kualiti, ketepatan, prestasi dan penggunaan mesin dari segi ekonomi. Pendedahan kepada tekanan air berkuasa tinggi serta agen penghakis atau pelepas menyebabkan nozel banyak mengalami hakisan dan perlu untuk diganti dengan kerap. Sebelum ini, terdapat kajian simulasi terhadap hakisan nozel didalam model berbentuk 2-D. Walaupun begitu, ianya penting untuk membuat simulasi didalam model 3-D dengan akurasi yang lebih tinggi. Didalam kajian ini, perisian berbentuk Komputasi Fluid Dinamik (CFD) didalam model 3-D yang lebih untuk penambahbaikan yang tidak dilakukan oleh kajian sebelumnya. Kaedah mesh dan model turbulens yang sesuai telah dipilih untuk simulasi hakisan nozel. Kaedah Fasa Diskrit (DPM) digunakan untuk simulasi model multi-fasa untuk air, angin dan bahan pelepas. Model pertambahan hakisan Finnie digunakan untuk mendapatkan kadar hakisan. Ketepatan kadar hakisan daripada kajian berbentuk eksperimen dan simulasi telah pun dibandingkan. Tambahan lagi, ketepatan kadar hakisan juga dibandingkan dengan parameter geometri dan kondisi penggunaan juga turut dibanding dan dikaji. Simulasi kaedah 'Quadrilateral' mempunyai kadar hakisan yang lebih tepat dengan ralat  $-5.645E^{-08}$  sehingga  $-1.591E^{-08}$  berbanding kaedah 'Cut-Cell' dan kaedah 'Tetrahedral' dengan kadar ralat  $6.750E^{-07}$  hingga  $-1.231E^{-08}$  dan  $1.868E^{-08}$  hingga  $-6.462E^{-08}$  mengikut turutan. Simulasi kaedah turbulens 'Realizable' menunjukkan lebih kurang ralat iaitu  $-3.266E^{-08}$  sehingga  $-1.592E^{-08}$  berbanding kaedah 'Standard' yang mempunyai ralat  $-4.281E^{-08}$  sehingga  $-1.290E^{-08}$ . Seterusnya, kajian didapati memperolehi bentuk beralun yang terhasil daripada simulasi dimana ia berkorelasi dengan kajian 2-D terdahulu. Keseluruhannya, didapati kajian simulasi terhadap parameter geometri dan kondisi operasi dan hasil telah dibandingkan dengan kadar hakisan yang diperoleh daripada model empirikal daripada kajian terdahulu mendapati kadar ralat diantara  $6.022E^{-09}$   $\text{kg/m}^2\text{s}^{-1}$  hingga  $1.063E^{-07}$   $\text{kg/m}^2\text{s}^{-1}$ .  $v$  dimana ianya konsisten dengan didalam keseluruhan simulasi. Walaupun begitu, kadar hakisan didapati rendah disbanding dengan hasil eksperimen. Namun, kadar hakisan adalah berada didalam nilai eksponen yang teramat rendah maka ianya boleh diterima pakai. Malahan, ianya konsisten dengan didalam keseluruhan simulasi perbandingan diantara simulasi dengan eksperimen. Walaupun begitu, kadar hakisan didapati rendah disbanding dengan hasil eksperimen. Kesimpulannya, kajian ini menunjukkan potensi yang tinggi untuk meramal jangkamasa kepenggunaan nozel Mesin Waterjet didalam aplikasi industri.

UNIVERSITI MALAYSIA PAHANG

## ABSTRACT

The nozzle of the Abrasive Waterjet (AWJ) machine is the most critical component that consequently affects the overall cutting quality, precision, performance and economy. Exposure to slurry of high velocity of water and abrasives makes it susceptible to wear erosion which requires for intermittent reinstatement. Previous simulation of AWJ nozzle erosion have been done by using a 2-D fluid flow model. However, it is important to conduct further simulation using a more accurate 3-D fluid flow model. The present work attempts to simulate the erosion of the nozzle wall using computational fluid dynamics-based software in 3-D. A suitable mesh assembly methods and turbulence model for the simulation of nozzle erosion was identified. Discrete Phase Method (DPM) model was used to simulate multiphase modelling of air, water and abrasives. The Finnie's erosion and accretion model were selected to find the erosion rate. The erosion profile based on the simulation was compared with the actual profile of worn out nozzle. Furthermore, the nozzle erosion rate for different geometric parameters and working conditions were analyzed based on simulation and experimental results. It was found that the simulations using Quadrilateral and mesh converged well with an error of  $.645E^{-08}$  to  $-1.591E^{-08}$  as compared to Cut-Cell and Tetrahedral mesh which produced some errors between  $6.750E^{-07}$  to  $-1.231E^{-08}$  and  $1.868E^{-08}$  to  $-6.462E^{-08}$ , respectively. The Realizable  $K-\epsilon$  turbulence model was selected as it shows less error of  $-3.266E^{-08}$  to  $-1.592E^{-08}$  as compared to Standard turbulence model which between  $-4.281E^{-08}$  to  $-1.290E^{-08}$ . Furthermore, it was found that the erosion profile with wavy patterns have correlated well past studies using 2-D model Overall, comparing the simulation results under different geometric parameters and operating conditions with empirical models obtained from past studies showed an error in the range of  $6.022E^{-09}$   $\text{kg/m}^2\text{s}^{-1}$  to  $1.063E^{-07}$   $\text{kg/m}^2\text{s}^{-1}$ . Also, there seems to be consistency in the erosion trend for different simulated parameters with experimental results although the erosion rates appeared to be mostly smaller in values. It can be concluded that the present work has shown an excellent potential for predicting the life of abrasive waterjet nozzle for industrial application.

اونيور سیتی ملیسیا قهغ

UNIVERSITI MALAYSIA PAHANG

## TABLE OF CONTENT

**DECLARATION**

**TITLE PAGE**

**ACKNOWLEDGEMENTS** **ii**

**ABSTRAK** **iii**

**ABSTRACT** **iv**

**TABLE OF CONTENT** **v**

**LIST OF TABLES** **viii**

**LIST OF FIGURES** **ix**

**LIST OF SYMBOLS** **xi**

**LIST OF ABBREVIATIONS** **xii**

**CHAPTER 1 INTRODUCTION** **1**

1.1 General Background 1

1.2 Problem Statement 2

**CHAPTER 2 LITERATURE REVIEW** **6**

2.1 Nozzle Wear 6

2.2 Empirical Model for Nozzle Wear 7

2.3 Assumptions and theoretical formulation 12

2.4 Applications of CFD in Erosion Modelling 14

2.5 CFD Numerical Model 17

2.5.1 Fluid Flow Model 18

2.5.2 Particle Motion Model 23

2.5.3	Erosion Model	28
2.6	Summary of Literature Review	31

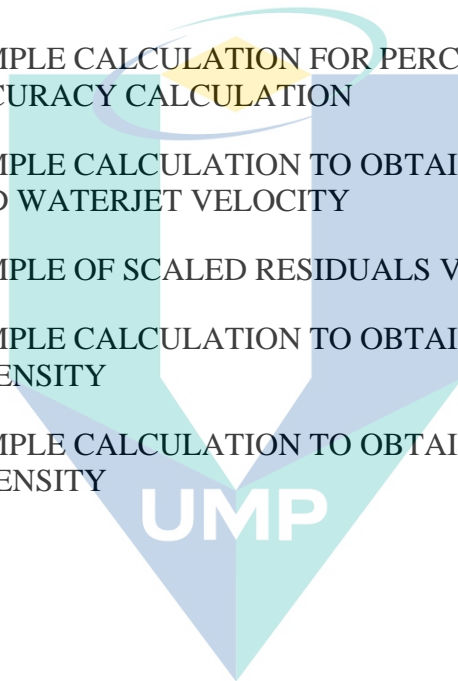
### **CHAPTER 3 METHODOLOGY** **32**

3.1	General	32
3.2	CFD Simulation	32
3.3	Pre-Processing	32
3.2.1	Geometry and System Parameters	35
3.2.2	Assembly Meshing	37
3.3	Solution Procedure	40
3.3.1	Solvers	40
3.3.2	Turbulence Modelling	40
3.3.3	Material Properties	42
3.3.4	Cell Zones and Boundary Conditions	42
3.4	Validation Methods	42

### **CHAPTER 4 RESULTS AND DISCUSSION** **43**

4.1	Modelling of Fluid Flow	43
4.2	Assembly Meshing Methods	47
4.3	Turbulence Modelling	53
4.4	Erosion Profile	56
4.5	Nozzle Length	64
4.6	Nozzle Diameter	71
4.7	Abrasive Flow Rate	73
4.8	Orifice Diameter	76

<b>CHAPTER 5 CONCLUSION</b>	<b>84</b>
5.1 Conclusion	84
5.2 Recommendation	85
<b>REFERENCES</b>	<b>87</b>
<b>APPENDICES</b>	
APPENDIX A: SAMPLE CALCULATION FOR PERCENTAGE OF ACCURACY CALCULATION	101
APPENDIX B: SAMPLE CALCULATION TO OBTAIN THEORETICAL AND WATERJET VELOCITY	102
APPENDIX C: SAMPLE OF SCALED RESIDUALS VERSUS ITERATIONS	103
APPENDIX D: SAMPLE CALCULATION TO OBTAIN PERCENTAGE INTENSITY	105
APPENDIX E: SAMPLE CALCULATION TO OBTAIN PERCENTAGE INTENSITY	106



اونيورسيتي مليسيا قهغ

UNIVERSITI MALAYSIA PAHANG

## LIST OF TABLES

Table 3.1	Boundary Condition and Parameter Values	36
Table 3.2	Nozzle Material Properties	37
Table 3.3	Abrasives Material Properties	37
Table 4.1	Comparison of Different Assembly Meshing Method	48
Table 4.2	Comparison of Erosion Rates and Nozzle Length in Different Assembly Meshing Methods	49
Table 4.3	Comparison of Erosion Rate and Nozzle Length for Different Turbulence Models	54
Table 4.4	Erosion Rate and Error between Experimental Model and Simulation Erosion at Different Nozzle Lengths	65
Table 4.5	Erosion Rate and Error comparison between Experimental Model and Simulated Erosion of AWJ Nozzle at different nozzle diameter	72
Table 4.6	Erosion Rate and Error of Experimental and Simulated Erosion Model in Different Abrasive Flow Rates	74
Table 4.7	Erosion Rate and Error between Experimental and Simulated Erosion Model in Different Diameters of Orifice Parameters	78
Table 4.8	Erosion Rate and Accuracy between Experimental And Simulated Erosion Model in Different Parameters of Water Pressure	80
Table 4.9	Summary of Nozzle Erosion Simulation of Different Parameters of Geometrical and Working Conditions	83
Table 5.1	Parameters used in Typical Simulation	102

اونيورسيتي ملايسيا قهغ

UNIVERSITI MALAYSIA PAHANG

## LIST OF FIGURES

Figure 2.1	Sectioned piece of a worn out AWJ nozzle	7
Figure 2.2	Bore profiles using plug gage method	9
Figure 2.3	Bore profiles using silicon casting method	9
Figure 3.1	Methodology Flowchart	33
Figure 3.2	Boundary conditions applied to the cutting head.	35
Figure 3.3	Designation values of dimensions applied to the nozzle geometrical model.	36
Figure 3.4	Quadrilateral assembly meshing model of AWJ nozzle.	38
Figure 3.5	Cut-cell assembly meshing model of AWJ nozzle.	39
Figure 3.6	Tetrahedral assembly meshing model of AWJ nozzle.	39
Figure 4.1	Waterjet velocity variations along the cutting head	44
Figure 4.2	Air and abrasives interacting with the water in the mixing chamber simulation.	45
Figure 4.3	Contours of erosion along the nozzle.	46
Figure 4.4	Waterjet abrasives particle tracking	47
Figure 4.5	Effect of nozzle length on erosion wear for different mesh assembly.	49
Figure 4.6	Contours of discrete phase method (DPM) erosion for different meshing methods (a) Quadrilateral mesh (b) Cut-cell mesh (c) Tetrahedral mesh	52
Figure 4.7	Effect of nozzle length on erosion rate for different turbulence modelling	54
Figure 4.8	(a) Realizable $k-\varepsilon$ volume model of turbulent kinetic energy and (b) Standard $k-\varepsilon$ volume modelling of turbulent kinetic energy.	55
Figure 4.9	Erosion profile of worn out nozzles and average erosion profile of simulated nozzle erosion.	56
Figure 4.10	Erosion profile of worn out nozzles and erosion profile of simulated nozzle erosion at different angle of rotation.	57
Figure 4.11	Exit diameter profile of AWJ nozzles where (a) New nozzle (b) Worn out nozzle erosion profile 1 (c) Worn out nozzle erosion profile 2.	58
Figure 4.12	Points of section taken for inner diameter erosion profile.	59
Figure 4.13	Inner diameter erosion profile (a) at section 1 (Inlet at 2 mm point).	60
Figure 4.14	Inner diameter erosion profile at section 2 (19 mm point).	60
Figure 4.15	Inner diameter erosion profile at section 3 (37 mm point).	61
Figure 4.16	Inner diameter erosion profile at section 4 (56 mm point).	61

Figure 4.17	Inner diameter erosion profile at section 5 (Outlet at 68 mm point).	62
Figure 4.18	Effect of nozzle length on erosion wear.	64
Figure 4.19	Boundary layer observation in AWJ nozzle wear simulation.	66
Figure 4.20	Contours of nozzle erosion for different nozzle sizes (a) 32.5mm (b) 50.8mm	67
Figure 4.21	Contours of nozzle erosion for different nozzle sizes (c) 76.2 mm (d) 101.6 mm	68
Figure 4.22	Effect of Nozzle diameter on nozzle erosion.	72
Figure 4.23	Contours of erosion for different nozzle diameters (a) 0.79 mm (b) 1.14 mm (c) 1.63 mm	73
Figure 4.24	Effect of abrasive flow rate on nozzle erosion.	74
Figure 4.25	Contours of erosion for different abrasive flow rate (a)1.9 g/s (b)3.8 g/s (c)5.7 g/s (d)7.6 g/s.	75
Figure 4.26	Effect of orifice diameter on nozzle erosion.	77
Figure 4.27	Contours of erosion for different nozzle orifice diameter (a) 0.28mm (b) 0.33mm (c) 0.38mm and (d) 0.43mm.	78
Figure 4.28	Effect of water pressure on nozzle erosion	80
Figure 4.29	Contours of erosion for different water pressure (a) 172 MPa (b) 241 MPa (c) 310 MPa and (d) 359 MPa	81
Figure 5.1	Residuals monitor for cut-cell mesh simulation	103
Figure 5.2	Residuals monitoring for tetrahedral mesh simulation	103
Figure 5.3	Residuals monitoring for quadrilateral mesh simulation	104

اونيورسيتي مليسيا قهغ

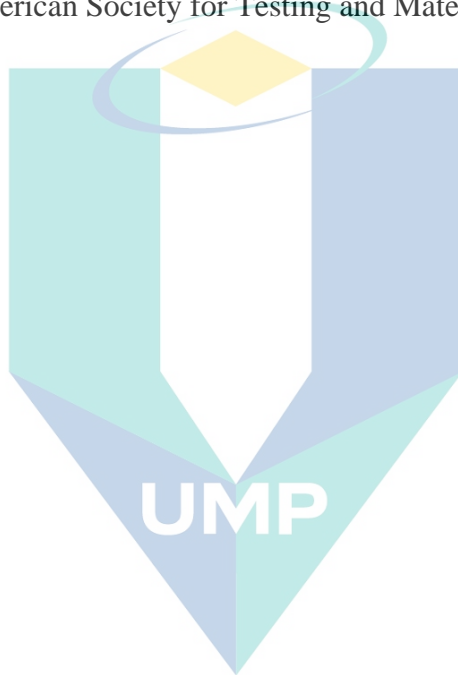
UNIVERSITI MALAYSIA PAHANG

## LIST OF SYMBOLS

$C$	Constant
$C_D$	Drag Coefficient
$D$	Constant
$d$	Diameter (mm)
$D_p$	Particle diameter
$E$	Erosion rate
$F_D$	Drag force [N]
$F_s$	Particle shape factor
$f$	Acceleration of gravity [ $m/s^2$ ]
$m$	Particle mass
$V$	Particle velocity[m/s]
$V_0$	Particle impingement velocity
$P$	Plastic flow stress
$K$	Ratio of force component
$\varphi$	Ratio between depth contact and cut
$\Delta E$	Total volume erosion rate
$E_{brass}$	Brass erosion rate
$E_{mild\ steel}$	Mild steel erosion rate
$E_{ratio}$	Erosion ratio [kg/kg]
$E_{deformation}$	Volume of erosion due to normal contact of particle impact
$E_{cutting}$	Volume of erosion due when the particle impact is not normal
$M$	Particle mass
$H$	Hardness
$\Omega_c$	Critical strain
$f$	Function
$\beta$	Constant
$\gamma$	Constant
$n$	Function
$f_a$	Abrasive flow rate

## LIST OF ABBREVIATIONS

AWJM	Abrasive Waterjet Machining (Machine)
CFD	Computational Fluid Dynamics
EDM	Wire electrical discharge machine
Eq.	Equation
ANSYS	CFD based software
ROC	Rapid Omni Directional Compaction
ASTM	American Society for Testing and Materials



اونيورسيتي ملايسيا قهغ

UNIVERSITI MALAYSIA PAHANG

# CHAPTER 1

## INTRODUCTION

### 1.1 General Background

Abrasive Water Jet (AWJ) machine is a versatile tool that can be used for many applications. The machine can be used for cutting, drilling, cleans and carves surface areas of a workpiece (Azhari, Schindler, Godard, Gibmeier, & Kerscher, 2016; Liu et al., 2018; Miller, 2018). The application of an AWJ machine is basically created by inserting abrasive grains into highly pressurized stream of water jet which then pulverizes the surface of the targeted work piece (Momber & Kovacevic, 2012). Compressed water was formed by forcing highly pressurized water which is around 350 MPa to 700 MPa to an orifice with a diameter of no less than 2.0 mm (Verma, Mishra, & Moulick, 2015). A stream of water which travels at a speed of more than 300 m/s is then discharged from the orifice to be mixed with the abrasives particles in a mixing chamber (Verma et al., 2015). Thus creates a slurry of stream further coursing into the nozzle producing a slurry of razor sharp current of water containing particles fast enough to lacerate through almost any materials and even hardened metals (Hashish, 1989).

Degradation of the nozzle is one of the most associated problems with AWJ machine where the wall of the nozzle are constantly eroded by abrasives particle (Humphrey, 1990). Nozzle erosion in AWJ is the process of being eroded or degradation by water, abrasives and other natural agents (Bhowmik & Ray, 2017). The typical lifecycle of a tungsten carbide nozzle is 12 to 13 hours (Jegaraj & Babu, 2016). The nozzle are required to be replaced constantly because the water travels at 80% of the water jet original velocity and contains abrasive particles that can be as large as 40% of the nozzle's diameter (Anand & Katz, 2003; Ness & Zibbell, 1996). The erosion of the internal bore of the nozzle reduces the mixing efficiency and lowers the consistency of the waterjet (Hashish, 1994). Kerf profile defects are one of the major problems that limits the cutting quality (Wang, Zhang, Wu, & Yang, 2017). An increase

in nozzle bore diameter will effectively decrease intersecting particle velocity which ultimately produce a wider kerf width of machined samples. A nozzle made using Rapid Omni Directional (ROC) technique has an approximate lifecycle of 50 – 100 hours (Nanduri, Taggart, Kim, Haney, & Skeele, 1997; Nanduri, Taggart, & Kim, 2002). There are studies that stated for the optimal cutting performance are starting to diminish when the diameter of the nozzle became 27% bigger from the original diameter of a nozzle (Kovacevic, 1992). Advanced erosion or increase in nozzle will induce a serious reduction in the extensity of the stream penetration and declination of the kerf surface quality (Hashish, 1994; Kovacevic, 1992; Manu & Babu, 2009; Momber & Kovacevic, 2012; Verma et al., 2015).

CFD can be a useful tool when implemented to study the effect of different factors on finding areas likely to be volatile to erosion and the prediction of the maximum erosion rate in complicated shapes whereby experimental study is difficult to be developed (Parsi et al., 2014). CFD is defined as a subsidiary of fluid mechanics studies that applies analysis of data structures and numerical data to investigate and solve fluid flows problems (Kinnell, 2018).

Assembly meshing were defined as a geometrical model is to be divided into many elements for the Computational Fluid Dynamics (CFD) solver to construct control volumes (Benzley, Perry, Merkley, Clark, & Sjaardama, 1995). The mesh is required to resolve the geometric features of interest in which this case is dealing with flow-aligned geometries (Magoulès, 2011).

Turbulence modeling is the mathematical model used to predict the effects of turbulence. In the current study, CFD simulations use turbulent models to predict the evolution of turbulence (Lyczkowski & Bouillard, 2002).

## 1.2 Problem Statement

There are vast studies that relates to erosion modeling. Finnie, (1960) have suggested a model of micro geometry for ductile material by proposing that mechanical erosion occurs in ductile material is the product of micro cutting. The model that was found were extensively enhanced to solve its flaws and applied on different conditions (Parsi, Vieira, Kesana, McLaury, & Shirazi, 2015). Aspects that influence erosion can

ranges to the material properties, geometrical shapes and particle size, water pressure, discharge velocity, types of turbulence, and interactions of particles multiphase flow (Blazek, 2015; Parsi et al., 2014). The mentioned factors are interacting with each other and developing experimental models of their contribution to erosion requires complicated studies (Parsi, Vieira, et al., 2015).

There are only a few studies which that investigates AWJ nozzle erosion which applies CFD based software. One of them is by (Mostofa, Kil, & Hwan, 2010) who have simulated the slurry of abrasives, water and air the mixing chamber of and AWJ machine to investigate the erosion rate at the wall of the nozzle and forecast the particle size effect of the abrasive against the different sizes nozzle's length. Finnie's erosion model of erosion in ductile material was used in the software to develop the erosion rate (Guide, 2016). There are other several CFD studies related with waterjet however most of the study are mainly on erosion on the work piece instead on the wear of nozzle (Aldaş & Yapıcı, 2014; Anantharamaiah, Tafreshi, & Pourdeyhimi, 2006; Arabnejad, Mansouri, Shirazi, & McLaurry, 2017; Duarte, de Souza, & dos Santos, 2015; Foldyna, Heiniger, Mettler, Sitek, & Scucka, 2007; Gou, Zhang, Li, Liu, & Lian, 2018; H. Liu, Wang, Brown, & Kelson, 2003; H. Liu, Wang, Kelson, & Brown, 2003; Maniadaki, Antoniadis, & Bilalis, 2011; Maniadaki, Kestis, Bilalis, & Antoniadis, 2007a; Messa, Ferrarese, & Malavasi, 2015; Ng & Guannan, 2015; Noon & Kim, 2017; Prisco & D'Onofrio, 2008; Thiana A Sedrez, Shirazi, Rajkumar, Sambath, & Subramani, 2019; Seehanam, Pianthong, Sittiwong, Milton, & Takayama, 2012; Shitole, Gawande, Desale, & Nandre, 2015; Sittiwong, Seehanam, Pianthong, & Matthujak, 2010; Tafreshi & Pourdeyhimi, 2003; Xie & Rittel, 2017).

A study has demonstrated nozzle wear rate using CFD however the study only attempted to simulate the erosion modelling in two dimensional analysis (Mostofa et al., 2010; Verma et al., 2015). The study also investigated nozzle erosion by varying the length of the nozzle and also changing the shape factor of the particle (Mostofa et al., 2010). Therefore, it would be interesting if other methods of erosion modelling can be investigated to understand their effects on the wear of the nozzle. It is hoped that a better prediction model can established to analyze the erosion effects on AWJ nozzle.

Furthermore, there is no ASTM test standards that can accurately represents the highly erosive condition of a AWJ nozzle mixing tube (Hashish, 1994; Nanduri, Taggart, & Kim, 1996). Research on nozzle wear have been mainly conducted by traditional experimental technique which is limited to predicting peak values of wear. CFD can give 3D insights of flow patterns that has been difficult to be performed since the nozzle is exposed to high velocity water jet

Studies of nozzle wear are mainly based on tests using traditional experimental which is costly and time consuming. A notable studies in regards with CFD to investigate nozzle wear were done by Mostofa et al. (2010) using an application called the ANSYS CFX. The study investigates the velocity of the waterjet velocity and erosion rate by varying the abrasive mass flow rate and shape factor. The present study further analyzes the effects of AWJ geometrical parameters and different working conditions using FLUENT. Discrete Phase Method (DPM) is utilized to predict the wear of the nozzle. The prediction results of the prediction are then validated with past experimental results as well as series of experimentation.

### 1.3 Objective

The followings are the objective of this study;

- i. To identify which Mesh Assembly methods and Turbulence model that is suitable for AWJ nozzle erosion simulation
- ii. To compare the accuracy of erosion profile of worn out nozzle between simulation and experimental.
- iii. To identify the accuracy of nozzle erosion rate for different parameters of geometry and working condition between simulation and experimental

### 1.4 Scope

The research approach uses CFD based approach by using features in ANSYS FLUENT as a tool to predict the erosion rate for abrasive waterjet nozzle in multiphase flow. The main approach is to use the DPM method to enable the identification of multi-phase flow of air, water and abrasive particle. The model is set to k-epsilon

turbulence model to replicate the flow condition of the high pressure within the mixing chamber of an abrasive waterjet machine. The boundary conditions are set to three condition which is the water inlet, outlet and the wall of the nozzle. The simulations were run in approximately 180000-time steps with 0.01 iteration time steps size. The variables include the assembly mesh methods and the geometrical parameters of the nozzle. The assembly mesh methods include the Quadrilateral, Cut-cell and Tetrahedral mesh. Whereas, the geometrical parameters include the nozzle length, nozzle diameter, orifice diameter and water pressure. The interdependent variable is the erosion rate. The computer specs used are I7 intel processor, 16 Gb ram and Xeon Graphic Card.

Samples of nozzle used in the industry are taken to identify the nozzle erosion pattern. The erosion profiles were acquired by using an optical video measuring system (ECON) for every 1mm. The nozzle erosion profiles were then compared with the simulation. Besides that, the erosion rates were also compared with erosion model made by past study.

The identification of mesh assembly to be used is by run simulations between different mesh methods which are the Quadrilateral, Cut-cell and Tetrahedral. Whereas the turbulence model is the Standard and the Realizable  $K-\varepsilon$  turbulence model. The comparison was made by comparing the the processing time, quality of convergence and accuracy between simulated and experimental results.

اونيورسيتي ملايسيا قهغ

UNIVERSITI MALAYSIA PAHANG

## CHAPTER 2

### LITERATURE REVIEW

#### 2.1 Nozzle Wear

There are two functions of AWJM nozzle which is mixing the water with abrasives and to form a concentrated high velocity abrasive water jet (Momber & Kovacevic, 2012). The nozzle is the most critical component that directly influences the performance, precision and economics of AWJM technology (Hashish, 1984). Even with the current system of AWJM, the life of a waterjet nozzle can vary depending on the type of nozzles and abrasive materials, nozzle length and diameter, water velocity and abrasives flow rate. The wear of the nozzle wall will lead to the jet becoming incoherent which causes increased kerf width on the work piece, deterioration of surface quality and loss of cutting accuracy (Anand & Katz, 2003).

In order for the nozzles to last longer, the nozzles must be made from very hard materials. Hashish (2009) has loosely specified two relationships for AWJ nozzles can follow to obtain longer life cycle which is the mixing tube length to nozzle diameter ratio is about three and the other relationship is mixing tube diameter to orifice diameter ratio is about three.

The nozzles are mostly made by hardened steel carbide and composites typically made from materials such as boron carbide, tungsten carbide and ROCTEC which is a composite carbide (Ness & Zibbell, 1996). Specially lubricated nozzles to improve the life of the nozzle are also introduced by Anand & Katz (2003). Apart from the high velocity of water jet, the abrasive grains are also another factor for contributing to nozzle wear. Typically, the abrasive is made from garnet with diameter which is no less than 40% of AWJ nozzle's diameter. Hashish (2009) have also suggested rough parameters for AWJ abrasives have to follow where the size for the abrasive particle should not exceed half the difference between mixing tube and orifice diameter and the abrasive mass flow rate can be no less than 10%-15% of the water mass flow rate.

Figure 2.1 shows a sectioned nozzle which has been cut by a wire electrical discharge machine (EDM). An erosion profile can be observed from the shape which gives a wave pattern throughout the nozzle tube. Other research also shows similar profile of wavy pattern (Nanduri et al., 2002). From the sectioned nozzle, the authors made a cast out of the profile by using silicon casting technique. This would be helpful to allow more insights in three dimensional.

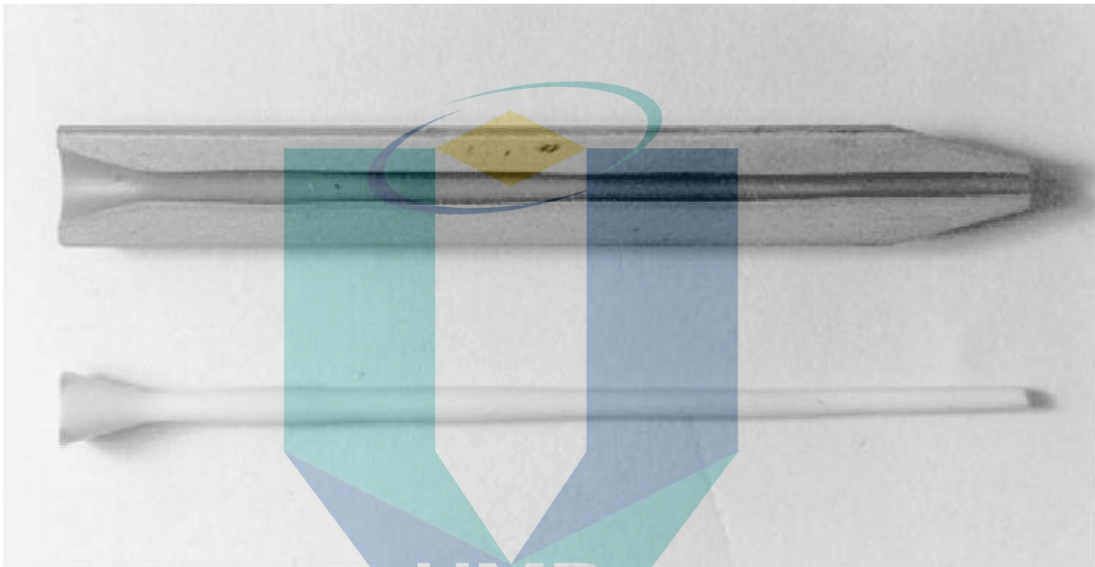


Figure 2.1 Sectioned piece of a worn out AWJ nozzle  
Source: Nanduri et al., (2002)

There are several studies on AWJ nozzle wear for variety of occasions and different parameters of the nozzle. Most of the studies requires the nozzle wear to be tested which prove to be a challenge. Hashish (1994) has stated that there is no ASTM standard that can replicate the erosive environment inside the nozzle mixing tube.

## 2.2 Empirical Model for Nozzle Wear

A comprehensive test procedures and outline of nozzle wear measurement conducted by Nanduri et al. (2002) have been useful for initiating future nozzle wear test. The test can be categorized into two; the first is the ‘Regular’ method which is using the garnet as the material for abrasive. The other is categorized as ‘Accelerated Wear Test’ which can further divide into two types. The first type of accelerated wear test replaces the nozzle and the abrasive into a softer material for nozzle and vice versa for the abrasives to accelerate the erosion rate. The second type of the test only replaces

the material of the abrasives with harder material, whereas, maintaining the nozzle of interest.

The nozzle wear was measured by measuring the growth of exit diameter and reduction of the nozzle weight. Nanduri et al. (2002) found that the increase of measurement of the exit diameter to be non-linear suggesting there is ambiguity in nozzle wear assessment however the growth of the bore profile can still be considered linear. It is observed that the increase of exit diameter is unstable. On a different note, the weight loss measurement is found to maintain a linear profile which. Therefore, weight loss is a more compelling measurement technique for characterization of nozzle wear. Both are results of an accelerated nozzle wear test with an initial bore of the nozzle to be of 1 mm using garnet abrasive. The experiment uses an orifice with 0.33 mm diameter, water pressure was set to 310 MPa and the flow rate of the abrasive applied was 7.6 g/s. Measurements are taken every interval of 30 minutes of testing.

Nanduri et al. (2002) also mentioned about measuring the nozzle bore profile as measuring the exit bore alone is not an accurate way to understand wear initiations and propagation. One of the methods used was by using GO - NO GO plug gage where the GO gage is to verify the upper limit and the NO GO gage is to verify the lower limit. The other method uses a destructive method where the nozzle is to be cut longitudinally, and a silicone casting is made out the bore profile. The finished mould will then be measured using a Coordinate Measurement Machine (CMM). Plug gage has the simplest working process whereby the size of the hole is determined by slotting the predefined gage size whether the gage can enter or not enter the hole. Therefore, the results of the measurement will show degradation profile in successive of steps as where in reality the profile should show pattern of waves. Figure 2.2 shows the data obtained using the plug gage method whose only limitation is that it cannot display the curvature of the actual wear profile. On the other hand, the silicone casting method can generate the wear profile limited by plug gage method. Figure 2.3 shows the initial and actual profile after 3 hours of testing. In term of nozzle wear profile obtained, the silicone casting is much preferred even though is a time and energy consuming method as compared to plug gage which is economical and convenient.

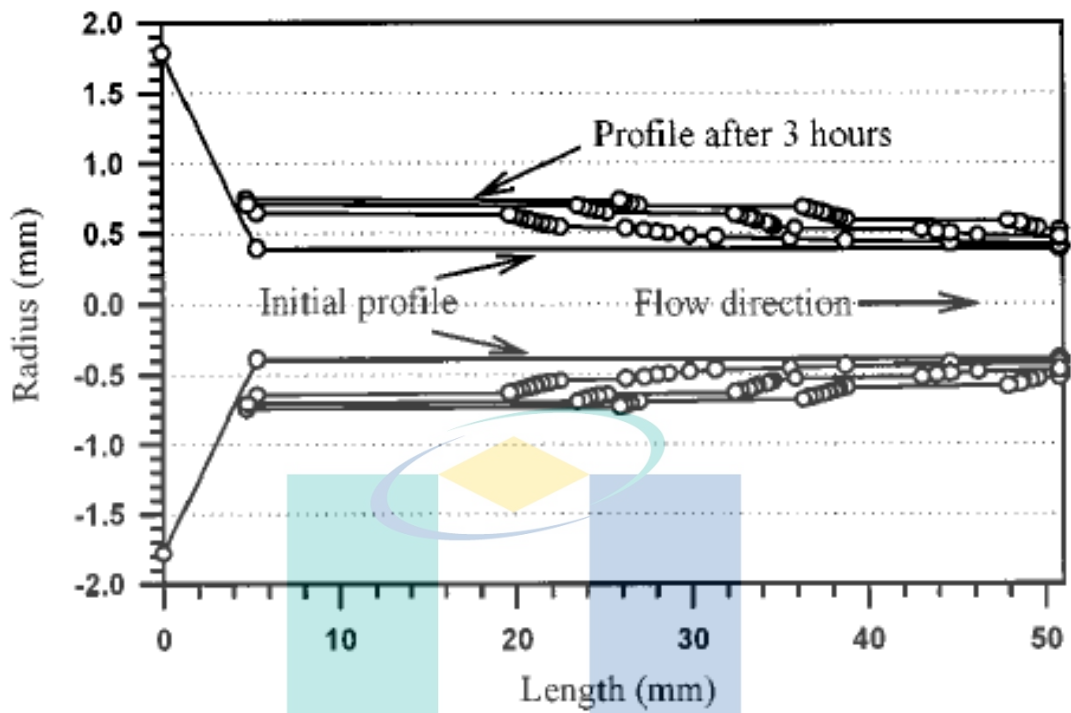


Figure 2.2 Bore profiles using plug gage method

Source: Nanduri et al., (2002)

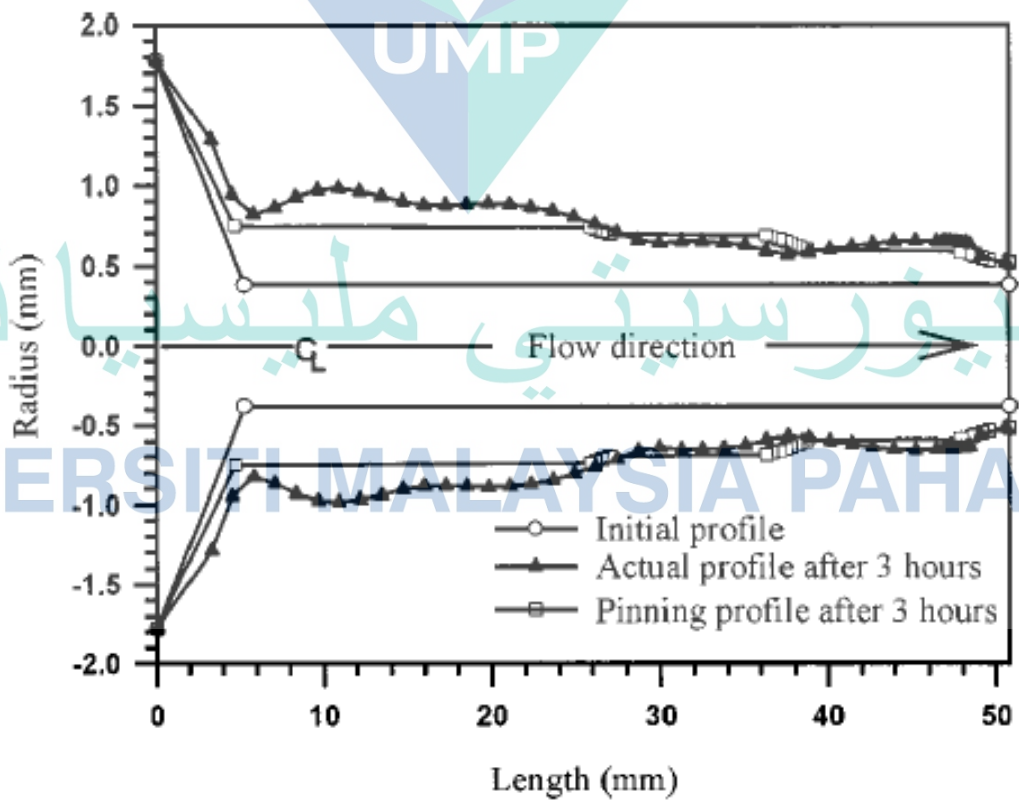


Figure 2.3 Bore profiles using silicon casting method

Source: Nanduri et al., (2002)

Similar accelerated wear tests have also been done to study the effect of nozzle materials on the erosion wear. Different nozzle of different materials are tested using alumina oxide abrasives and garnet abrasives. For the test using alumina oxide as the abrasives, it was found that the hardest material which is boron carbide shows lowest wear rate whereas tungsten carbide had the highest wear rate. A reverse trend was observed when garnet was used as abrasives where tungsten carbide exhibits highest wear rate instead of boron carbide which have come to exhibits the higher wear rate. It also shows that tungsten carbide grades exhibited longer lifecycle than the harder boron carbide when garnet abrasives were used (Hashish, 1994).

Accelerated nozzle wear tests were conducted to determine the critical ratio of particle diameter at which a stable wear rate were produced and becomes slow. The nozzles were manufactured from tool steel, hardened to about 62 Rockwell C.

In the end results, Hashish (1994) made some conclusions that were to improve nozzle lifetime. It was specified that effective performance of the nozzle life can be identified through quantitative property identification which basically needed the nozzle material to be high value of toughness and hardness. The study also concludes that to improve wear performance is by making the nozzle entrance section to have high toughness properties and the exit to have high hardness properties.

Using similar testing conditions, Nanduri et al. (2002) also made an accelerated nozzle wear experiment in AWJ machining process with adding different parameters and conditions. Mainly the nozzle materials used are tungsten carbide Cobalt (WC/Co), and ROCTEC nozzle (Tungsten carbide nozzles made with rapid Omnidirectional compaction process).

Instead of investigating the nozzle wear by measuring the change of exit diameter, the nozzle wear is assessed by weighing the loss of nozzle volume by measuring the nozzle after an interval of time. It is also shown that the addition of the length of the nozzle will reduce the exit bore increment and weight reduction rate. Furthermore, the eroded outlet diameter profiles of the nozzles revealed that although the interior erosion contour were shown to be identical, the nozzle length has an explicit effect on the increase of outlet diameter by increasing the time of the wear profile built

up from spanning the outlet. The increase of nozzle length has no effect on the flow pattern upstream within the nozzle. The erratic trend of the outlet diameter growth was not affected by the increment of the nozzle (Nanduri et al., 2002).

A trend of reduction of nozzle outlet incrementation with increasing the angle of the was detected in 15 minutes' duration test (Nanduri et al., 1997). On the other hand, a same experiment was done to investigate the life cycle of the nozzle using the same parameters of inlet angle and found that the life cycle are almost the same (Nanduri et al., 1997). The profiles of the outlet diameter show that there was compelling difference in the erosion profiles of different inlet angle of the nozzles to the distribution of erosion along the length. As the angle of the nozzle inlet increases, the distribution of erosion produces increased oscillation therefore contributed to the erratic nozzle outlet increment. It was then concluded that smaller angle of the nozzle inlet produces a more linear incrementation of the nozzle outlet.

For the effect of nozzle diameter on erosion of the AWJ nozzle. The profile of the nozzle outlet curve indicates that the ratio of the orifice to nozzle have an effects to cutting performance (Hashish et al., 1994; Nanduri et al., 1997). According to an experiment to investigate the different particle distribution in nozzles under different mixing conditions found that by preserving the ratio,  $Ro$ , of orifice diameter to nozzle diameter around 0.3–0.4 and maintaining other parameters to a constant value produced an outcome where the optimum cutting and mixing setting was achieved (Nanduri et al., 1996).

By comparing the erosion rates of AWJ nozzles under different conditions, the erosion rate of the nozzle,  $E$ , as a function of AWJ system and nozzle parameters is obtained as the following Equation 2.1 (Nanduri et al., 2002);

$$E = f(P, d_o, d_n, L, \dot{m}_a) \quad 2.1$$

Where  $P, d_o, d_n, L$  and  $\dot{m}_a$  is water pressure, orifice diameter, nozzle diameter, nozzle length and abrasive flow rate respectively. Thus, an empirical model for the nozzle wear rate was obtained as following Equation 2.2 (Nanduri et al., 2002);

$$E = (8.07E^{-4}) \frac{P^{0.9} d_o^{0.38} \dot{m}_a^{0.7}}{d_n^{0.5} L^{0.8}}$$

This erosion model is important for the research to compare between an experimental model of the nozzle erosion with the CFD based erosion model.

### 2.3 Assumptions and theoretical formulation

The simulation assumed that the flow to be treated as multiphase and the fluid to be considered as incompressible and continuum. Since the abrasive are entrained in the flow therefore particle's abrasive velocity is simulated to have equal velocity with the slurry. The interaction between fluid flow and abrasives were solved with using Langrangian-Eulerian model. It is also defined a discrete particle modelling, which deals with the equations of each particle individually through which the stable stage is modelled using a Eulerian structure and the particles directional trajectories are solved within a Lagrangian structure. Two-way coupling is defined for each particle interaction of momentum, mass and energy with the fluid domain were applied for the current work (Deepak, Anjaiah, Karanth, & Sharma, 2012; Hu, Zhu, Yu, & Yuan, 2008; Ng & Guannan, 2015; Y Zhang, Reuterfors, McLaury, Shirazi, & Rybicki, 2007). Similar simulation model to validate the work by Mostofa et al. (2010) by using theoretical waterjet velocity. Same methods of validation were used to further approves the simulation model for the present work alike. Equation 2.3 to Equation 2.7 forms the theoretical formulation to obtain the velocity of the waterjet at the at the orifice.

Theoretical waterjet velocity,  $V_{th}$ ;

$$V_{th} = \sqrt{\frac{2p}{\rho}} \quad 2.3$$

Water compressibility;

$$\frac{\rho}{\rho_0} = \left(1 + \frac{P}{L}\right)^n \quad 2.4$$

Whereby  $p$ ,  $\rho$  and  $L$  is the operating pressure, water density ( $kg/m^3$ ) and pumping pressure. Whereas  $n = 0.162$  at  $25^0$  C. The value of  $L$  were relying on the pumping pressure of the AWJ machine. Which is when plunging process of the pump before any water starts to discharge by the check valve which is 345 MPa to be used in this simulation.

Waterjet velocity produced from the resulting equation;

$$V_j = \sqrt{\frac{2L}{(1-n)\rho_0} \left[ \left(1 + \frac{P}{L}\right)^{1-n} - 1 \right]} \quad 2.5$$

Compressibility factor:

$$\varphi = \frac{V_j}{V_{th}} = \sqrt{\frac{L}{P(1-n)} \left[ \left(1 + \frac{P}{L}\right)^{1-n} - 1 \right]} \quad 2.6$$

The following equation expressed the waterjet velocity:

$$V_J = C_d \varphi V_{th} \quad 2.7$$

Where discharge coefficients,  $C_d = 0.85$ . The value was obtained past research function of jet size (Mostofa et al., 2010).

Utilizing the particle erosion and accretion feature to have the monitoring of the erosion rates at wall boundaries. Equation 2.8 defines the erosion rate equation:

$$R_{erosion} = \sum_{p=1}^n \frac{\dot{m}_p C(d_p) f(a) v^{b(v)}}{A_{face}} \quad 2.8$$

Where  $a$  is the impact trajectory of the abrasive particle direction to the wall surface,  $C(d_p)$  is a particle diameter function,  $f(a)$  is an impact angle function,  $v$  is the relative velocity of the relative particle,  $b(v)$  is a relative particle velocity function, and

$A_{face}$  is the cell surface area of the wall.  $C = 1.8 \times 10^9$  are a default value,  $b=0$  and  $f = 1$ . The unit of  $\text{kg/m}^2\text{s}^2$  is the erosion rate density. It is also noted that this value just represents the value of the qualitative characteristic of the actual materials being used instead of the physical value.

The turbulence simulation for the flow of water, air and abrasive of an AWJ process is presented in an  $K-\epsilon$  turbulence model. The Percentage Intensity,  $I$ , which is defined as the root-mean-square of the velocity fluctuations,  $u'$ , to the mean velocity  $u_{average}$  specifies the turbulence quantity. Equation 2.9 defines the value of the turbulence intensity conditions which is the process occurring at water pressure inlet area;

$$I = \frac{u'}{u_{average}} = 0.16(Re_{Dh})^{-1/8} \quad 2.9$$

Equation 2.10 shows how to obtain the Reynold's number,  $Re$ , for the AWJ waterjet circular tube when the size of the hydraulic diameter,  $D_h$  is given;

$$Re_{Dh} = \frac{\rho u D_h}{\mu} \quad 2.10$$

Where  $L$  is the characteristic length [m],  $\mu$  is the dynamic viscosity [ $\text{Ns/m}^2$ ]  $u$  is velocity based on the actual cross sectional area of the tube [m/s] and  $\nu$  is the value of the kinematic viscosity [ $\text{m}^2/\text{s}$ ].

#### 2.4 Applications of CFD in Erosion Modelling

Computational Fluid Dynamics (CFD) is a technique to solve and analyze problems that involves fluid flows using numerical methods and algorithms. Using computers to perform modelling, simulations and analysis of fluid flow enables CFD practitioners to have insights of flow patterns that have been difficult to be performed using traditional experimental techniques. Currently, CFD applications can be found in the field of aerospace, turbo machinery, automotive and maritime. The capabilities of CFD also made it way in geography, oceanography, astrology, meteorology, oil recovery and architecture. A comprehensive explanation of CFD principles and

applications have been done by Blazek (2015). Currently, the development of CFD software has been very promising. ANSYS Fluent software is well known and widely used CFD engineering software for modelling fluid flow.

Vast research have been put effort on the study of multiphase flow sand erosion in horizontal pipe (Jafari, Mansoori, Saffar Avval, Ahmadi, & Ebadi, 2014), pipe bends (Njobuenwu & Fairweather, 2012; Pereira, de Souza, & de Moro Martins, 2014) and in complex geometries(Gandhi, Vuthaluru, Vuthaluru, French, & Shah, 2012). CFD applications in AWJ machining have been a prevalent tool to simulate many processes involving AWJ machining. Liu, Wang, Kelson, et al (2003) used the Fluent6 flow solver to study the attributes of abrasive waterjet by CFD simulation and CFD models were made for abrasive waterjet and high-speed velocity waterjets. Kerf profile process in AWJ cutting Particle and water velocities were achieved under multiple input and boundary conditions to provide a greater observation into the jet attributes and more basic understanding. For the multiple of postliminary ranges engaged, the observation shows that a jet is characterized by an initial rapid erosion of the axial velocity at the middle of the jet whereas the cross-sectional flow shows changes towards the upper profile at the end of the jet stream. The study then uses smaller diameter nozzles and made simulations using multiple flow conditions to study the attributes of the dynamicity of the jet to the flow at the end of the jet stream.

Chen, McLaury, & Shirazi (2006) prediction of erosion model used three steps process methods which includes the extended medium of fluid flow simulation, using the Lagrangian approach for particle monitoring and calculation of erosion by harnessing the data of particle breaches on the surface wall. The continuous carrier fluid flow equations are given by CFX software. The results found that fluid properties had significant effects on erosion.

Hadžiahmetović, Hodžić, Kahrmanović, & Džaferović (2014) have made an erosion model prediction based from Finnie's erosion equation for elbow erosion using the ANSYS software. Comparisons with experimental studies done by Chen et al. (2006) found positive correlations.

Jafari et al. (2014) developed a modified model for predicting erosion rate in pipe flows that accounts for the effect of particle size to simulate the wall impact velocity caused by fluid turbulence. Discrete random walk model was used as the basis in the modeling of the fluid oscillating velocities. The phases of gas and solids in horizontal pipe was analytically investigated utilizing four-way coupling of Lagrangian and Eulerian approach. Equation 2.11 shows the modified erosion rate from Huang, Minev, Luo, & Nandakumar (2010) which have been simplified to deal with the effect of mediatory abrasive size on the surface wall impingement velocity which is generated by the flow turbulence.

$$\Delta E = \frac{D\rho_p^{1+3(1-n)/4}d_p^{2(1-n)}U_0^2\varphi^{\dagger}}{\varepsilon_0^i P_t P_n^{3(1-n)/4}} \left( \frac{0.0116b_2 U_0 \sqrt{0.5a/R_{ed}^m (y^+)^2}}{1 + 0.203y^+ + 0.0014(y^+)^{2.421}} \right)^2 + \frac{d_p^2 g(1-\varphi)(\rho_p \rho_f) \cos(\alpha)}{18\mu(1 + 0.1Re_p^{0.75})} \quad (2.11)$$

Where  $\Delta E$  is the erosion rate in [mm/year], the information for  $D$  and  $b_2$  values can be obtained through experiment (Bitter, 1963; Karabelas, 1978).

An AWJ related study was conducted to study the effect of erosion impact of a single particle abrasive with the target workpiece which is stainless steel (AISI 304). The research was done using LS Dyna where the crater sphericity in the simulation was used to compare with the observation of experimental shapes of craters on the workpiece material. The study is emphasized only in the measurements of the sphericity of the impact crater and limited parameters of abrasive and workpiece material (Junkar, Jurisevic, Fajdiga, & Grah, 2006).

Maniadaki, Kestis, Bilalis, & Antoniadis (2007) introduced a computerized method model for AWJ simulation for the purpose to study and evaluate in comprehensive the material assessment of a work piece under waterjet impingement. The model developed using LS-DYNA 3D cipher to model the impingement of the workpiece caused by the waterjet flow high impact pressure.

Deepak et al. (2012) had also apply the features of ANSYS application to observe the cause of pressure at the inlet of nozzle on surface friction coefficient and

flow outlet kinetic energy. The observation shows that by rising the pressure at the inlet causes compelling increase to the surface friction coefficient and the flow kinetic energy increased as well. Further observation then shows that by raising the volume fraction of abrasives particles causes a compelling decrease on both surface friction coefficient and flow kinetic energy.

Baisheng et al. (2011) have performed analytical simulation of the flow field of abrasive waterjet nozzle under deluging setting based on application of FLUENT software. The research used RNG  $\kappa$ - $\epsilon$  turbulent model and finer algorithm for modelling to simulate flow field from generated from an abrasive waterjet nozzle. The research indicated that there are three areas of zones which are shock zone, free flow zone and wall flow zone. Shock zone suggest the distance for the best cutting distance which is shown to be within the scope of 2 – 7 times the nozzle exit diameter.

It is known that investigations using Computational Fluid Dynamics (CFD) in studying erosion prediction and modelling in AWJ nozzle were very few. Mostofa et al. (2010) uses the ANSYS CFX application to model multiple flow of water, air and abrasives phases in the AWJ nozzle to observe the erosion rate at surface wall of the nozzle and investigate the effect of the size of abrasive particle with multiple conditions of the nozzle lengths. Finnie's erosion model of ductile material was used as the base model. Observation demonstrated that the geometry of the abrasive and flow velocity have influence on the erosion rate value. It was monitored that the rate of erosion identical linear trending as attained by Nanduri et al. (2002).

## 2.5 CFD Numerical Model

The CFD analytical model mainly repose of three parts which is the fluid jet model, the particle trajectory model and the erosion impingement model. First, jet flow model is obtained. After that, the jet flow were analytically computing to track the trajectory of solid particles (abrasives) in the fluid domain. Finally, once the abrasive impacted the target face (nozzle wall), the mass loss then calculated through the data gathered throughout the process.

### 2.5.1 Fluid Flow Model

The general equation for conservation of mass (continuity equation) is written as Equation 2.12;

$$\frac{\partial \rho}{\partial t} + \nabla \cdot (\rho \vec{v}) = S_m \quad 2.12$$

The equation above shows the general form of the mass conservation equation and is valid for incompressible as well as compressible flows. The source  $S_m$  is the mass added to the continuous phase from the dispersed second phase (gas, liquid, solid) and any user-defined sources.

The general equation for the conservation of momentum in an inertial (non-accelerating) reference frame is expressed as Equation 2.13;

$$\frac{\partial \rho}{\partial t} (\rho \vec{v}) + \nabla \cdot (\rho \vec{v} \cdot \vec{v}) = -\nabla p + \nabla \cdot (\bar{\tau}) + \rho \vec{g} + \vec{F} \quad 2.13$$

Where  $p$  is the static pressure,  $\tau$  is the stress tensor and  $\rho \vec{g}$  and  $\vec{F}$  are the gravitational body force and external body forces, respectively. Example of external body forces are the forces arise as per interaction of primary phase and dispersed phase.

$\vec{F}$  also contains other model-dependent source terms such as user-defined sources and porous-media which is defined in Equation 2.14;

$$\bar{\tau} = \mu [(\nabla \vec{v} + \nabla \vec{v}^T) - \frac{2}{3} \nabla \cdot \vec{v} I] \quad 2.14$$

In the first term on the left-hand side,  $\mu$  is the molecular viscosity,  $I$  is the unit tensor and the second term on the right hand side is the effect of volume dilation

#### 2.5.1.1 Multiphase Flow

Multiphase flow is any domain of flow which imposed of multiple phase for example a blend of abrasives, liquids, gasses, bubbles or drops (Al-Baghdadi, Resan, &

Al-Waily, 2017; Darihaki, Hajidavalloo, Ghasemzadeh, & Safian, 2017; Parsi, Agrawal, et al., 2015; Parsi, Kara, et al., 2017; Shabarchin & Tesfamariam, 2016; R E Vieira, Sajeev, Shirazi, McLaury, & Kouba, 2015; Ronald E Vieira, Mansouri, McLaury, & Shirazi, 2016; Zahedi, Karimi, Mahdavi, McLaury, & Shirazi, 2016; Zheng et al., 2017). In another context, liquids and gases are multiphase flows that are categorized as detached phase while particles such as sand and abrasives are categorized as the circulating phase (Brennen, 2005).

In pipe flows especially in oil and gas industry, this configuration is observed in types of gas-liquid, gas-solid, liquid-liquid and liquid-solid (Lin, Arabnejad, Shirazi, McLaury, & Lan, 2018; A Mansouri, Arabnejad, Shirazi, & McLaury, 2015; Amir Mansouri, Arabnejad, Karimi, Shirazi, & McLaury, 2015; Olsen et al., 2017; Parsi, Vieira, et al., 2015; Peng & Cao, 2016a; Shirazi, McLaury, & Arabnejad, 2016; Zahedi et al., 2018; Zamani, Seddighi, & Nazif, 2017; Zheng et al., 2016; H. Zhu, Han, Wang, He, & Wang, 2015).

In an AWJ mixing chamber, there are two main flows where one phase is composed of continuous (primary) flow which is water and abrasives particles which can be characterized as dispersed flow. Therefore, it can be logical to identify the multiphase flow inside the mixing chamber of and AWJ machine to be liquid-solid interaction.

There are several multiphase models that are available in CFD cipher and three of them are the Eulerian, Langrangian and volume of fluid (VOF) model. This thesis will approach the study of multiphase flow in two approach. The first approach is where gas and solid phase interaction is studied. The base equation for detached phase of water is presented in Eulerian form and the circulating phase of abrasive particle is presented in Langrangian form.

For the second approach, three phases of gas, liquid and solid was investigated where the VOF method is applied. The abrasive particle still presented in the Langrangian form the same with the first case.

### 2.5.1.2 Primary Phase Flow Modelling

The interaction between the primary (continuous phase) with the abrasive's particles are required to be modelled. Mass, momentum and energy are transferred between the phases which controls the interaction between the phases (Al-Khayat, Al-Baghdadi, Neama, & Al-Waily, 2018; Banakermani, Naderan, & Saffar-Avval, 2018; M.-J. Li, Tang, Wang, Zhao, & Tao, 2017; J. Liu et al., 2017; Morrison et al., 2017; Pandya, Dennis, & Russell, 2017; Parsi, Kara, Sharma, McLaury, & Shirazi, 2016; Parvaz, Hosseini, Elsayed, & Ahmadi, 2018; Peng & Cao, 2016b; C. Zhu, Qiu, Cao, Rao, & Hu, 2016). The flows are solved in general mathematical form which includes mass and momentum conservation and the summarization can be concluded as the Navier-Stokes equations. Therefore, the turbulence modelling are taken as a solution for the major influence of turbulence in the model

### 2.5.1.3 Turbulence Model

It is a general idea that most engineering flows are turbulent as it is essentially a random process (Barkley et al., 2015; Lee, Lamar, Mudrow, Weissinger, & Shanbhag, 2018; Priyadarshana, Weaver, Szymyk, & Goodson, 2018; Schubauer & Tchen, 2015; Sheikholeslami, Jafaryar, & Li, 2018). Therefore, a Turbulence model is needed as we cannot perfectly represents the effects of turbulence in the CFD simulation (Jafari et al., 2014). The Reynolds-Averaged Navier Stokes (RANS) was used to solve the average time and flow behaviour and finding the magnitude of turbulence oscillation which is defined by Equation 2.15.

$$\frac{\partial(\rho\bar{u}_i)}{\partial t} + \frac{\partial(\rho\bar{u}_i\bar{u}_j)}{\partial t} = -\frac{\partial}{\partial X_i} + \frac{\partial\bar{p}}{\partial X_j} \left[ \mu \left( \frac{\partial\bar{u}_i}{\partial X_i} + \frac{\partial\bar{u}_j}{\partial X_j} - \frac{2}{3}\delta_{ij} \frac{\partial\bar{u}_m}{\partial\bar{u}_x} \right) \right] + \frac{\partial}{\partial X_j} (-\rho u'_i u'_j) \quad 2.15$$

The Standard  $k-\varepsilon$  Model is a two-equation turbulence model which solves the assurance of the length of turbulence and scale of time by equating two deliverable equations. A model was developed which is based on model deliverable equations for the turbulence flow kinetic energy,  $k$ , and its degradation rate,  $\varepsilon$  (Launder & Shima, 1989). The model transport equation for  $k$  remained the same whereas the transport equation has been modified  $\varepsilon$  using physical evidence and similar with its counterpart. It is assumed that flow is fully turbulent and the other factors effecting the flow such as

viscosity are to be negligible. Therefore, the method used are only applicable for flow under full turbulence. There are two variants of the Standard  $k-\varepsilon$  Model which is the RNG  $k-\varepsilon$  Model (Yakhot & Orszag, 1986) and the Realizable  $k-\varepsilon$  Model (Shih, Liou, Shabbir, Yang, & Zhu, 1994).

Transport deliverable equation for the Standard  $k-\varepsilon$  Model can be presented in the following Equation 2.16 and Equation 2.17 for the turbulence kinetic energy,  $k$ , and rate dissipation,  $\varepsilon$ .

$$\frac{\partial}{\partial t}(\rho k) + \frac{\partial}{\partial x_i}(\rho k u_i) = \frac{\partial}{\partial x_j} \left[ \left( \mu + \frac{\mu_t}{\sigma_k} \right) \frac{\partial k}{\partial x_j} \right] + G_k + G_b - \rho \varepsilon - Y_M + S_K \quad 2.16$$

$$\frac{\partial}{\partial t}(\rho \varepsilon) + \frac{\partial}{\partial x_i}(\rho \varepsilon u_i) = \frac{\partial}{\partial x_j} \left[ \left( \mu + \frac{\mu_t}{\sigma_\varepsilon} \right) \frac{\partial \varepsilon}{\partial x_j} \right] + C_{1\varepsilon} \frac{\varepsilon}{k} (G_k + C_{3\varepsilon} G_b) - C_{2\varepsilon} \frac{\varepsilon^2}{k} + S_\varepsilon \quad 2.17$$

These equations,  $G_k$ , can be expressed as the production of turbulent kinetic energy because of the mean velocity gradients.  $G_b$  is the production of turbulent kinetic energy caused by buoyancy  $Y_M$ , is the production of oscillating dilatation in compressible turbulence to the overall degradation rate.  $C_{1\varepsilon}$ ,  $C_{2\varepsilon}$  and  $C_{3\varepsilon}$  are constants.  $\sigma_k$  and  $\sigma_\varepsilon$  are the turbulent Prandtl numbers for  $k$  and  $\varepsilon$  respectively.  $S_\varepsilon$  and  $S_k$  are terms specified by users.

Equation 2.18 shows the transport equations for the RNG  $k-\varepsilon$  Model which is similar to the standard form of  $k-\varepsilon$  Model;

$$\frac{\partial}{\partial t}(\rho k) + \frac{\partial}{\partial x_i}(\rho k u_i) = \frac{\partial}{\partial x_j} \left[ (\alpha_\varepsilon \mu_{tlf}) \frac{\partial k}{\partial x_j} \right] + G_k + G_b - \rho \varepsilon - Y_M + S_K \quad 2.18$$

$$\frac{\partial}{\partial t}(\rho \varepsilon) + \frac{\partial}{\partial x_i}(\rho \varepsilon u_i) = \frac{\partial}{\partial x_j} \left[ (\alpha_\varepsilon \mu_{tlf}) \frac{\partial \varepsilon}{\partial x_j} \right] + C_{1\varepsilon} \frac{\varepsilon}{k} (G_k + C_{3\varepsilon} G_b) - C_{2\varepsilon} \frac{\varepsilon^2}{k} + S_\varepsilon \quad 2.19$$

Where  $G_k$  expressed as the production of turbulent kinetic energy due to the mean velocity gradients.  $G_b$  is the production of turbulent kinetic energy due to buoyancy,  $Y_M$ , is the contribution of the fluctuating dilatation in compressible turbulence to the overall dissipation rate. The quantities  $a_k$  and  $a_\varepsilon$  are the inverse of effective Prandtl numbers for  $k$  and  $\varepsilon$  respectively.  $S_\varepsilon$  and  $S_k$  are terms specified by users.

Realizable  $k$ - $\varepsilon$  Model and standard  $k$ - $\varepsilon$  Model are different in two critical ways

- The model composed of different alternative formulation for solving viscosity in turbulence.
- The transport deliverable equation of the degradation rate,  $\varepsilon$ , has been acquired from an exact equation for the transport deliverable of the mean-square vorticity oscillation.

The term “realizable” came to define that the model can solve certain analytical problems on the Reynolds stresses which is always come about with the physics of turbulent flows. Neither the standard or RNG  $k$ - $\varepsilon$  Model is realizable. Equation 2.20 to Equation 2.22 shows the transport equation for the Realizable  $k$ - $\varepsilon$  Model

$$\frac{\partial}{\partial t}(\rho k) + \frac{\partial}{\partial x_j}(\rho k u_j) = \frac{\partial}{\partial x_j} \left[ \left( \mu + \frac{\mu_t}{\sigma_\varepsilon} \right) \frac{\partial k}{\partial x_j} \right] + G_k + G_b - \rho \varepsilon - Y_M + S_k \quad 2.20$$

$$\frac{\partial}{\partial t}(\rho \varepsilon) + \frac{\partial}{\partial x_j}(\rho \varepsilon u_j) = \frac{\partial}{\partial x_j} \left[ \left( \mu + \frac{\mu_t}{\sigma_\varepsilon} \right) \frac{\partial \varepsilon}{\partial x_j} \right] + \rho C_1 S_\varepsilon - \rho C_2 \frac{\varepsilon^2}{k + \sqrt{\nu \varepsilon}} C_{1\varepsilon} \frac{\varepsilon}{k} + C_{3\varepsilon} G_b + S_\varepsilon \quad 2.21$$

Where

$$C_1 = \max \left[ 0.43, \frac{\pi}{\pi + 5} \right], \pi = S \frac{k}{\varepsilon}, S = \sqrt{2 S_j S_j} \quad 2.22$$

These equations,  $G_k$ , expressed the production of turbulent kinetic energy because of mean velocity gradients.  $G_b$  is the production of turbulent kinetic energy

because of buoyancy,  $Y_M$ , is the contribution of the fluctuating dilatation in compressible turbulence to the overall dissipation rate.  $C_{1\varepsilon}$ ,  $C_{2\varepsilon}$  and  $C_{3\varepsilon}$  are constants.  $\sigma_k$  and  $\sigma_\varepsilon$  are the turbulent Prandtl numbers for  $k$  and  $\varepsilon$  respectively.  $S_\varepsilon$  and  $S_k$  are terms specified by users.

To simulate the turbulence near the wall, a surface wall domain function is required and the standard wall functions in ANSYS which are based on the work on CFD erosion rate on AWJ nozzle (Mostofa et al., 2010). As in the  $k-\varepsilon$  models, the  $k$  equation is solved in the entire domain which also includes the wall-adjacent cells. It is stated that the boundary condition for  $k$  imposed at the wall as Equation 2.23.

$$\frac{\partial k}{\partial n} = 0 \quad 2.23$$

The above  $n$  is the local coordinate normal to the wall. The equation for production of kinetic energy is as Equation 2.24.

$$G_k \approx \tau_w \frac{\partial U}{\partial y} = \tau_w \frac{\tau_w}{K \rho k_p^{1/2} y_p} \quad 2.24$$

Where  $G_k$  is the kinetic energy and its dissipation rate,  $\varepsilon$ , at the wall-adjacent cells where the source term in  $k$  equation are computed in the basis of the local equilibrium hypothesis. It is assumed that the production  $k$  and its dissipation rate are assumed to be equal in the wall-adjacent control volume. Thus  $\varepsilon$  is computed using Equation 2.25.

$$\varepsilon_p = \frac{C_\mu^{3/4} k_p^{3/2}}{K y_p} \quad 2.25$$

### 2.5.2 Particle Motion Model

In this work, dispersed phase is the finite number of the abrasive particles which are injected into the primary phase. Dispersed phase model are commonly treated in two models which is the particle trajectory models and the multiphase fluid models (Brennen, 2005). In the particle trajectory model, the Lagrangian approach can be used to predict the projection of abrasive particles by composing the balance of the force

which is the drag, lift and moment force on the abrasive particle. Whereas in the multiphase fluid models, the Eulerian method were used, therefore, the abrasive abrasives particles can be treated as both dispersed and continuous phase.

Coupling is another issue that is needed to be addressed as there are interaction between continuous and dispersed phase. There are four types of coupling which is the One-way coupling, Two-way coupling, Three-way coupling and Four-way coupling. In One-Way coupling, the effect of the dispersed phase is considered to be ignored as it is used in model where the concentration of dispersed phase is very small. Two-way coupling is used when the dispersed phase has effect onto the interacting phase. Three-way and Four-way coupling is where there are additional numbers of dispersed phase interaction. In this work, the Two-way coupling were adopted for the phase interaction.

### 2.5.2.1 Governing Equations

The conservation of mass common equation can be expressed by equation of balance of mass of the element of fluid flow which can be produced in Equation 2.26.

$$\frac{\partial}{\partial t}(\rho_q \alpha_q) + \nabla \cdot (\rho_q \alpha_q \vec{v}_q) = \sum (\dot{m}_{pq} - \dot{m}_{qp}) \quad 2.26$$

The first expression and second expression of the term shows the value of rate of change of density in time, the value of rate of increase of mass (mass per unit of volume) and the net value of rate of flow of mass outlet of the element of fluid.

Whereby  $a$  is the fraction of volume,  $i$  is the phase number for liquid, solid and gas and  $\nabla$  is the quantity of partial derivative with respect to all projection. The sum accumulation of  $a_i$  is equal to 1 as shown in Equation 2.27.

$$\sum_i a_i = a_{gas} + a_{liquid} + a_{solid} = 1 \quad 2.27$$

The basic term of the conservation of momentum describes that the value for the rate of change of the momentum of a particle fluid is equal to the sum of the forces acting on the particle which can be shown as Equation

2.28 to Equation 2.31 2.31 (Poirier & Geiger, 2016);

$$\frac{\partial}{\partial t} (\rho_i \alpha_i V_i) + \nabla \cdot (\rho_i \alpha_i V_i V_i) = -\alpha_i \nabla p + \nabla \cdot [\alpha_i (\tau_i + \tau_i^t)] + \rho_i \alpha_i g + M_i \quad 2.28$$

$$\nabla \cdot [\alpha_i (\tau_i + \tau_i^t)] = \nabla \cdot [\alpha_i \mu_i (\nabla V_i + \nabla V_i^T)] \quad 2.29$$

For two phases (gas and liquid)

$$\frac{\partial}{\partial t} (\rho_g \alpha_g V_g) + \nabla \cdot (\rho_g \alpha_g V_g V_g) = -\alpha_g \nabla p + \nabla \cdot [\alpha_g (\tau_g + \tau_g^t)] + \rho_g \alpha_g g + M_g \quad 2.30$$

$$\nabla \cdot [\alpha_l (\tau_l + \tau_l^t)] = \nabla \cdot [\alpha_l \mu_l (\nabla V_l + \nabla V_l^T)] + \rho_l \alpha_l g - M_l \quad 2.31$$

Which  $\alpha_i$  is the fraction of volume and  $i$  is the number of phases which is in this contact are the liquid, solid and gas. The accumulation of summation of  $\alpha_i$  is equal to 1,  $p$  is the pressure and it is assumed to be the same in all phases of the process,  $\tau_i$  is the stress at molecular state,  $\tau^t$  is the stress and turbulent state,  $M_i$  is the momentum at different phase of exchange which is expressed in per unit volume.

The interphase momentum transfer includes the drag, virtual mass, lift and turbulent dispersion force in all projection. Equation 2.32 shows the accumulation of summation of all the mentioned forces;

$$M_i = \sum F = \sum F_{Drag} + F_{virtual\ mass\ force} + F_{Lift} + F_{Turbulent\ Dispersion} \quad 2.32$$

### 2.5.2.2 Drag force

Drag force is the one of the most important interaction terms since this demonstrate the two-phase flows effects which determine the flow fields of the dispersed and continuous phases. It has two sources which is the skin friction and form drag. Surface friction is associated to stresses of shear of the solid particle when there is entrainment and interaction with the flow of the fluid and it is reliant on the viscous surface friction between fluid and particle.

Pressure drag or also called a form of drag composed due to normal stresses and it reliant on the geometry of the abrasive particle. The drag force equation can be expressed in the term reflected in Equation 2.33 and Equation 2.34 (Gosman, Lekakou, Politis, Issa, & Looney, 1992);

$$F_{Drag} = \frac{3}{4} \rho_c \alpha_d \frac{C_D}{d_p} |V_r| V_r \quad 2.33$$

$$V_r = V_c + V_D \quad 2.34$$

Whereby,  $F_D$  is the force of the drag,  $V_r$  is the relative velocity between continuous phase and dispersed,  $V_d$  is the velocity of the dispersed phase process,  $V_c$  is the velocity of the continuous phase, c and d subscript represents dispersed and continuous phase respectively,  $d_p$  is the diameter of the particle and  $C_D$  is the drag coefficient for the standard round spherical particles (Ochieng & Onyango, 2008). The drag coefficient are defined in Equation 2.35 to Equation 2.36 (Flemmer & Banks, 1986);

$$C_D = \begin{cases} \frac{24}{Re_D} (1 + 0.15 Re_d^{0.678}) & \text{for } 0 < Re_D \leq 1000 \\ 0.44 & \text{for } Re_D > 1000 \end{cases} \quad 2.35$$

Where

$$Re_D = \frac{\rho_c d_p |V_r|}{\mu_c} \quad 2.36$$

Spherical drag law is given when the particles are treated as a smooth which can be expressed as in Equation 2.37;

$$C_D = a_1 + \frac{a_2}{Re} + \frac{a_3}{Re^2} \quad 2.37$$

Where  $a_1$ ,  $a_2$  and  $a_3$  are constants that apply over several ranges of  $Re$  (Morsi & Alexander, 1972).

The following correlation in Equation 2.38 of Non-spherical drag law is also to be considered as abrasives particles are not completely round in shape (Haider & Levenspiel, 1989).

$$C_D = \frac{24}{Re_{ph}} \left( 1 + b_1 Re_{ph}^{b_2} + \frac{b_3 Re_{ph}}{b_4 + Re_{ph}} \right) \quad 2.38$$

Where

$$b_1 = \exp(2.3288 - 6.4581\phi + 2.4486\phi^2)$$

$$b_2 = 0.0964 + 0.5565\phi$$

$$b_3 = \exp(4.905 - 13.8944\phi + 18.4222\phi^2 - 10.2599\phi^3)$$

$$b_4 = \exp(1.4681 + 12.2584\phi - 20.73222\phi^2 + 15.8855\phi^3)$$

Where the shape factor  $\phi$ , is defined as in Equation 2.39;

$$\phi = \frac{s}{S} \quad 2.39$$

Where  $s$  is the surface area of a sphere having the same volume as the particle.  $S$  is the actual surface area of the particle.  $Re_{ph}$  represents the drag force and  $d_p$  is the particle size.

### 2.5.2.3 Virtual mass force

Virtual mass force or also called additional mass force is the supplementary force added to increase the acceleration of the particle and other part of the fluid flow surrounded. A compelling are affected when the density of the dispersed phase state is less than the density of the primary phase state. Thus, this presented the equation of virtual mass flow is as in Equation 2.40;

$$F_{VM} = C_{VM} \alpha_d \rho_c \left[ \left( \frac{DV}{Dt} \right)_c - \left( \frac{DV}{Dt} \right)_d \right] \quad 2.40$$

Which  $\left( \frac{DV}{Dt} \right)_c$  and  $\left( \frac{DV}{Dt} \right)_d$  are derivative of material for the phase continuity and

the dispersed phase condition respectively and  $C_{vm}$  is the coefficient of the virtual mass which is equal to 0.5. Whereas  $F_{Drag}$  is the drag force,  $C_{Drag}$  is the drag coefficient,  $A$  is the reference area,  $\rho$  is the density of the mass of the fluid and  $u$  is the relative velocity of the flow of the object.

### 2.5.3 Erosion Model

Erosion on the surface of AWJ nozzle is simply the process of removal of material or degradation impinged by high velocity abrasives particles or others which is circulating in a jet flow on to the surface of the nozzle wall (Bitter, 1963). Other definition are the continuous removal of material through repeating impingement of small particles streaming in a fluid flow crazing against the surface of the nozzle wall (Hutchings & Winter, 1974). The equatio to obtain the erosion rate at surfaces of nozzle wall due to solid particles impact impingement can be expressed from Equation 2.41 (Finnie, 1960).

$$E = \begin{cases} \frac{mV^2}{P\phi K} \left[ \sin 2\alpha - \frac{6}{K} \sin \alpha \right], & \tan \alpha < \frac{K}{6} \\ \frac{mV^2}{P\phi K} \left( \frac{K \cos^2 \alpha}{6} \right), & \tan \alpha \geq \frac{K}{6} \end{cases} \quad 2.41$$

Where  $m$  is the mass of the particle,  $V$  is the velocity of the particle,  $P$  is the stress of the plastic flow which is a constant,  $\alpha$  is the angle of the particle impact,  $K$  is the components of the forces ratio in all direction and trajectories,  $\phi$  is the ratio between cut and contact of the depth which is equal to the value of 2 and  $E$  is the volume of material degraded by a individual particle. Finnie's model have been long-established and modified through countless times, however, it is still considered to be relevant and provides the basis for erosion modeling in all of areas (ElTobgy, Ng, & Elbestawi, 2005).

Bitter (1963) later introduced an erosion model basically composed of erosion wear and degradation of the surface of materials or workpiece caused by particles impingement or impact. Bitter's mechanism states that the cutting erosion process occurs when the particle impacts together with surface of a material or workpiece with approximately smaller impact angle, therefore gradually removed a fine amount of surface material which produces wear erosion or grinding effect on the surface of the material. Whereas, when the particle impacting the surface of the wall with higher value of impact angle, increased amount of material was detached which leads to the term called micro cracking on the surface material and fragmentation of the surface of the material or workpiece. Later on, Hashish (1989) made a modification to Finnie's model which considers the effect of particle's shape. It is introduced to replicate the AWJ erosion condition which the abrasives particle is used to erode work piece. Also related with erosion by solid particles, Hutchings (1981) introduced an erosion model for spherical particles at normal incidence.

Chen et al. (2006) have conducted both experimental and CFD based erosion prediction to predict the erosion in plugged tees and elbows for a wide range of dilute air and sand flows. The erosion results found that fluid properties had significant effects on erosion. The study evaluates the erosion data which is gathered from impingement information of impact speed and impact angle. Many studies have used an empirical relation for estimation of erosion wear through numbers of experimental data developed (Desale, Gandhi, & Jain, 2008; Elkholy, 1983; B. K. Gandhi, Singh, & Seshadri, 1999; Gupta, Singh, & Sehadri, 1995; Simon Ka-Keung, Humphrey, & Levy, 1981; Tsai, Humphrey, Cornet, & Levy, 1981).

Currently there are many studies of CFD based erosion model which mainly concentrates under the oil and gas industries involving slurry erosions in pipelines, tanks and burners (Arabnejad, Mansouri, Shirazi, & McLaury, 2015b, 2015a; Arabnejad et al., 2017; Barton, Lewis, & Emmerson, 2016; Lin, Lan, Xu, Dong, & Barber, 2015; Marzen, Iserloh, de Lima, Fister, & Ries, 2017; Parsi, Al-Sarkhi, et al., 2017; Thiana Alexandra Sedrez, Decker, da Silva, Noriler, & Meier, 2017; J. Zhang, Kang, Fan, & Gao, 2016). There are also erosion models that studies he development of soil erosion and applied it to CFD software (Baggaley & Potts, 2017; Hernandez et al., 2016; Kinnell, 2018; Klavon et al., 2017; Long et al., 2018, 2018; López-Vicente, Quijano, Palazón, Gaspar, & Izquierdo, 2015; Nearing, Lane, & Lopes, 2017). Erosion models are also developed for studies related to wind which are applied to land degradation, climate prediction, agricultural industry and sands trend development in arid or desert regions (Borrelli, Lugato, Montanarella, & Panagos, 2017; Chappell & Webb, 2016; Chappell et al., 2018, 2019; Mezósi, Blanka, Bata, Kovács, & Meyer, 2015; H. Pi, Sharratt, Feng, & Lei, 2017; Pierre et al., 2018; Rezazadeh, Irannejad, & Shao, 2016; Touré et al., 2018; Van Pelt et al., 2017; Webb et al., 2016).

Elkholy (1983) have done modification to the erosion equation specifically for expressing wear for cast iron Gupta et al. (1995) have produced an erosion model to predict wear in multi sized particulate slurries for brass and mild steel. Desale et al. (2008) used the empirical equation to investigate the parameter affecting erosion wear of ductile materials under normal impact conditions. It is found out that erosion wear of ductile materials at normal impact condition appears to be a function of the ratio of the abrasive material hardness to target material hardness. Velocity and particle size have large impact on erosion wear whereas smaller impact from solid concentration.

Huang, Chiovelli, Minev, Luo, & Nandakumar (2008) produces an erosion model which incorporates removal of material due to both deformation damage and cutting action removal. The study produces an equation for deformation damage which is obtained by analyzing the force, volume of indentation, strain introduced into the surface layer of target, critical strain and Coffin-Manson equation includes the effect of particle's shape mass, size, velocity, impact angle and properties of target on the volume loss. The study shows that the model of cutting removal indicated that erosion rate has a weak dependence on particle size.

Oka, Ohnogi, Hosokawa, & Matsumura (1997) have developed a separate erosion model which is derived from trigonometric functions where erosion damage is expressed by the product of two factors in which one for repeated deformation erosion and one is for cutting erosion. The first factor is related to the vertical component of the impact energy and approximates repeated plastic deformation. Where the second factor are related with cutting action.

There are many studies that considers the effect of incident angles, velocity and abrasives size to erosion rate (Hadavi, Moreno, & Papini, 2016). An erosion model which considers ploughing and fracture mechanism were proposed whereby the predictions are governed by the ratio of the target material fracture toughness to hardness (Ben-Ami, Uzi, & Levy, 2016). An energy dissipation of particle impact was derived by means of tangential and normal coefficients of restitution models which allows different energy dissipation mechanism to be recognized (Uzi & Levy, 2018).

Nanduri et al. (2002) have done a very comprehensive experimentation to study the erosions on AWJ nozzle wear specifically. The study covers the effect of system and geometric parameters on abrasive water jet nozzle wear thus came out with an erosion model to predict the erosion rate. A comprehensive description of the findings is discussed in detail in the next sub chapter.

## **2.6 Summary of Literature Review**

There are several studies on AWJ nozzle wear for variety of occasions and different parameters of the nozzle. Most of the studies requires the nozzle wear to be tested which prove to be a challenge. Hashish (1994) has stated that there is no ASTM standard that can replicate the erosive environment inside the nozzle mixing tube. CFD studies of erosion are used widely in the oil and gas pipeline industry as mentioned earlier in the chapter. Studies of nozzle wear are mainly based on tests using traditional experimental which is costly and time consuming Nanduri et al. (2002). Whereas, few have studied simulation of erosion in AWJ nozzle erosion as have been done by Mostofa et al. (2010) using an application called the ANSYS CFX. Therefore, the present study further analyzes the methods to simulate AWJ nozzle erosion.

## CHAPTER 3

### METHODOLOGY

#### 3.1 General

The simulation of the AWJ nozzle erosion consist of the following steps as shown in Figure 3.1. The Finnie's erosion and accretion model which was already available in the ANSYS software were used (Aslam Noon & Kim, 2017; Finnie, 1960). The simulation was validated through comparing the fluid flow simulation where the velocity profile was compared with the theoretical calculation which were also used by Mostofa et al. (2010) to validate their simulation. The simulation results are further compared with the erosion profile obtained from sectioned worn out nozzle used in the industry. Whereas, the parametric study replicates the geometry and system parameters studies done previously in which the empirical model obtained were used as a measurement for measuring the accuracy of the simulation (Nanduri et al., 2002).

#### 3.2 CFD Simulation

The CFD simulation process for AWJM nozzle erosion simulation consist of several steps that are involved in the analysis of the fluid flow. The primary steps of a CFD process for its analysis is Pre-Processing, applying the Solver and getting results through Post Processing.

#### 3.3 Pre-Processing

This is the first step of CFD simulation process which helps conceptualizing the geometry of the model. It is important to identify the fluid domain of interest. In this study, the fluid domain is the area bounded by the wall of the inlet of the mixing chamber to the nozzle outlet of the nozzle.

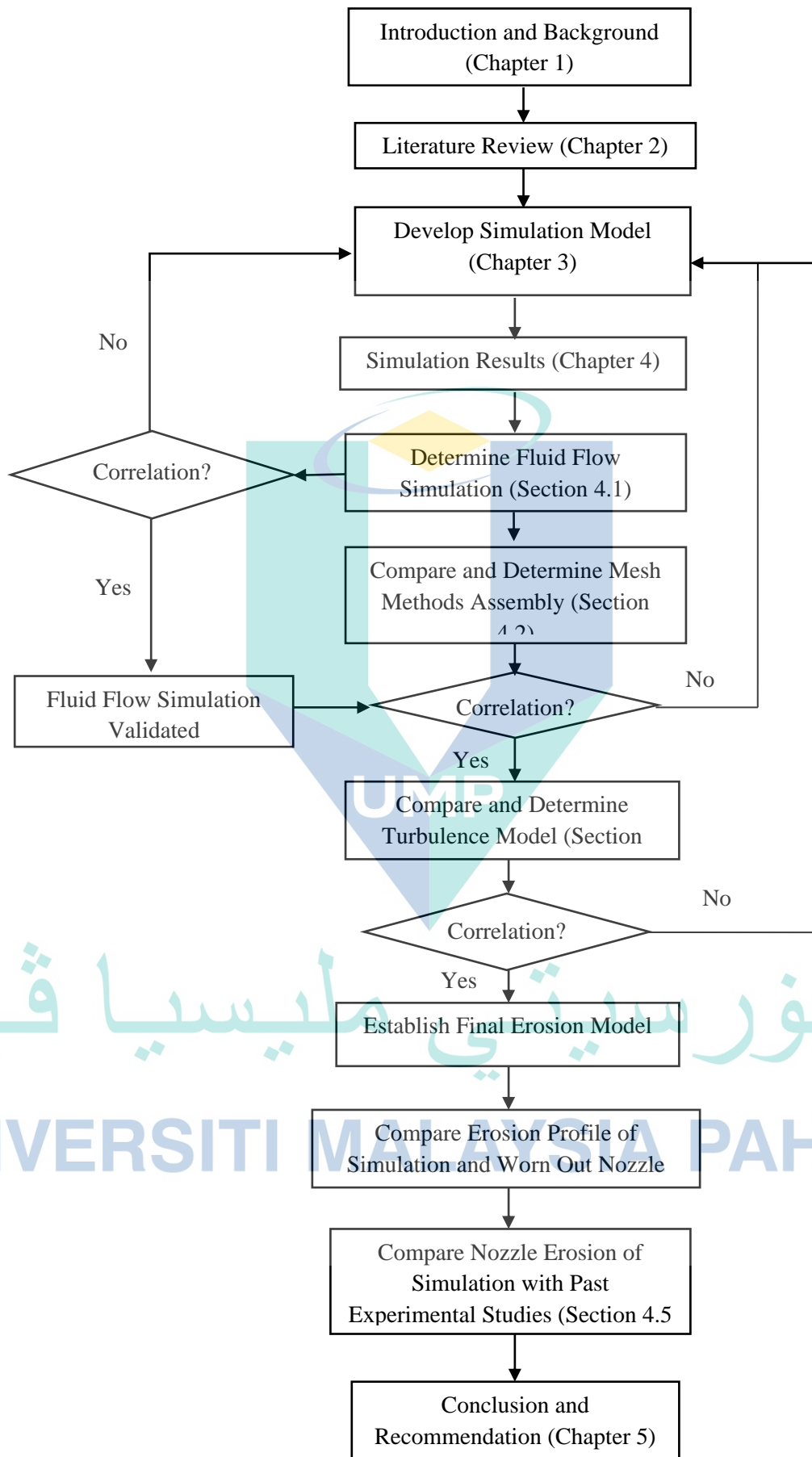
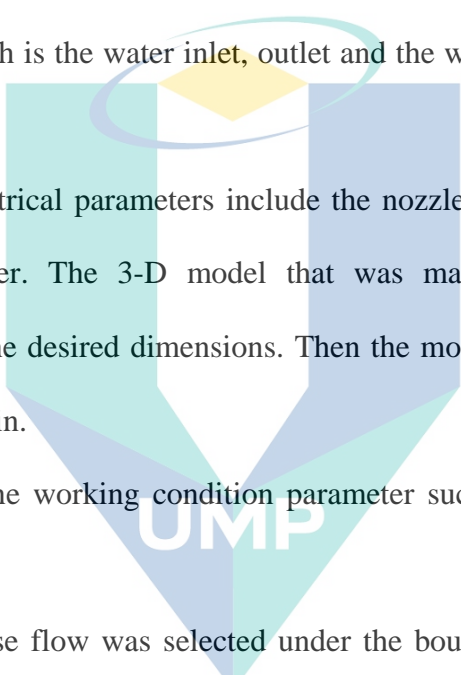


Figure 3.1 Methodology Flowchart

As shown in Figure 3.2, the 3-d conceptualization of the fluid domain was made. Below shows the steps of pre-processing;

- a) Under the mesh methods, there are the Quadrilateral, Cutcell and tetrahedral mesh. The 3-D model that was made are to be meshed to the mesh method mentioned.
- b) After that, under the grid section, the surface conditions are set to three condition which is the water inlet, outlet and the wall of the nozzle as shown in Figure 3.2.
- c) For the geometrical parameters include the nozzle length, nozzle diameter and orifice diameter. The 3-D model that was made need to be re-modelled according to the desired dimensions. Then the model were to repeat step (a) to be meshed again.
- d) Whereas for the working condition parameter such as the water pressure and abrasive size.
- e) The multi-phase flow was selected under the boundary condition section. The properties of air, water and abrasive particle were defined.
- f) Under the turbulence model, there options which are the Standard  $k-\varepsilon$  turbulence model and the Realizable  $k-\varepsilon$  turbulence model. In this study, both turbulences were simulated to identify which turbulence model have better accuracy.
- g) Start the simulation under the initialization section with setting the time steps to 180000 with 0.01 iteration time steps size.

### 3.2.1 Geometry and System Parameters

The geometrical and system parameters were based on the 3-D model of commercial AWJ cutting head from past research (Mostofa et al., 2010; Nanduri et al., 2002). Figure 3.2 represents the fluid phase of the model and is labelled per their boundary conditions. It shows a sectioned meshed model which includes the cutting head and the nozzle. The cutting head and abrasive delivery system were based on PASER® II abrasive cutting head. A distinctive characteristic of the model type is the abrasive system in which the abrasives were inserted diagonally into the mixing chamber.



Figure 3.2 Boundary conditions applied to the cutting head.

Figure 3.3 shows the designation of values applied to the nozzle geometrical model. In this simulation, the values for the cutting head remained the same whereas the parameters of the nozzle as well as other defined parameters were changed as per Table 3.1. The typical operating and values tested were based on the experimental design of past research in which the geometrical parameters were either already available in the industry or modified (Nanduri et al., 2002). This is to identify the potentially influential parameters that affects the behaviour of the nozzle erosion.

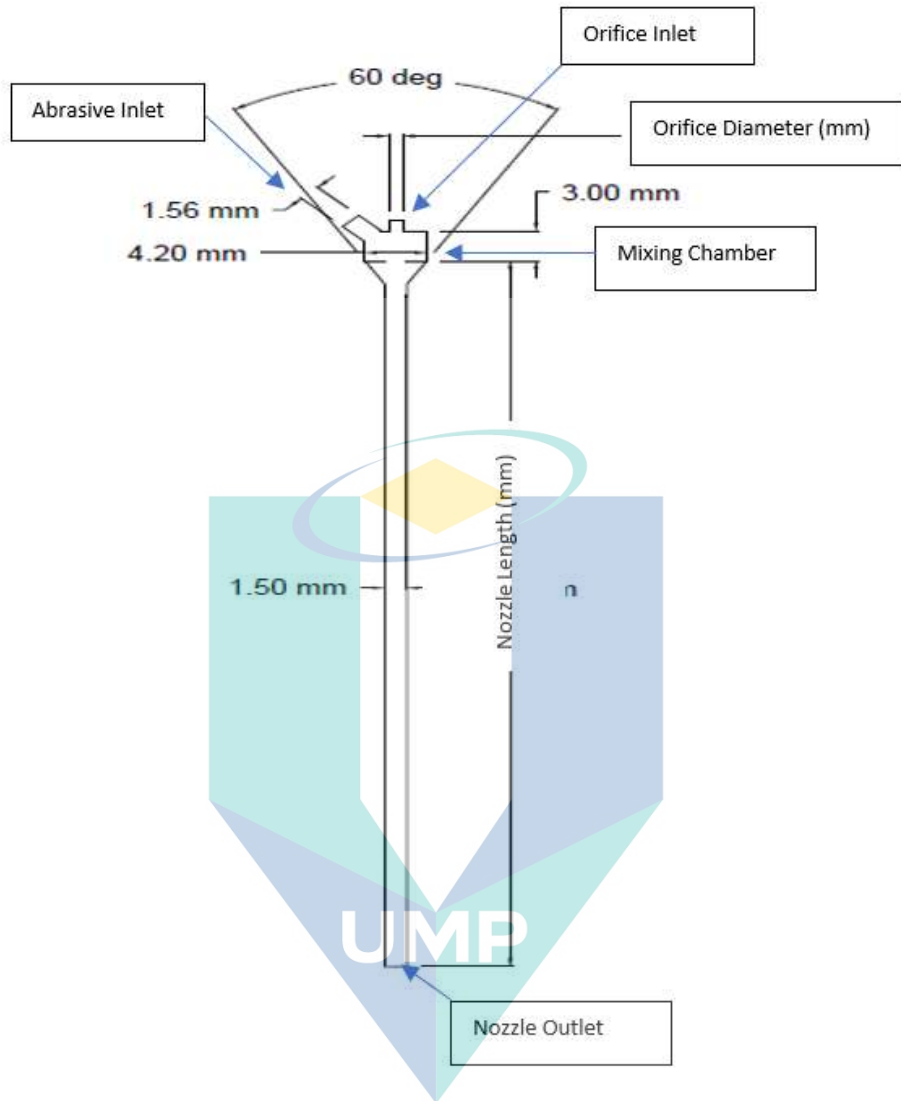


Figure 3.3 Designation values of dimensions applied to the nozzle geometrical model.

Table 3.1 Boundary Condition and Parameter Values

Parameters	Values Tested	Typical Values
Nozzle length, $L$ [mm]	32.5, 50.8, 76.2, 101.6	50.8
Nozzle diameter, $d_n$ [mm]	0.4, 0.5, 0.79, 1.14, 1.2, 1.4 1.63	1.14
Orifice diameter, $d_o$ [mm]	0.28, 0.33, 0.38 and 0.48	0.38
Water pressure, $P$ [MPa]	172, 241, 310, 359	310
Abrasive flow rate, $f$ [g/s]	1.9, 3.8, 5.7, 7.6, 9.5, 11.4	3.8

Table 3.2 Nozzle Material Properties

Material	Density, $\rho$ (kg/m <sup>3</sup> )	Specific Heat, $C_p$ (J/kg-k)	Thermal Conductivity, $\lambda$
Tungsten Carbide (WC/Co)	15680	39.8	100

Table 3.3 Abrasives Material Properties

Material	Density, $\rho$ (kg/m <sup>3</sup> )	Specific Heat, $C_p$ (J/kg-k)
Aluminium Oxide ( $Al_2O_3$ )	3950	880

Table 3.2 and Table 3.3 shows the nozzle and abrasives material properties respectively. Tungsten Carbide is the basic material used for AWJM nozzle and is widely used in the industry. Garnet is the common material used for the abrasives however Aluminium Oxide ( $Al_2O_3$ ) is the choice for accelerated wear test. This is due to its higher abrasiveness properties shortens the life of the nozzle which benefits in experimental time. The values of both material of the nozzle and abrasives were taken from multiple sources and were applied for the simulation (M Hashish, 1994; Ness & Zibbell, 1996).

The parameters used in Table 3.1, 3.2 and 3.3 are taken from studies done by Nanduri et. Al (2002). The same modelling parameters are applied so that the results can be compared to a valid experiment. The values tested by Nanduri et. Al (2002) are commonly used in the AWJM industry.

### 3.2.2 Assembly Meshing

After defining the geometric and boundary conditions for the base model of the simulation. In this simulation, three methods of meshing algorithm are chosen which is the Quadrilateral, Tetrahedron and Cut cell elements. This method is chosen mainly because it is the meshing methods that are featured in the current ANSYS FLUENT package for this study. Currently the study does not have access to other meshing methods would be to use other software package for assembly meshing during this study.

### 3.2.2.1 Quadrilateral Meshing

Figure 3.4 shows an overview of Quadrilateral meshing after being implemented to the model geometry. The characteristic of Quadrilateral cell shape is that it has a basic four sides and four edges (Benzley et al., 1995). A Quad based meshes are expected to provide higher quality solutions with fewer cells and nodes (Lewis, n.d.).

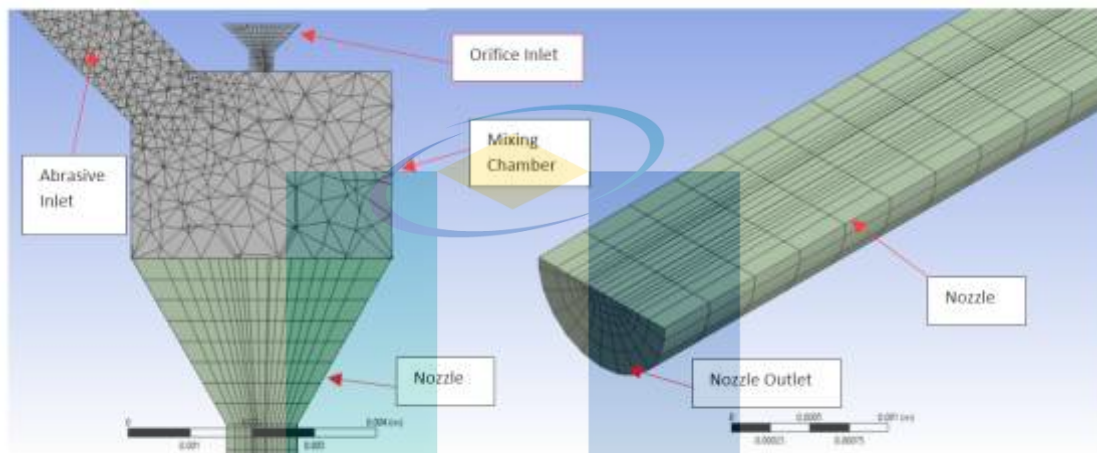


Figure 3.4 Quadrilateral assembly meshing model of AWJ nozzle.

### 3.2.2.2 Cut-Cell Meshing

As shown in Figure 3.5, the Cut-Cell meshing uses a bit fragmentation of volume patching meshing method where the surface meshing are analytically formed from the border zone mesh of volume avoiding the need required of manually geometry cleaning up or fragmentizing in where the cycle time requirement were reduced for meshing process (Benzley et al., 1995). It is very useful when the fluid flow is required to be meshed or fragmentized and assemblies of disarrayed domains of solids. The large hexagonal cells in the mesh allows for wide range of applications and complex algorithm (Benzley et al., 1995; Lewis, n.d.). The cons of Cut-cell meshing are that they are much more irregular than unstructured meshes such as Tetrahedral mesh. There are no grid smoothness at cut-cell therefore it will contribute to error during simulation (Benzley et al., 1995).

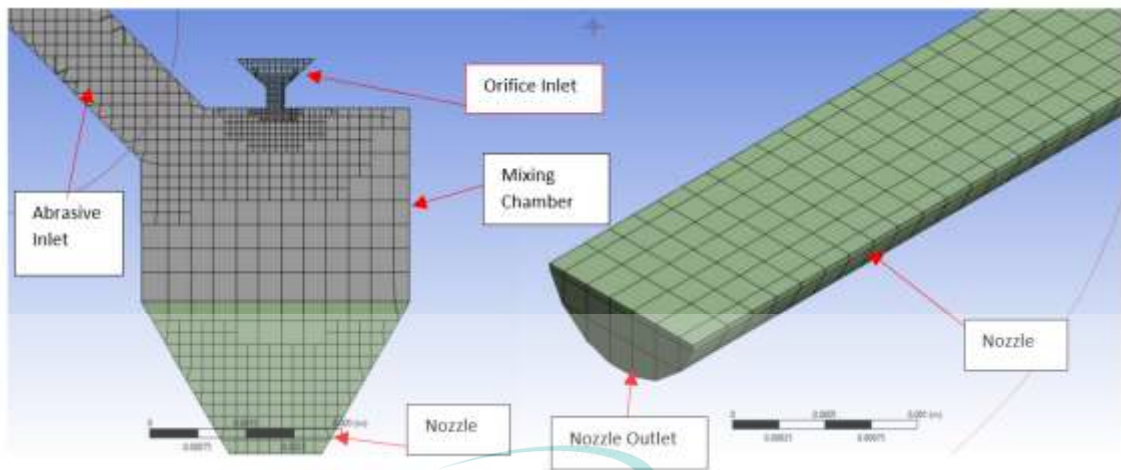


Figure 3.5 Cut-cell assembly meshing model of AWJ nozzle.

### 3.2.2.3 Tetrahedral Meshing

Figure 3.6 shows tetrahedral cell shaped consist of four vertices, six edges and is bounded by 4 triangular faces (Benzley et al., 1995; Edelsbrunner & Edelsbrunner, 2009; Lewis, n.d.). The Tetrahedral assembly meshing algorithm is a by-product related of the Cut-Cell algorithm which shares similar trades in pros and cons to those of Cut-Cell (Benzley et al., 1995; Lewis, n.d.).

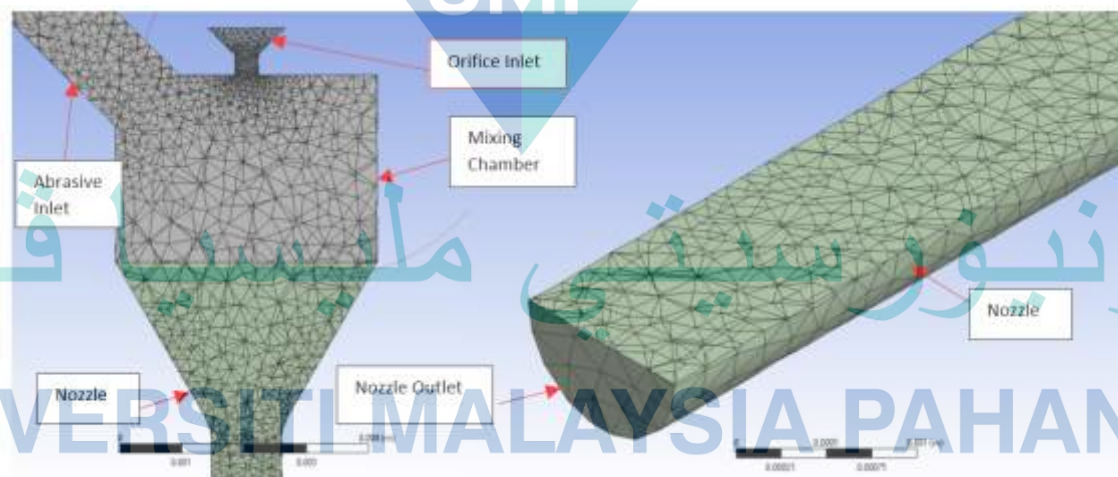


Figure 3.6 Tetrahedral assembly meshing model of AWJ nozzle.

Conversely, tetrahedral mesh are widely known for drastic simplification of 2D surface meshes while maintaining a very good accuracy as compared in 3D meshes (Cignoni, Constanza, Montani, Rocchini, & Scopigno, 2000).

### 3.3 Solution Procedure

The next process is to setup the solver, fluid material properties, flow physics model and boundary conditions required to run the simulation. A considerable understanding of the underlying principles to produce the ideal model is essential which have been laid out in the previous chapter. The solver will transfer the information of the defined fluid domain and labelled boundary from the previous meshed model.

#### 3.3.1 Solvers

The pressure-based solvers were chosen as the model takes momentum and pressure as the primary variables. It is applicable for a wide range of flow regimes and primarily in multiphase flow problems. The implicit solution approach is taken as the simulation need to be limited to a duration of time. The standard interpolation scheme is used for face pressure as the flows are expected to have swirling flows with considerable pressure gradients in the fluid domain. As pressure-based solver was used, the pressure-velocity couplings are apparent. The pressure-pressure coupling refers to the numerical algorithm which uses a combination continuity (Equation 2.12) and momentum equations (Equation 2.13 and 2.14) to derive an equation for pressure. Semi-Implicit Method for Pressure Linked Equations (SIMPLE) scheme algorithms were applied as it is robust and is expected to work well with the current model. The pressure-based solvers were used because the process condition are based on flow which are produced through the differences of flow. Enabling this function allows the manipulation of pressure condition on the point selected in the 3-D model.

#### 3.3.2 Turbulence Modelling

Turbulence modelling is required for modelling the complex multiphase flow of water, air and abrasives. The main tool used in approaching turbulence model is the Reynolds-Averaged Navier Stokes (RANS) model. As explained in the previous chapter in Equation 2.15. Under the RANS based model, the two-equations models which is the Standard  $k-\varepsilon$  (Equation 2.16 and 2.17) and Realizable  $k-\varepsilon$  (Equation 2.18 and 2.19) is to be used.

There are two ways that the realizable  $k-\varepsilon$  model differs from the standard  $k-\varepsilon$  model. Firstly it contains the turbulent viscosity,  $C\mu$ , formula where it is not a constant

like in the standard model but is a variable (Blazek, 2015; Guide, 2016). The second difference is the transport equation for the dissipation rate,  $\varepsilon$ , that is derived from an exact equation for the transport of the mean-square vorticity fluctuation (Blazek, 2015; Guide, 2016).

Therefore, it is thought to give improved predictions for the spreading rate of jets, a superior ability to capture the mean flow of complex structures and for flows involving rotation, boundary layers under strong adverse pressure gradients, separation and recirculation (Blazek, 2015; Guide, 2016). The other reasons were that the turbulence model enables the wall function which are important to define the boundary conditions (Blazek, 2015; Guide, 2016).

The simulations were run using the mentioned turbulence model and the most accurate method was chosen. For turbulence near the wall, the standard wall function is chosen. The inlet boundary conditions are specified using the Turbulence intensity and hydraulic diameter because the models are based on internal flows.

The simulations were done for three different cases in term of the build of meshing which are quadrilateral, cut cell and tetrahedral. Previous studies of erosion modelling commonly used the Tetrahedral elements as the method for meshing (Baisheng et al., 2011; Deepak et al., 2012; Junkar et al., 2006; Kamarudin, Rao, & Azhari, 2016; Lebar & Junkar, 2004; Mostofa et al., 2010). This is due to the common knowledge that tetrahedral elements provides finer mesh, better accuracy and efficiency for three-dimensional meshes as compared to quadrilateral elements which are prevalent in two-dimensional meshes (Benzley et al., 1995). It is important to choose the assembly meshing methods as it has compelling causes that affect the merging profile of finite element methods that is composed of the materials geometrical shape, distortion of elements, elements of polynomial order, polynomial functions of solutions, methods of integration and incompressibility of fluid (Brauer, 1993; Taylor & Zienkiewicz, 1989). However, triangular elements that have higher level of arrangement assumptions can produce comprehensible results and convergence profile (Benzley et al., 1995). In another observation, mesh locking due to material incompressibility can become a critical setbacks of triangular elements (Hughes, 1987).

### 3.3.3 Material Properties

The material properties need to be defined for the all solids and fluids to be simulated. The values that are specified in Table 3.2 and Table 3.3 were inputted to the software. The materials are either already defined in the FLUENT database or defined by the user using User Defined Function (UDF).

### 3.3.4 Cell Zones and Boundary Conditions

The boundary conditions have been stated in Figure 3.2 where the boundary conditions are consisting of the orifice inlet, nozzle wall, abrasive inlet and nozzle outlet. The material in the cell zone must be declared in which all the zones are defined as the fluid domain except for the nozzle wall which is solid. The material for solid zone for this case should be Tungsten Carbide Cobalt (WC-Co). The motion for solid zone is defined as reflect. Pressure inlet boundary conditions was set for the inlet at the orifice, while pressure outlet boundary conditions were used for the outlet at the nozzle. The abrasives inlet is programmed from the DPM by selecting the face of the abrasives inlet to become the injection point. The data for the pressure inlet is based on the water pressure as listed in Table 3.1

## 3.4 Validation Methods

The simulation was validated through several ways;

- a) Comparing the theoretical waterjet velocity with the velocity produced in the simulation (Mostofa et al., 2010).
- b) Comparing the erosion profiles of the worn-out sample of AWJM nozzles with the erosion profiles from the simulation (Nanduri et al., 1996).
- c) Comparing the erosion rate accuracy of the experimental result with the simulation (Nanduri et al., 1996).

## CHAPTER 4

### RESULTS AND DISCUSSION

#### 4.1 Modelling of Fluid Flow

The validation of the fluid flow model was conducted by first completing Equation 2.7 solved for the inlet pressure of water at the set value of 470 MPa and obtain the following values of theoretical velocity and jet velocity where  $V_{th}$  was approximately 970 m/s,  $V_j$  was obtained at 934 m/s and the value of  $\varphi$  is 0.96. The values gotten from the mention equations are then used to solve equation 2.5 and  $V_j$  and the value of 791 m/s was obtained. The simulation was ran and the similar results were observed for the velocity contour monitored along the  $x$  axis and the maximum velocity monitored at orifice as shown in Figure 4.1. The chart was composed of two parts which is the waterjet velocity domain where the mixing chamber is set at 3 mm in length. The second part was from 3 mm to 54 mm where the trend continues onto the nozzle section. It can be observed that the start of the flow, the velocity of the water was around 790 m/s and 800 m/s. This value is not far from the values calculated from the theory therefore it can be concluded that the model are validated.

The waterjet velocity was observed to fell at the inlet when it is entering the mixing chamber. It was assumed that the higher diameter of the mixing chambers geometry affects the velocity and causes it to drop. In the mixing chamber, the abrasives are mixed together with stream of waterjet. Going further into the length of the nozzle, it can be observed that the waterjet velocity was beginning to increase. Proceeds on to the next section, the monitoring shows that the waterjet velocity remained constant and then gradually dropping velocity until it finally exits the nozzle outlet at around 370 m/s to 400 m/s. This further shows that the models have the similar results of velocity distribution as to were other models simulated in other similar studies (Deepak et al., 2012; Mostofa et al., 2010).

Figure 4.2 shows projectile trajectory of the different flow of abrasives, water and air in blending cell of the AWJ nozzle. In this simulation the  $K-\epsilon$  turbulence model was generated to simulate the turbulence of different phases of abrasive, water and air.

This is where the water is categorized as the multiphase flow whereas the abrasives and air are categorized as the dispersed phase. The intensity of the turbulence are acquired using equation 2.9 and the calculation sample can be referred in Appendix B. It can be observed that the rise of intensity of the turbulence affects the turbulence between the different phases in distinct ways. When water was released from the orifice, he scream created a very powerful vacuum thus attracting the air and abrasives back to the inlet of the nozzle. The oscillations fuse the different phases of water, air and abrasives and entrained into the stream of waterjet. As the waterjet released from the orifice at high velocity, the air and abrasives were drawn into closer to the inlet of the orifice before getting entrained with the flow of waterjet. Powell (2009) also describes the same phenomenon when there are introduction of high pressure and low-pressure creating vortex. This is further validated by the simulation done by Mostofa et al. (2010) which have the same similar results. The phenomenon was explained that the waterjet created a vortex at the outlet of the orifice that attracts the abrasive, air and other particles into the AWJ nozzle tube. The dragging or entrainment of the particles have factors to do with the shape factor. The geometrical shapes of the particles are defined in its shape's irregularity whereby the shape factor of 1.0 were to state that the particle was round and circular in geometry. Decreasing the shape factor value states that the geometry of the particle is set to be irregular. In further simulation, the typical parameter was set to 80 and around 0.1 mm in diameter for particle mesh size. Whereas the abrasives particle geometry was set to be round for the simplification of the simulation.

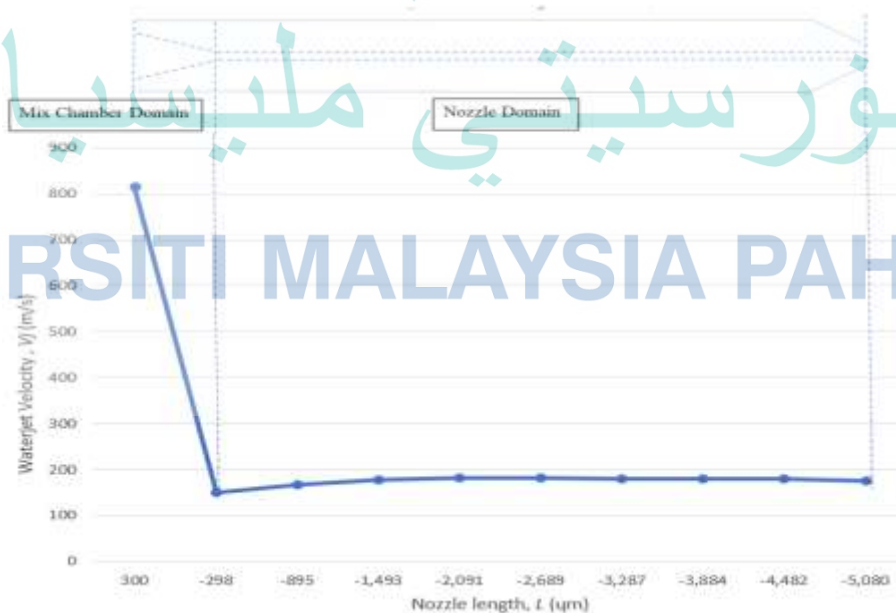


Figure 4.1 Waterjet velocity variations along the cutting head

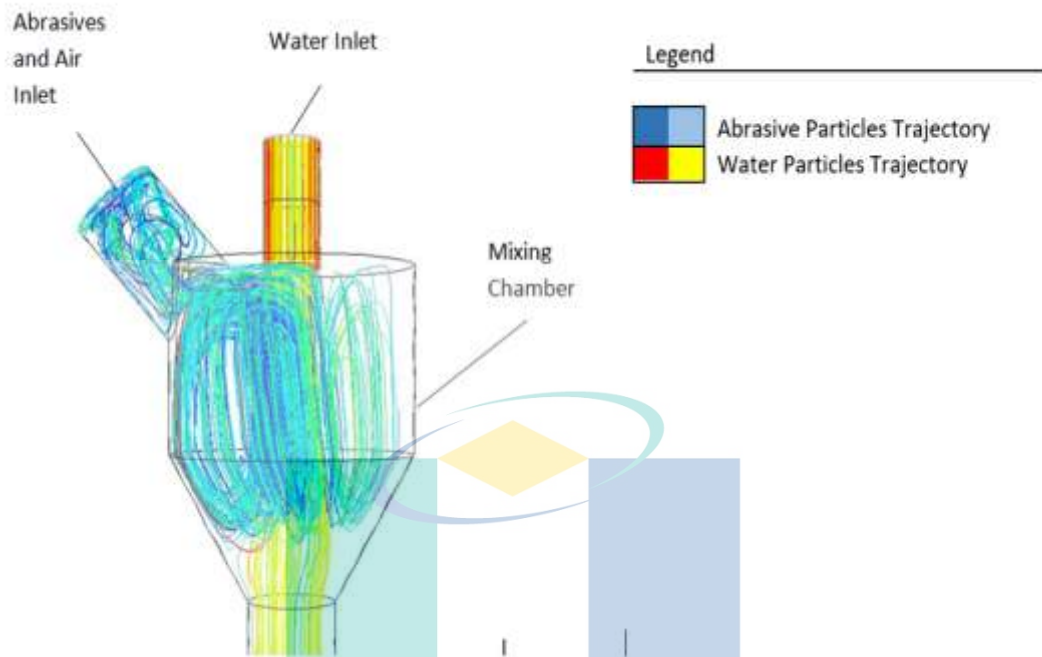


Figure 4.2 Air and abrasives interacting with the water in the mixing chamber simulation.

Figure 4.3 is the contour of erosion rate produced from the simulation. It basically shows the erosion contour throughout the nozzle. From the observation it can be found that there are high concentration of particle impingement activity at the nozzle inlet tube or the beginning of the fusing chamber. The contour of erosion shows pattern of degradation along the nozzle wall which is consistent with the findings by other studies (Mostofa et al., 2010). As was shown in Figure 4.4, the high amount of erosion at the inlet of the nozzle are largely because of the high turbulence. Vortex were created in the mentioned section and the fusion of different phases of liquids and solids causes more activities of degradation. Abrasives particle moved into the inlet and throughout the nozzle, the particles were impacting the nozzle wall and bounced on multiple sections. This bouncing and deflection trends throughout the surface of the nozzle wall thus causes the erosion profile to the indication of wavy patterns which were consistent with past studies (Nanduri et al., 1996).

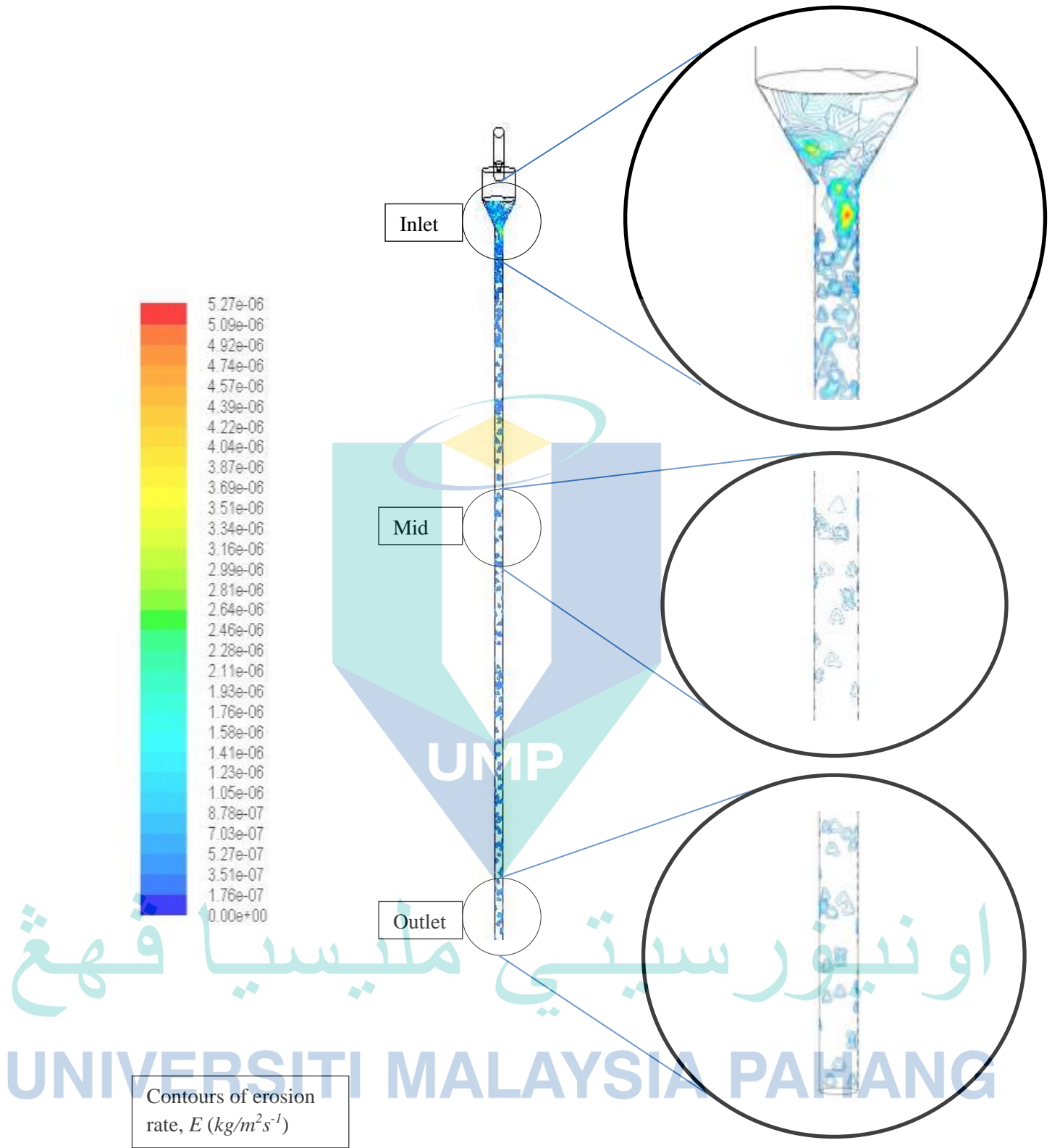


Figure 4.3 Contours of erosion along the nozzle.

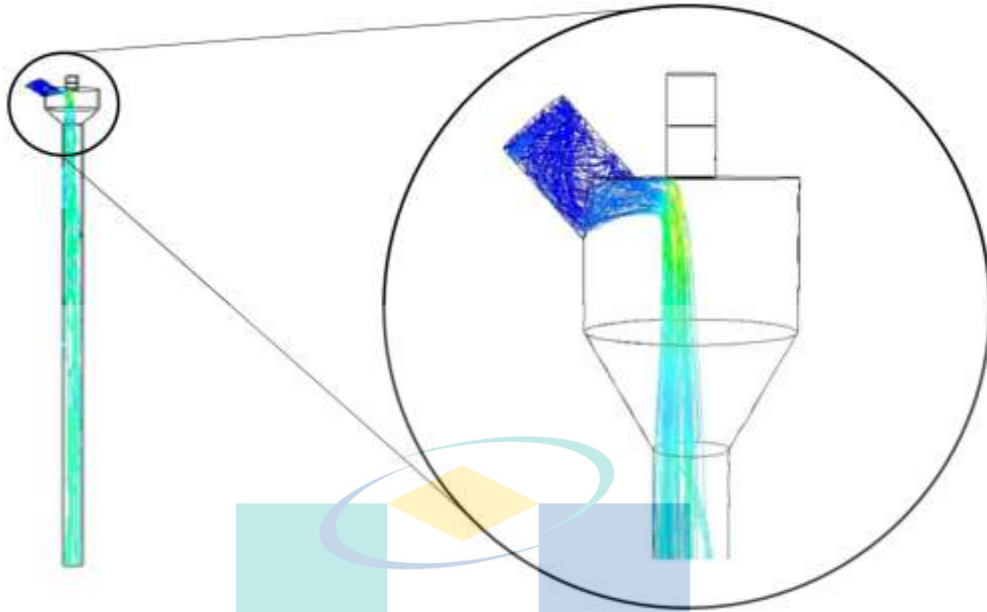


Figure 4.4 Waterjet abrasives particle tracking

The actual and the predicted erosion wear are presented by showing the maximum erosion rate. In all cases, the actual nozzle wear was obtained from the empirical model provided by Nanduri et al. (2002) which held accurate presentation of predicted erosion wear rate on specific system and geometric parameters. The empirical model were further tested and validated by other researchers for predicting nozzle wear (Mostofa et al., 2010; V. N. Pi & Tuan, 2009).

#### 4.2 Assembly Meshing Methods

Table 4.1 shows the maximum value of the size, nodes and number of elements which the ANSYS software allows on meshing of the nozzle model according the mesh methods. Inputting finer values of size were declined and it will be automatically adjusted as the software have its own size ratio to follow. The table also shows the processing in which the Quadrilateral mesh methods have the fastest processing time followed by Cut cell and Tetrahedral assembly meshing. It is predicted that the tetrahedral have the highest processing time as it has almost triple the number of elements compared to Cut-cell and Quadrilateral.

Table 4.1 Comparison of Different Assembly Meshing Method

Assembly Methods	Quadrilateral	Cut cell	Tetrahedral
Min Size	3.03E-05	4.69E-05	4.69E-05
Max Face Size	3.03E-03	6.07E-03	6.07E-03
Nodes	22205	26037	20416
Elements	30482	23682	95680
Processing time	3 Days	3 – 4 Days	7 Days
Convergence	Converged Well	Converged well however shows error in some runs	Converged well however shows error in some runs
Under Relaxation Factor	None	Minimal	High

The residuals monitoring to evaluate the convergence quality is shown in Appendix C. For this case which involves turbulence quantities, the residuals are acceptable as the scaled residuals starts low, increase as non-linear sources build up, and eventually decrease (Guide, 2016). Therefore, it can be ensured that the simulations were converged. The simulations were also ran in 70 iterations for every time steps which is more from the suggested iterations which is 50 (Guide, 2016). Errors in producing the residuals monitoring to show convergence were prevalent in Tetrahedral and Cut-cell elements as the complex triangular elements will leads to a stress quantity that continually increases, thus, error encountered as the load transfer concentrates in the geometry at a sharp corner (Sinclair, Beisheim, & Sezer, 2006). To decrease the errors, Under-Relaxation Factor (URF) were applied to stabilize calculations by limiting the rate of change of both fields and equations which will keep the stress quantity to a limit. The errors in this context is when the results failed to show any data after running the simulation.

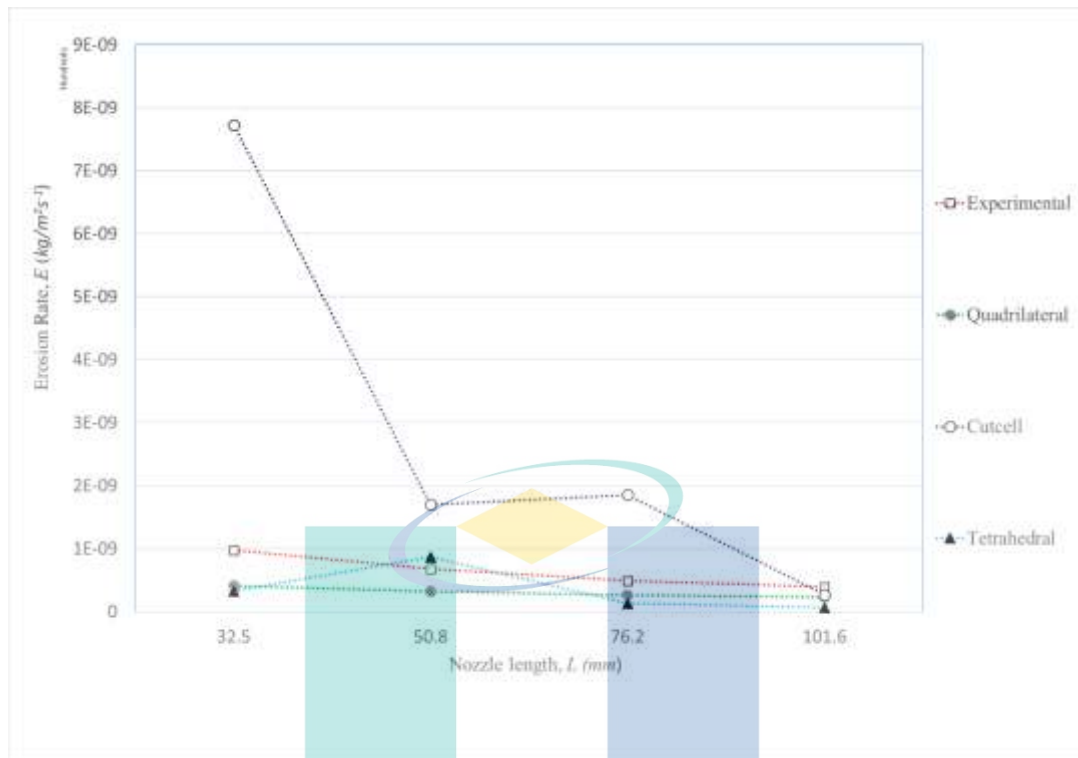


Figure 4.5 Effect of nozzle length on erosion wear for different mesh assembly.

As shown in Figure 4.5, the quadrilateral meshing shows the closest accuracy with the experimental result methods. This is followed by tetrahedral with a minor accuracy difference between quadrilateral mesh. In contrast, cut cell assembly has the biggest differences in comparison with the result in comparison with the others.

Table 4.2 Comparison of Erosion Rates and Nozzle Length in Different Assembly Meshing Methods

Experimental model		Quadrilateral		Cut cell		Tetrahedral	
Nozzle length, L (mm)	Erosion Rate, E (kg/m²s⁻¹)	Erosion rate, E (kg/m²s⁻¹)	Error (Unitless)	Erosion rate, E (kg/m²s⁻¹)	Error (Unitless)	Erosion rate, E (kg/m²s⁻¹)	Error (Unitless)
32.5	9.723E-08	4.078E-08	-5.645E-08	7.722E-07	6.750E-07	3.261E-08	-6.462E-08
50.8	6.802E-08	3.180E-08	-3.622E-08	1.701E-07	1.021E-07	8.670E-08	1.868E-08
76.2	4.918E-08	2.621E-08	-2.297E-08	1.854E-07	1.362E-07	1.290E-08	-3.628E-08
101.6	3.907E-08	2.315E-08	-1.591E-08	2.676E-08	-1.231E-08	6.588E-09	-3.248E-08

Table 4.2 shows the comparison of erosion rate at different nozzle length for different assembly meshing methods. It is also shown that quadrilateral meshing has a consistent trend with the actual erosion rate in which in general the erosion rate declines as the length of the nozzle increases. The tetrahedral assembly has a considerable accuracy for the shortest nozzle length of 32.5 mm. The erosion wear rate however had increased when nozzle length was increased to 50.8 mm. The erosion rate reduced again as the length increases.

Whereas for cut cell mesh assembly, a contrasting value were shown when the nozzle length is at 32.5 mm. In term of the effect of the nozzle length in results accuracy as compared to the experimentation. It can be said that the quadrilateral assembly meshing shows the most consistent trend of erosion rate.

The geometries of the model simulation can be categorized as a flow-aligned geometry. The higher quality solutions provided by the quad based assembly is due to the fewer cells and nodes than the tetrahedral based assembly. The quad based meshes shows reduced numerical diffusion when the mesh is aligned with the flow. In term of generating the quad based mesh, it does take more effort to generate the mesh the cut-cell based meshing. However, it still does take lesser time than the comparable tetrahedral meshing. The findings are further supported by Yongjie Zhang, Bajaj, & Xu (2009) in their approach in improving geometric flow using different meshes. It was found that the quadrilateral meshing improves the quality of the geometric flow which works well with the current simulation. In another finding, it was found that it would be impractical to generate quadrilateral mesh for complex geometries. Meshing are quicker to generate by using the tetrahedral mesh instead. Another type of meshing which is the hybrid meshing can combine the tetrahedral elements with other elements in selected region. It may be used in the conical the cylindrical region of the nozzle which have a wedge characteristic which can beneficial in improving the mesh.

Out of the three methods, the Quadrilateral mesh showed promising results in term of processing time, convergence quality and erosion rate accuracy followed by cut-cell and tetrahedrons mesh, respectively. The cut-cell and tetrahedrons methods require significant processing time that will cause divergence and ultimately, repetitions of simulations. Adjusting the URF will also affect the accuracy of the calculation.

Therefore, the Quadrilateral mesh method were chosen to for the proceeding simulations.

In Figure 4.6, the contours of the erosion rate for the three mesh methods shown for nozzle with the length of 32.5 mm. The level of erosion was set to 50 to enhance the contours pattern. It is observed that there are obvious differences in pattern erosion along the nozzle. The common pattern of erosion for all three-mesh method is that there are extensive erosion at the inlet and the erosion were beginning to decline as it reaches the outlet. These patterns are irregular and are expected as to compare with worn out experimental nozzles. However, there are differences in the case if the tetrahedral mesh as compared to other mesh methods which are there are less erosion activity at the inlet especially at the focusing area and also slight increase of erosion activity towards the end of the outlet. Cignoni, Constanza, Montani, Rocchini, & Scopigno (2000) suggested that there is a certain amount of value data set for it to maintain geometrical or topological shape and the information encoded in an attached scalar field. There are also techniques proposed by introducing modification to the domain and the approximation of the field of the original volume dataset. This can be achieved by adjusting the elements numbers and sizes in the assembly methods as shown in Table 4.1.

It is proposed that a new error function should be devised by considering the 2D mesh and introducing an original heuristic. It is assumed that the proposed changes especially by reducing mesh size and increasing mesh volume will improve accuracy (Cignoni et al., 2000). However, this will further increase processing time and less chances for it to converge. It is further found that the problem of accurate simplification of tetrahedral mesh is more difficult than simplification of standard 3D surfaces. For certain meshes, obtaining high simplification rates that will introduce a low or negligible error is a very complicated task, even if a slow but accurate error criterion is adopted (Cignoni et al., 2000).

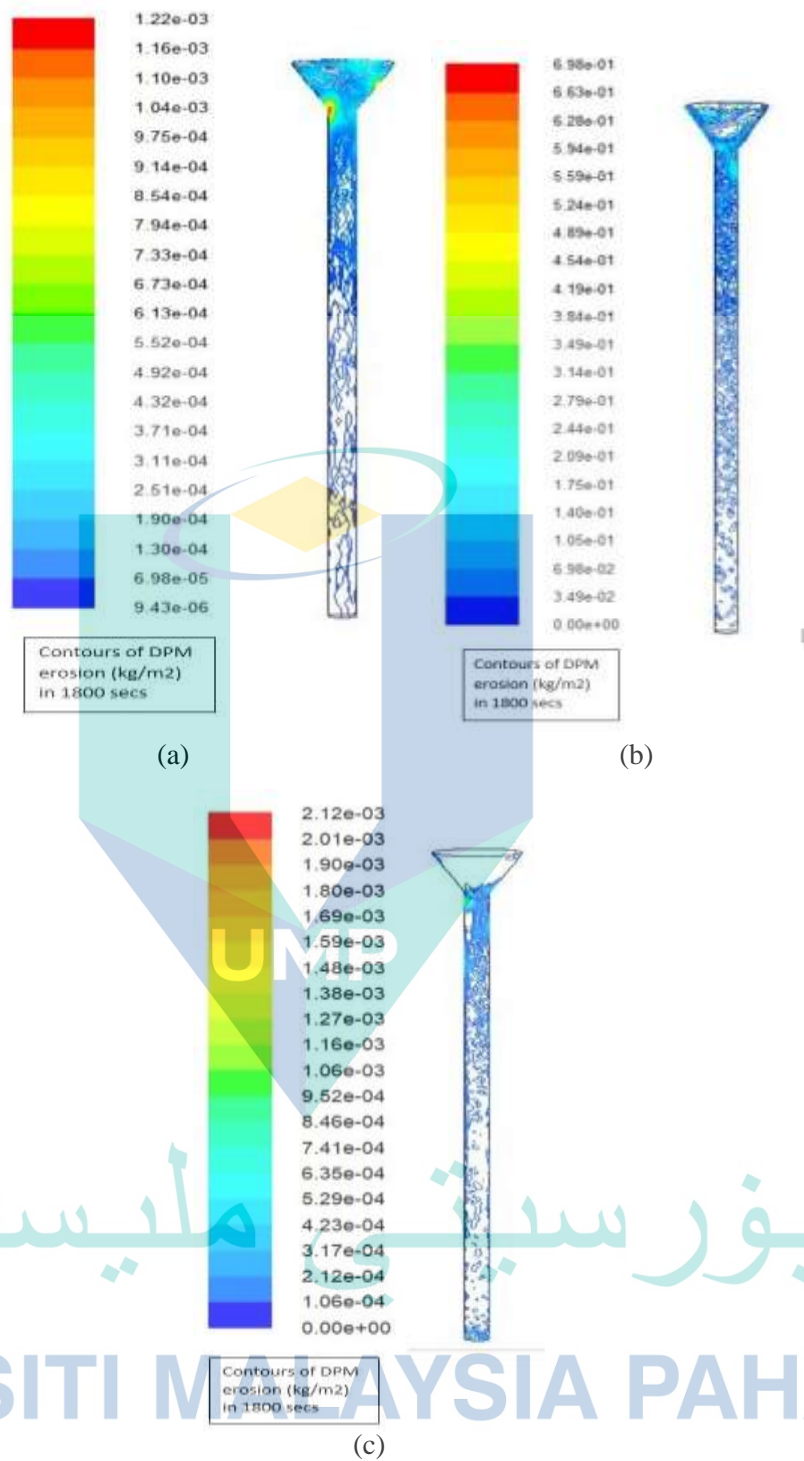


Figure 4.6 Contours of discrete phase method (DPM) erosion for different meshing methods (a) Quadrilateral mesh (b) Cut-cell mesh (c) Tetrahedral mesh

A closer look on Figure 4.6 reveals different pattern of erosion. For the Quadrilateral Mesh, the patterns appeared lacerated whereby the length of lacerations is shorter at the inlet area. As the distance progresses, the lacerations appear to be longer in size. As for Cut-cell mesh model, the shapes are appeared to be in smaller, rounder and in dots. The quantities are higher at the beginning of the inlet and decreases in numbers as it progresses to the outlet. Different patterns were also shown in the Tetrahedral meshing where it was found that there is no erosion activity at the top areas of the inlet which is unlike the first two mentioned modelling methods. The patterns beginning to emerge at the end of the slope whereby the patterns are similar as of that of Cut-cell modelling. As it progresses, the erosion pattern began to show less activities as compared to the other models.

Reviewing to the actual erosion patterns, it can be assumed that the erosion pattern is more similar to the Quadrilateral meshing as compared to the other mesh model methods. The patterns supposed to appear wavy and as comparing it to the bore profile, there are highest in in their similarities of producing erosion shapes and patterns to the nozzle.

### 4.3 Turbulence Modelling

Figure 4.7 represents the effect of nozzle length on erosion rate for different turbulence model. There are two turbulence model that were tested which are the standard and realizable turbulence model. The standard  $k-\epsilon$  model is to be expected to be robust and accurate. From the figure mentioned, the model shows irregular values that is against the desired trend. While the realizable  $k-\epsilon$  model shows promising trend with the experimental erosion rate. However, the accuracy in Table 4.3 shows values of between 53% to 47% as compared to the Standard  $k-\epsilon$  model which is between 33% to 63%. The inaccuracy is maybe due to limitations that Standard  $k-\epsilon$  model commonly known to performs poorly for flows with strong separation, large streamline curvature and significant pressure gradient (Kim & Boysan, 1999).

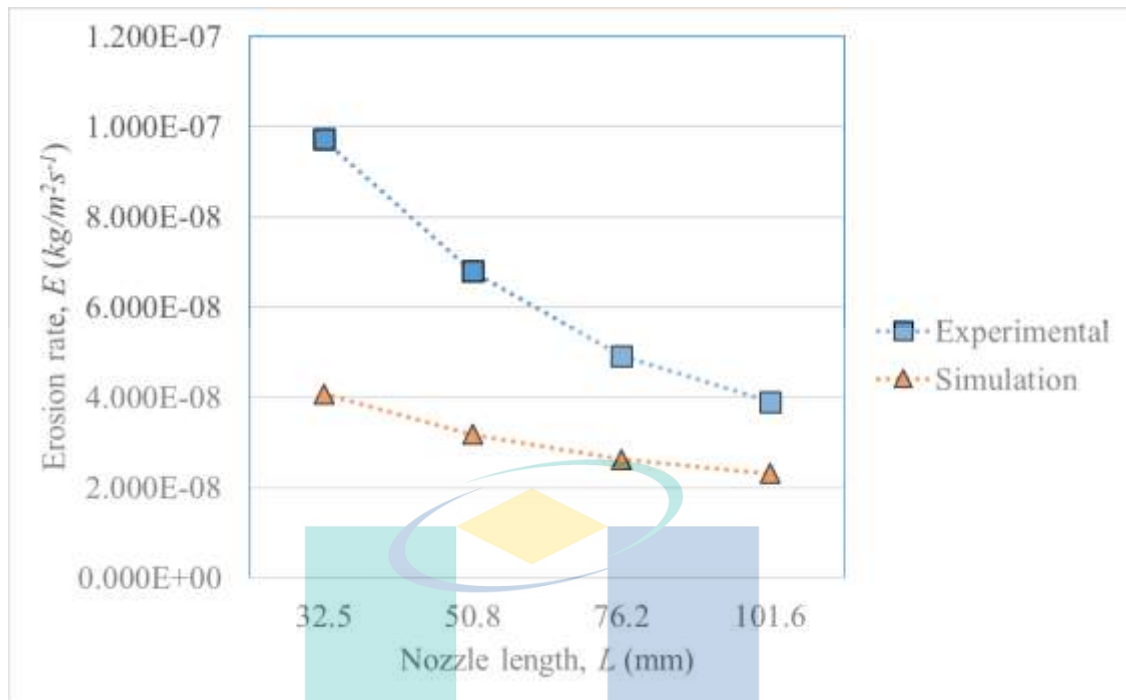


Figure 4.7 Effect of nozzle length on erosion rate for different turbulence modelling

Table 4.3 Comparison of Erosion Rate and Nozzle Length for Different Turbulence Models

Experimental model		Realizable		Standard	
Nozzle length, L (mm)	Erosion Rate, E (kg/m²s-1)	Erosion Rate, E (kg/m²s-1)	Error (Unitless)	Erosion Rate, E (kg/m²s-1)	Error (Unitless)
50.8	6.802E-08	3.180E-08	-3.622E-08	2.521E-08	-4.281E-08
76.2	4.918E-08	2.621E-08	-2.297E-08	2.173E-08	-2.745E-08
101.6	3.907E-08	2.315E-08	-1.592E-08	2.617E-08	-1.290E-08

The realizable  $k-\varepsilon$  model is mainly chosen for turbulent flows as the model satisfies certain mathematical constraints on the Reynold's stresses. The benefits of using the model is that it will likely provide superior performance for flows involving rotation, boundary layers under strong adverse pressure gradients and recirculation in which meets with the traits/characteristics of the multiphase interaction of the simulation model.

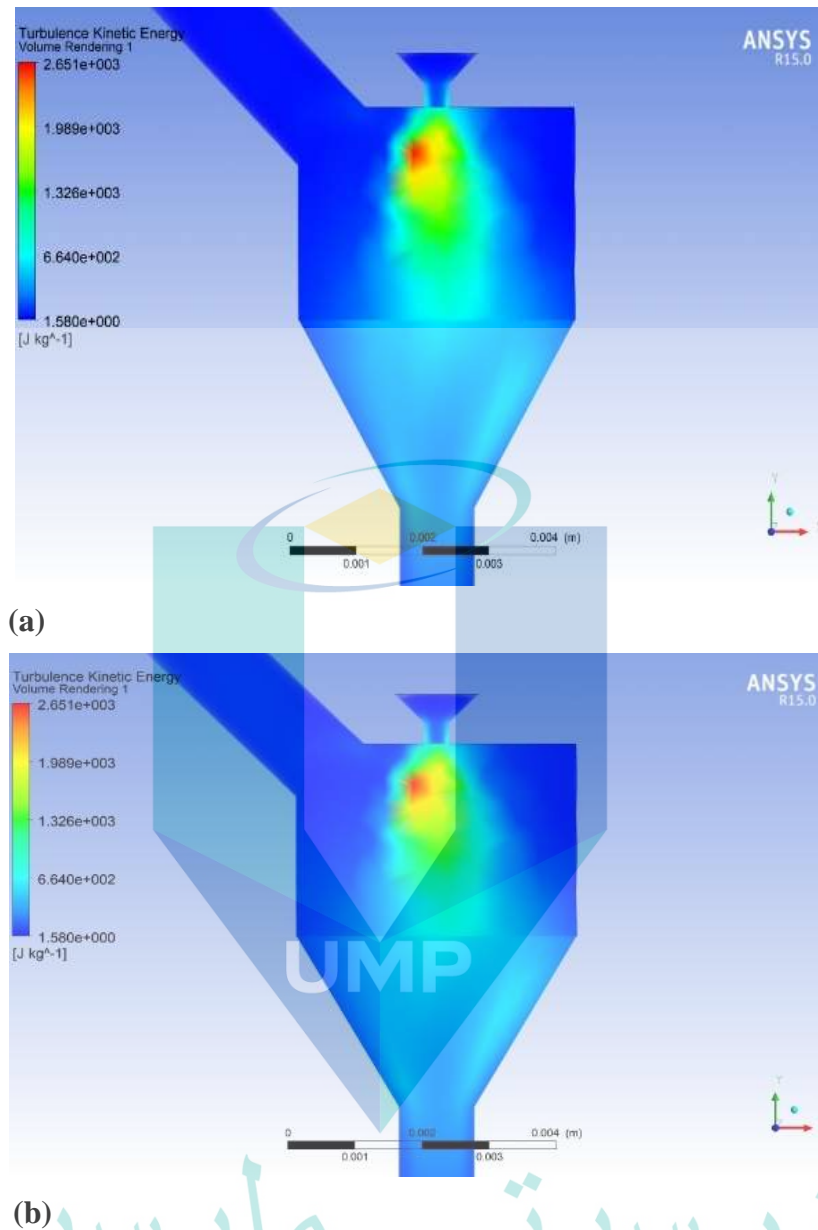


Figure 4.8 (a) Realizable  $k-\varepsilon$  volume model of turbulent kinetic energy and (b) Standard  $k-\varepsilon$  volume modelling of turbulent kinetic energy.

Figure 4.8 (a) and (b) shows the volume rendering of turbulent kinetic energy for realizable  $k-\varepsilon$  and standard  $k-\varepsilon$  respectively. There is not much difference in pattern between the two. Application of an appropriate CFD solver to simulate and model the flow process is thus appealing. It was stated that whether existing CFD based analysis could capture adequately the supersonic and compressible flow features of these jets was of concern (Y. Li, Kirkpatrick, Mitchell, & Willson, 2004). The results obtained from the turbulence kinetic energy shows an expanded contour which were similar from past conducted study (Y. Li et al., 2004).

#### 4.4 Erosion Profile

Figure 4.9 shows the erosion profile of worn-out nozzle that collected by measuring the value of the new inner diameter along the length of the nozzle. The nozzles were obtained from the industry were made of WC/Co with length of 76.2 mm and initial diameter of the bore was 0.76 mm. The worn-out nozzles were cut vertically using EDM wire cut (Sodick VZ300L) with wire diameter of 0.2 mm, wire speed (WS) of 80 mm/min and servo speed (SF) of 8 mm/min. The diameters of the bore were taken using optical video measuring system (Econ) for every 1mm. The data from the graph profile then are compared with the simulated results.

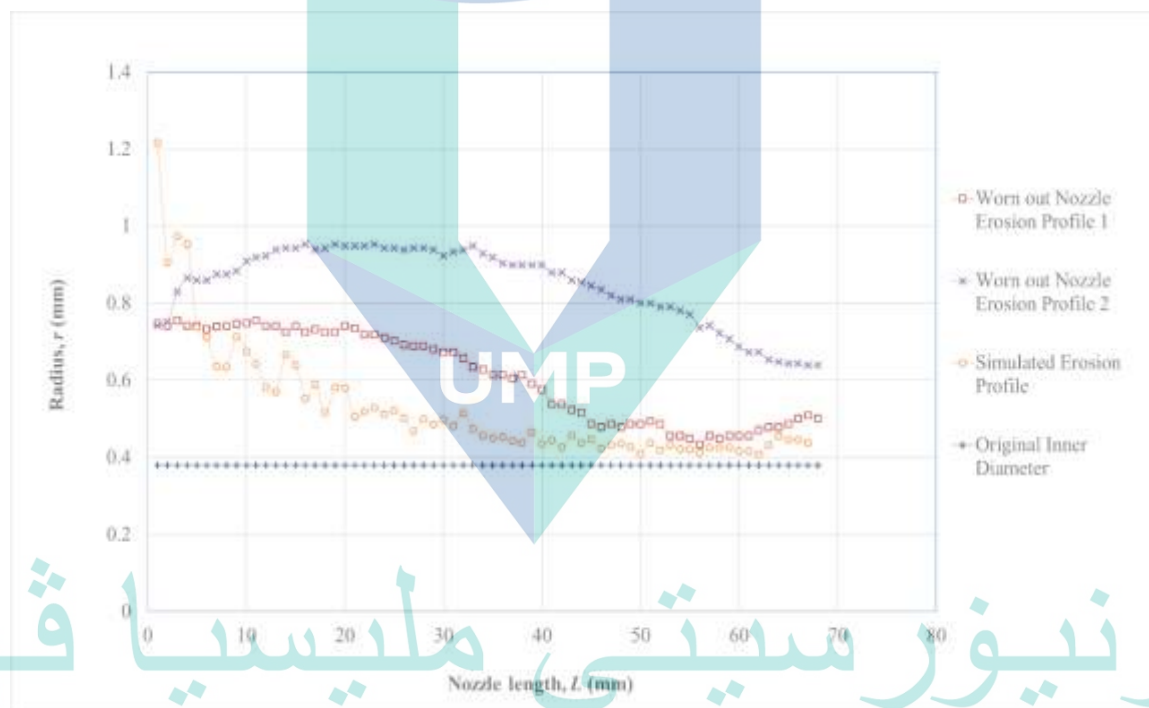


Figure 4.9 Erosion profile of worn out nozzles and average erosion profile of simulated nozzle erosion.

It can be observed from Figure 4.10 the erosion profile of two samples of worn out nozzle as well as one from the simulation. The nozzles have actual length of 76.2 mm which were then cut off at the inlet leaving only the straight profile of the nozzle which have total length of 67 mm. The graph takes the radius of the eroded nozzle in which the original radius of the nozzle was 0.38 mm.

The inlet section of the nozzle shows a comparable erosion profile between the worn-out nozzle and the simulation. Along the length, the simulation shows a similar trend with one of the samples; the sample had a low erosion rate at the outlet section of the nozzle before increasing linearly as it reached the exit. Apart from that, the simulation and the sample had no significant changes to their erosion profiles at the middle towards the end length of the nozzle. The other sample on the other hand showed a higher erosion rate at the middle section of the nozzle before decreasing steadily towards the outlet.

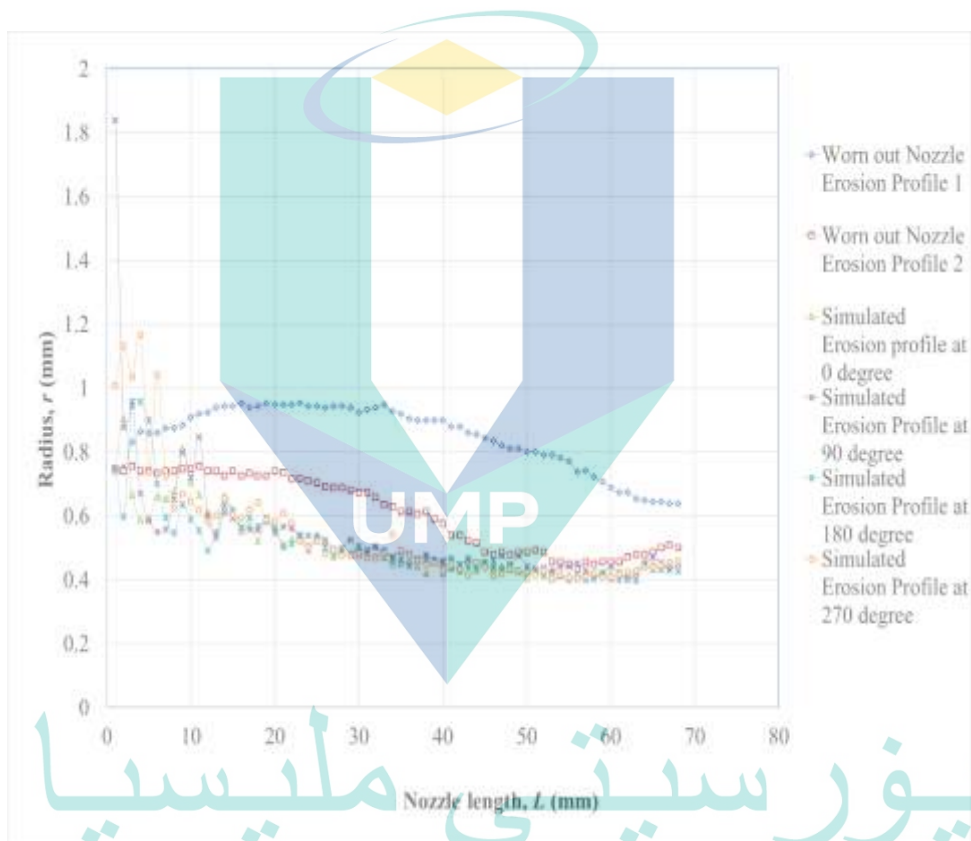


Figure 4.10 Erosion profile of worn out nozzles and erosion profile of simulated nozzle erosion at different angle of rotation.

In Figure 4.11, the diameter profile of the exit AWJM nozzle were taken. From the observation, Figure 4.11 (a) reflects the diameter profile of the new nozzle. Next, Figure 4.11 (b) demonstrate a severe erosion at one end of the outlet. Another erosion profile as shown in Figure 4.11 (c) had a significantly different pattern of erosion. Instead of following its counterpart, the profile shows an almost uniform erosion at most orientation of the nozzle.

This gave assumptions that the patterns of erosion can be very different depending on unknown factors implemented in the industry. A highly dynamic process influenced the factors that can affect the AWJM nozzle wear (M Hashish, 1994b; Madhusarathi Nanduri et al., 2002). Another explainable factor that contributes to this discrepancy is due to the turbulence flow that is unsteady and irregular. It is observable in Figure 4.3 that the erosion pattern produced is erratic in nature yet conform to the wavy pattern. Therefore, it expected that there are non-uniform erosion profile along the length of the nozzle.

The study then move on to the erosion profile at different angle of rotation as shown in Figure 4.12. Different from the last results, the different angle of the wall was observed as the simulation are simulated in three-dimensional model. Similar trend and accuracy as compared to the last perimeter, however, there are some deviations at the inlet where there is large activity of erosion at 180-degree and 270-degree angle.

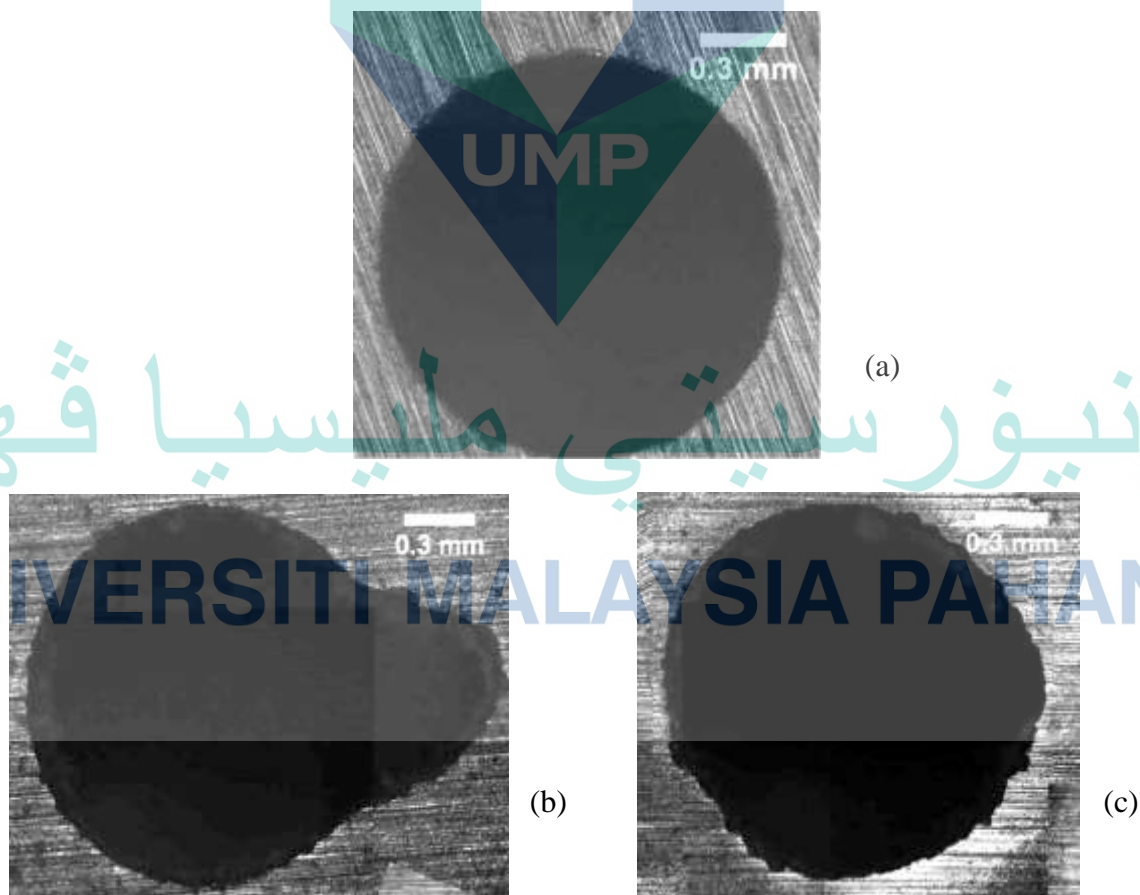


Figure 4.11 Exit diameter profile of AWJ nozzles where (a) New nozzle (b) Worn out nozzle erosion profile 1 (c) Worn out nozzle erosion profile 2.

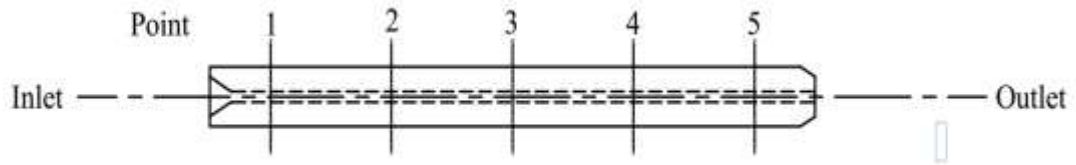


Figure 4.12 Points of section taken for inner diameter erosion profile.

Figure 4.12 shows a nozzle with 76.2 mm length with inner diameter and outer diameter of 0.79 mm and 6.3 mm respectively. The nozzle were divided into 5 sections to observe the changes of the inner diameter caused by erosion throughout the length of the nozzle. At the opening of the inlet, there are noticeable amount of erosion activity. The profile of the erosion is not constant throughout the angle where there are extreme erosion activity especially at the 90 degrees section of the nozzle. It then bounded to the 250 – 210 degrees section of the nozzle. This is as expected of the erosion profile where the effect of the hitting angle of the abrasives and waterjet velocity were likely produces unstable slurry of water and abrasives (Anand & Katz, 2003; M Hashish, 1994b; M Nanduri et al., 1997; M Nanduri et al., 2002). The erosion activity then consistently came to a slow throughout the length of nozzle.

The results obtained from the erosion profile suggest that there are factors that produces such profile of erosion from the worn-out nozzle obtained from the industry. One was consistent with the simulation throughout the length of the nozzle but begins to lose erosion activity as it reaches the outlet. On the other hand, the other worn out nozzle went through excessive erosion as it made to the middle section of the nozzle. This suggest that there is unknown factor whether there are due to geometrical parameters or working conditions which will further discussed in this chapter.

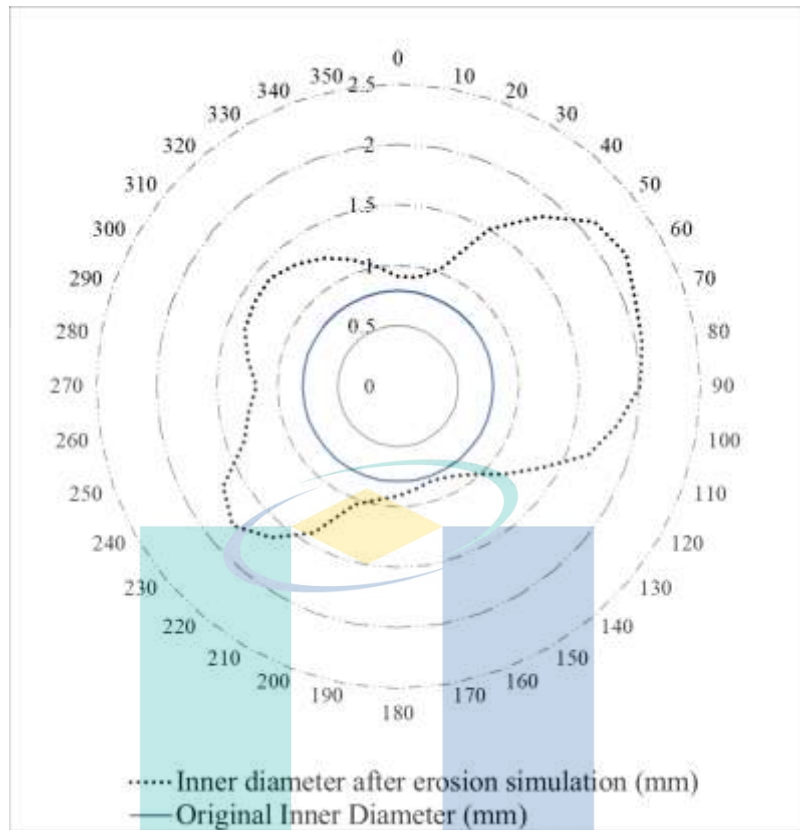


Figure 4.13 Inner diameter erosion profile (a) at section 1 (Inlet at 2 mm point).

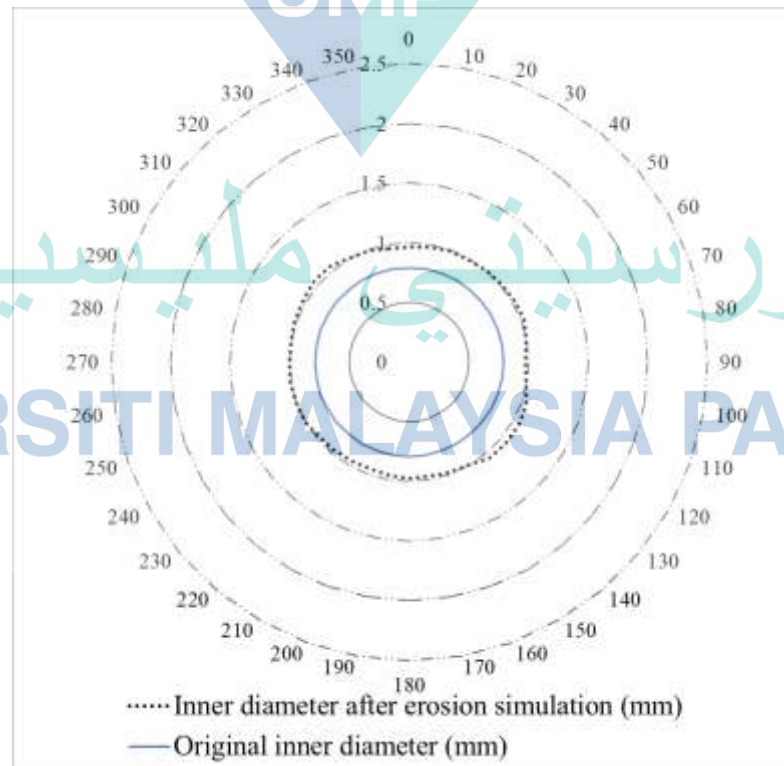


Figure 4.14 Inner diameter erosion profile at section 2 (19 mm point).



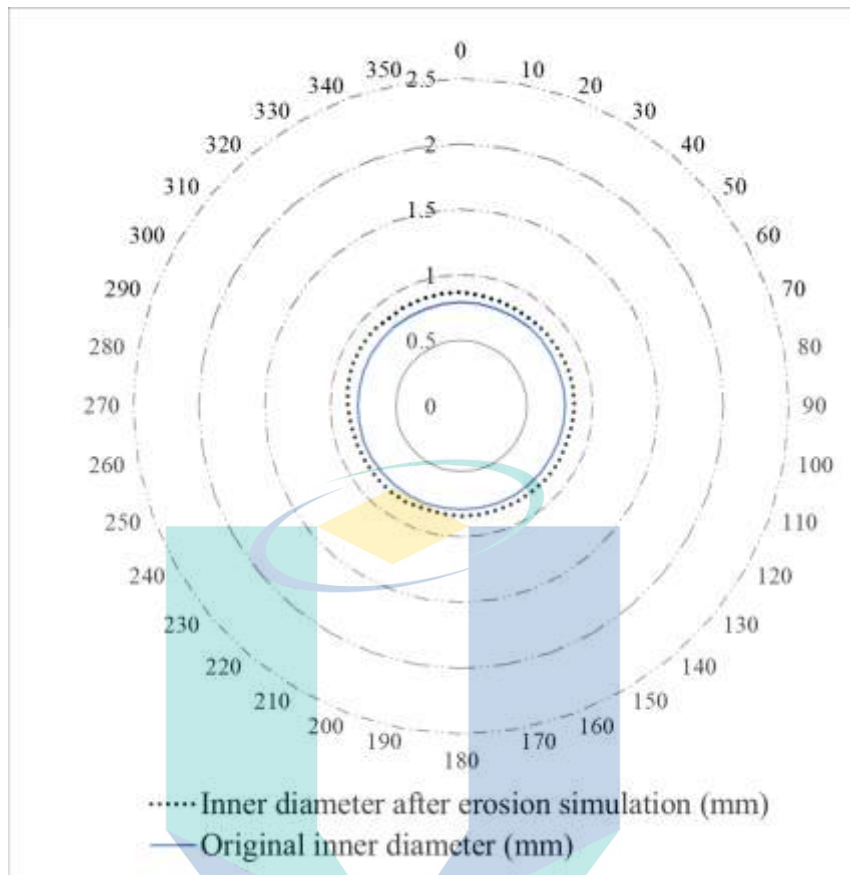


Figure 4.17 Inner diameter erosion profile at section 5 (Outlet at 68 mm point).

In Figure 4.13, it can be observed that the inlet of the nozzle has the most erosion activity. Another familiar observation that can be made is that there are more erosion activities towards a certain degree of orientation that also can be found in Figure 4.4 (b). Although they are opposite in side of the nozzle, it proclaims that the simulation model has its affect in producing such pattern. To validate the results at the nozzle inlet based on the erosion profile in and, the same erosion profile is documented by through casting of the nozzle after three hours of erosion testing. The erosion profile at the nozzle inlet in Figure 4.10 and Figure 4.13 is consistent with the profile in a study by Nanduri et al. (2002), who performed casting of the nozzle after three hours of erosion testing. Figure 2.1 shows the sectioned nozzle along with the casting which clearly shows the larger erosion activity at the inlet and the erosion begins to decrease in a wavy pattern as it goes along the nozzle.

Moving on to Figure 4.14, the erosion activity started to go down as it reaches the second point (19 mm from the inlet) of the nozzle. Again, this conforms the observation from past experimental results (M Nanduri et al., 2002). The erosion

activity continued to decrease as it went along the third and the fourth point (36 mm and 57 mm from the inlet respectively) the nozzle which can be shown in Figure 4.15 to Figure 4.16. In Figure 4.17 (68 mm from the inlet) shows the section near the outlet, it was observed that there are very slight difference from previous erosion profile at point four which suggest a very slight increase in erosion activity increases. Recent studies of nozzle wear by Xiaochen Chen, Deng, Guan, & Hua (2017) also shows similar results where the internal surface of the wear distribution shown using the accumulation data of erosion rate at different nodes. The study stated that wear occurs throughout the whole nozzle inner surface and is inhomogeneous in erosion pattern supporting the mentioned findings.

According to experimental analysis, one of the factors that contributes to this is due to lesser mechanical strength at the edge of the outlet of the nozzle can leads to chipping. As the erosion process continues, the chipping propagates as it has limited properties thus erodes more than the earlier parts before reaching the exit. However, this is non-relevant to the simulation model which leads to different factors of geometrical or system parameters. Previously in Figure 4.1 where the variations of waterjet velocity were shown in the cutting head points out slight increase of velocity at the exit. Increase of erosion rate is determined by Equation 2.8 where the velocity of the water effects directly to the particle velocity thus resulting an increase erosion rate.

Previous studies also support the findings as the wear characteristic of the cylinder section is related to the movement of the abrasive particles (Xiaochen Chen et al., 2017; Deepak et al., 2012; Mostofa et al., 2010). Further explanation reveals that the concentration at the cone section (inlet) causes the abrasives particles to produce a high radial velocity, however, the radial velocity decreases due to constant collision of the particles with the nozzle wall (Xiaochen Chen et al., 2017). When the radial velocity decreases, the abrasives particle begins to have an increase in axial velocity due to acceleration produced from the stream of high velocity waterjet. Another explanation by Abdolkarimi & Mohammadikhah (2013) are that erosion activity are higher when radial velocity are at peak value. The contours of erosion rate and numerical rate in are higher when the impact angle of particle is between 50 degrees to 60 degrees.

In Huang et al. (2010) study of producing phenomenological model in jet flow categorized the higher impact angle impact to be erosion by deformation damage removal and the lower impact angle to be erosion by cutting removal. It is conceivable that a similar phenomenon occurred in the AWJM flow as the deformation damage removal is dominant at the inlet. Also, the cutting removal of the lower erosion activity took place throughout the nozzle until its outlet.

#### 4.5 Nozzle Length

Figure 4.18 shows the effect of nozzle length with the erosion wear rate. It is revealed that the length of the nozzle has a direct influence on the nozzle wear rate. However, the simulated nozzle wear shows varied results as the length of the nozzle increases. General pattern indicates that the erosion of nozzle decreases as the nozzle length increases which is similar to results acquired in past experimental results (Hashish, 1994; Nanduri et al., 2002; V. N. Pi & Tuan, 2009).

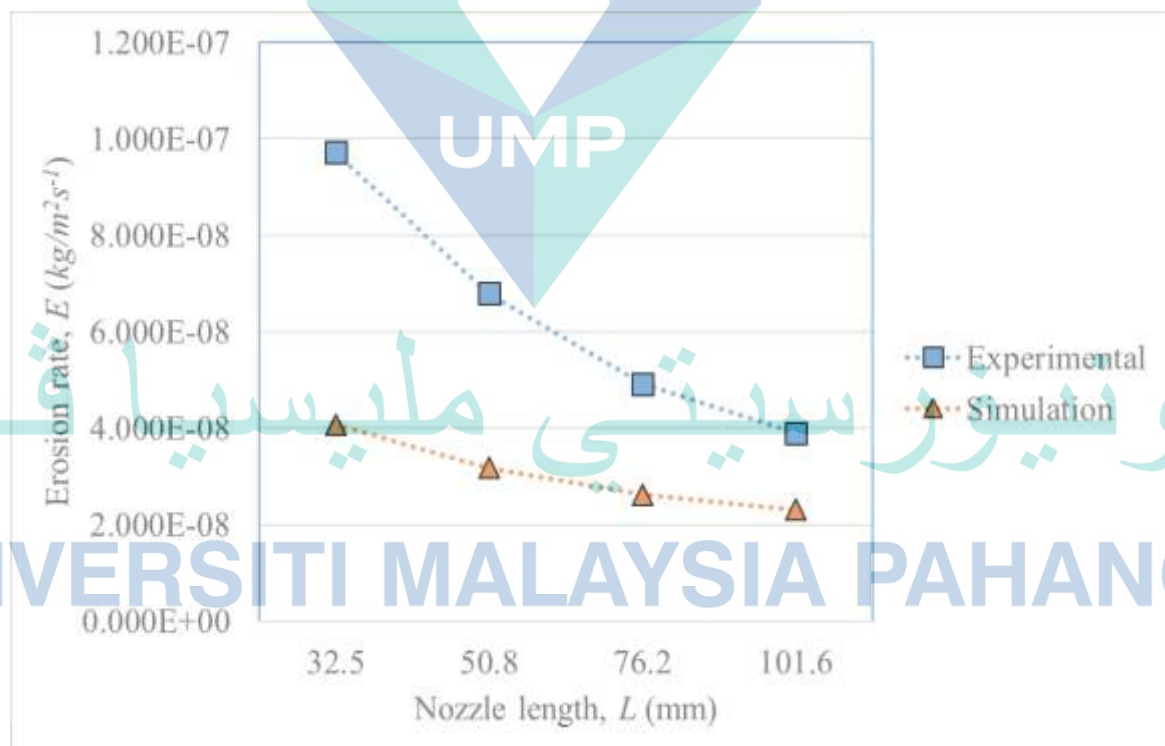


Figure 4.18 Effect of nozzle length on erosion wear.

Table 4.4 Erosion Rate and Error between Experimental Model and Simulation Erosion at Different Nozzle Lengths

Experimental model		Simulation	
Nozzle length, $L$ (mm)	Erosion Rate, $E$ (kg/m <sup>2</sup> s <sup>-1</sup> )	Erosion Rate, $E$ (kg/m <sup>2</sup> s <sup>-1</sup> )	Error (Unitless)
32.5	9.723E-08	4.078E-08	-5.645E-08
50.8	6.802E-08	3.180E-08	-3.622E-08
76.2	4.918E-08	2.621E-08	-2.297E-08
101.6	3.907E-08	2.315E-08	-1.591E-08

The decrease in erosion rate as the nozzle length increases is due to few factors which is change of impact angle of particle and wall boundary layer's effect (M Hashish, 1994). As the length of the nozzle increase, the velocity vectors of the particle become parallel to the wall, thus shallow angle impact and abrasion types of erosion became prevalent. Shorter nozzles tend to have stronger erosion impact and higher erosion which the particle have a higher angle of impact erosion. This mainly occurs at the inlet area of the nozzle where mixing of abrasive particles and highly entrained water produces a considerable amount of turbulence thus affecting the particle impact trajectories (Dosanjh & Humphrey, 1985). As the length of nozzle became longer, a velocity profile was starting to gradually build up as it enters the nozzle and eventually produces a phenomenon called the boundary layer (Schlichting, Gersten, Krause, Oertel, & Mayes, 1960). It is stated that as a fluid flow enters a stationary surface, the fluid touching the surface is brought to rest by the shear stress at the wall and thus the velocity increases from the wall to maximum in the main stream of the flow (Cengel, 2010). The boundary layer acts as coat that minimize the impact of abrasive against the wall of the nozzle.

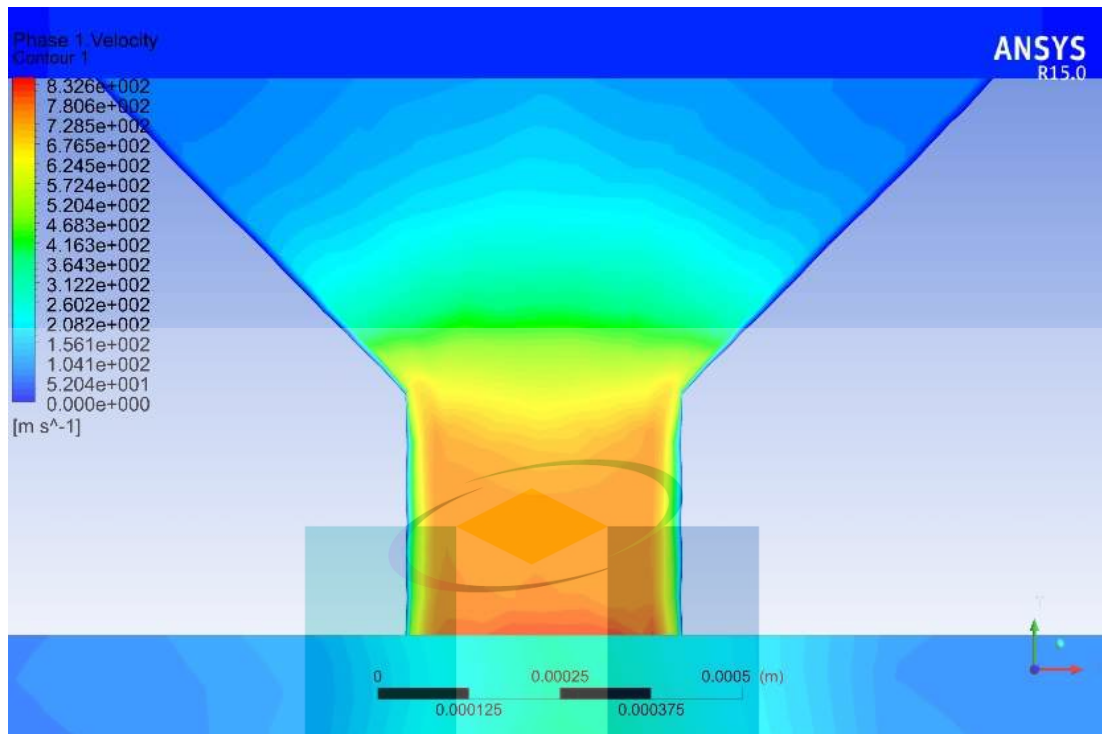


Figure 4.19 Boundary layer observation in AWJ nozzle wear simulation.

Other causes for lesser erosion wear as the length of the nozzle increases is due to the particles loss of energy, shape and material properties. This occurrence is prevalent in pipelines in oil and gas industry where Clark & Wong (1995) did a study on the comparison of the rate of erosion and the rate of dissipation of kinetic energy of impact with impact angle and angular location of a pipe cylinder. Although primary flow of the fluid would be unaffected, the particles that have undergone deformation at the earlier phase of entrance of the nozzle inlet and went on to the wall will obviously shows sign of decay and thus results in lesser erosion throughout the end of the nozzle length. A study done was done through different inlet operating pressure and volume fraction showed that the skin friction coefficient at the wall begins to decrease as the length of nozzle increases (Xiaochen Chen et al., 2017).

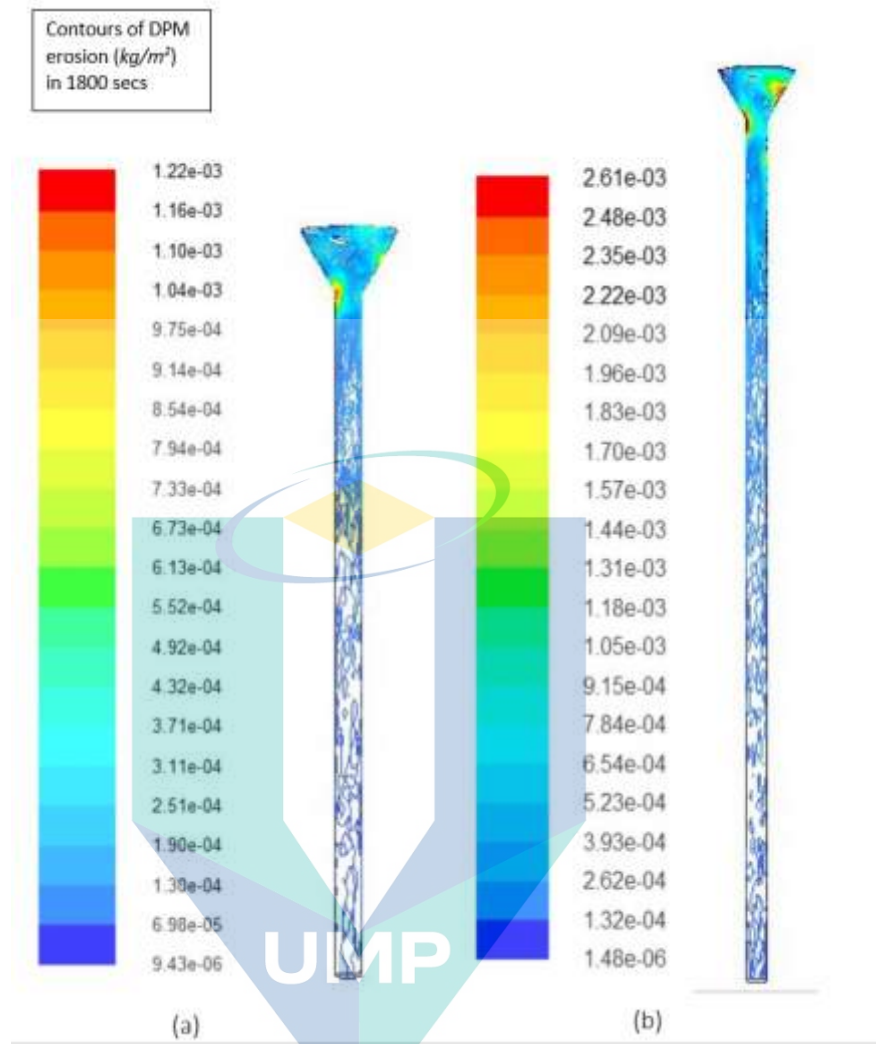


Figure 4.20 Contours of nozzle erosion for different nozzle sizes (a) 32.5mm (b) 50.8mm

اونيورسيتي ملايسيا فهاغ

UNIVERSITI MALAYSIA PAHANG

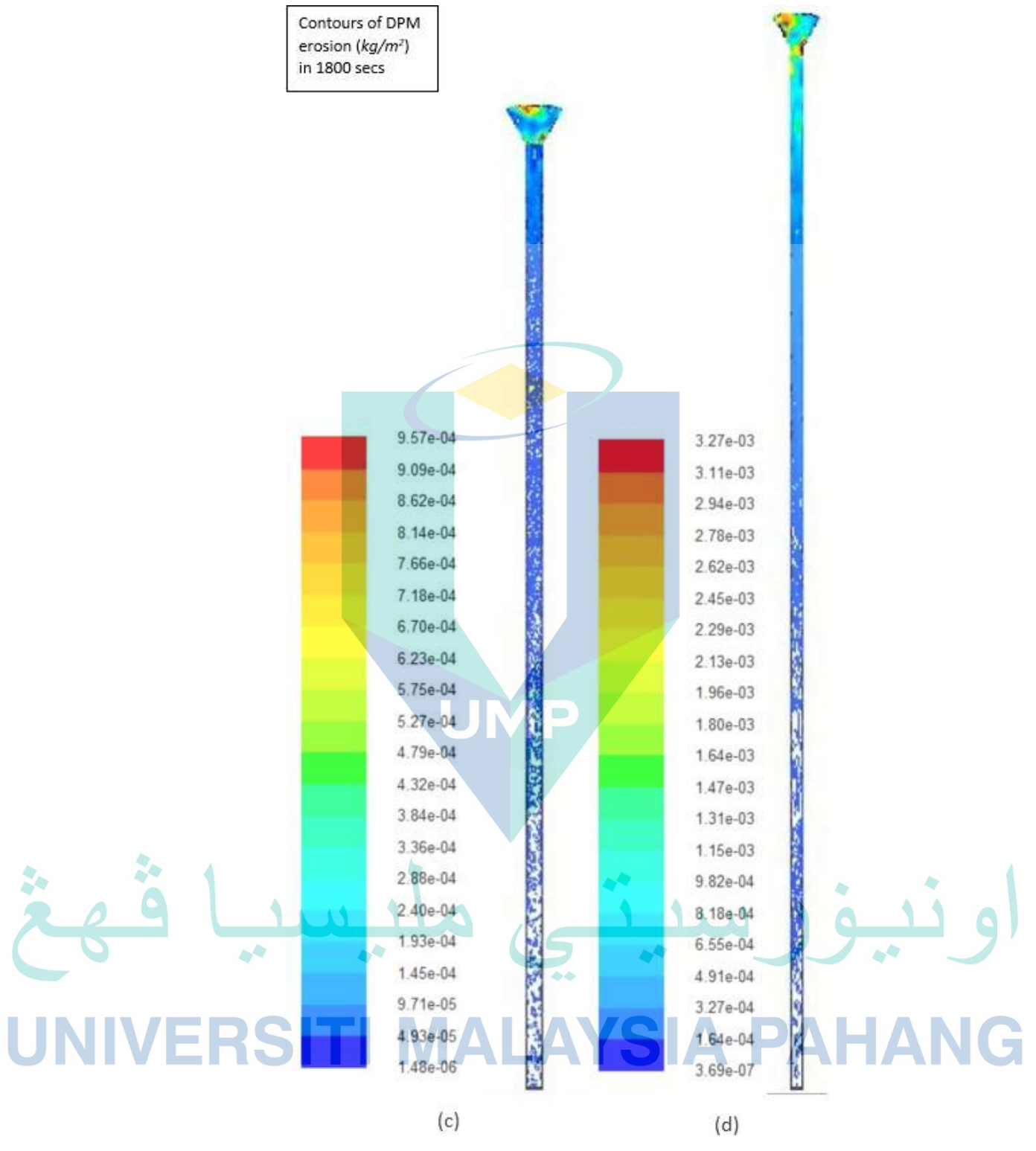


Figure 4.21 Contours of nozzle erosion for different nozzle sizes (c) 76.2 mm (d) 101.6 mm

The contours of erosion are shown in Figure 4.20 and Figure 4.21 for different nozzle length. The nozzle image is scaled down as the nozzle length size's increases, therefore, other dimensions stays the same except for the nozzle's length. The contours of erosion are represented by the coloured bar where the smallest erosion is designated as blue and the highest erosion rate is in red. The highest and lowest value of erosion is different between the samples and does not represent the entire quantity of erosion rate throughout the nozzle.

In Figure 4.20 and Figure 4.21, the recorded data was expected to be similar to previous findings. It can be observed from the figures that all the nozzles have a similar erosion pattern, where the highest erosion rate is recorded at inlet of the nozzle, then a decrease in activity is seen upon reaching the outlet. This is as to be expected where from previous findings it was found that the highest erosion activity to be at the inlet and will gradually decreases as it reaches the outlet. The other pattern that can be observed is the wavy pattern of erosion in which the erosion rate is alternating as it heads towards the outlet. The pattern is prevalent in the longer nozzles where such can be seen at the 101.6 mm nozzle. For the 32.5 mm nozzle, it can be observed that there is larger amount of erosion activity at the inlet. The nozzle has highest erosion rate of  $1.22E^{-03}$  kg/m<sup>2</sup> whereas the lowest erosion rate is  $9.43E^{-09}$  kg/m<sup>2</sup>.

As the nozzle increase in length, even though the accumulated erosion rate shows that the erosion rate gradually declines as the nozzle increase in size. The highest erosion rate for the longest nozzle in the sample is slightly higher which is at  $3.27E^{-03}$  kg/m<sup>2</sup> whereas the lowest erosion rate for the nozzle is  $3.69E^{-07}$  kg/m<sup>2</sup>. This was followed by the 50.8 mm nozzle and the subsequent 76.2 mm nozzle, with the latter having the smallest erosion rate altogether and its highest erosion rate at  $9.57E^{-04}$  kg/m<sup>2</sup>.

There is no definite pattern for the highest erosion rate, however, the value of the lowest erosion rate has shown clearer pattern of erosion rate decrement when the nozzle size increases. One of the factors that may affect the value of erosion rate can be due to the introduction of turbulence to the model. When the fluid flow enters the inlet, a maintained velocity of stream impacts the border of the conical shaped focusing tube;

a lower turbulence boundary layer was created. Therefore, the flow will be very predictable in this region. After some sections in acceptable distance, minor anarchic swaying of flow begins to develop in the boundary layer and the flow was transitioning to different turbulence process where gradually became fully turbulent phase. The  $k-\varepsilon$  model solves for two variables which is  $k$ , the turbulence kinetic energy and  $\varepsilon$  (epsilon), the rate of dissipation of turbulence kinetic energy. This model used a wall function, so the flow in the buffer region is negligible and not simulated.

The erosion of the surface is largely depending on the numbers of particles striking the surface, their velocity and the direction which is relative to the surface. The flow condition made will determine the quantities of the particle strikes. It is also known that the flow conditions can also greatly increase or decrease erosion. The erosion is considerably to be more severe at the focusing section rather than the straight run of the nozzle. The uneven surface at the focusing section greatly increases erosion. The wear erosion of AWJ nozzle have also been studied using plastic as a material (Syazwani, Mebrahitom, & Azmir, 2016). From the observation, the increased wear or degradation at the nozzle inlet have similitude with the simulation done. The simulation was further validated when there are huge change of diameter at around 50 mm section. After that there are promising evidence that there is degradation. It is found that longer nozzles have lower erosion rate and higher lifecycle (M Nanduri et al., 1996). It is understood that the longer length of a nozzle provides a condition where the degradation wear was delayed as the wear profile were forming to the outlet thus producing a stable and less oscillation in wear profile. Figure 4.21 shows this condition mentioned and this contributes the less erosion at the outlet compared to shorter nozzles.

It can be observed that as the length of the nozzle tube increases, the erosion rate correspondently decreases. The outlet pattern of the nozzles contour shows a similar profile to all the nozzle length. It shows that the erosion profile is distinctively affected to the addition of the length of the nozzle. Similar studies have been done to investigate the length of the nozzle to the erosion rate and shows that increase of nozzle length brought a more focused kerf width and higher jets efficiency to the workpiece (M Hashish, 1994b; M Nanduri et al., 1997). It is further explained that when the length of

the nozzle is added, the abrasives particle became uniformed with the jet flow to the outlet of the nozzle. In addition, longer nozzles found to be better in aspect of growth of exit bore, lifecycle of nozzle, width of waterjet kerf and cutting depth. At certain length of nozzle, the nozzle efficiency does not justify the production cost of the nozzle. However, the wear profile is only consistent when the nozzles are at the early process of erosion wear. After the wear have reached certain time, the nozzle will begin to show deterioration in jets efficiency. Increase of nozzle length is dubbed to be only a temporary option to solving irregular and high outlet wear rate.

#### 4.6 Nozzle Diameter

It is known that to achieve optimum mixing and cutting conditions, the orifice diameter to nozzle diameter ratio,  $R_o$ , is to be in the value of 0.3 to 0.4 (Momber & Kovacevic, 2012; M Nanduri et al., 2002). The ratio for typical values of orifice diameter 0.38 and nozzle diameter 1.14 is calculated to be 0.333 which is within the range of optimum mixing and cutting conditions.

It is shown in Table 4.5 the effect of nozzle diameter on nozzle erosion on three different diameter which is 0.79 mm, 1.14 mm and 1.63 mm. From the observation of the actual experimentation of the nozzle wear, the erosion rate of the nozzle is decreasing as the size of the nozzle diameter increases. The simulation also shows favorable trend and had the closest accuracy to the actual nozzle wear. The value of erosion rate was obviously high for 0.79 mm of diameter and it begins to deviate more when the nozzle diameter was change to 1.14 mm. However, the trend drops to a very close accuracy with the actual erosion at larger diameter of 1.63 mm. The loss of erosion activity is mainly due to the increasing diameter of the nozzle where it is too big to provide condition for efficient transfer of momentum (M Nanduri et al., 2002). The observation shows that as the nozzle increase in diameter, distinctively lower impact and resistance produces a drop in the trend of nozzle erosion degradation.

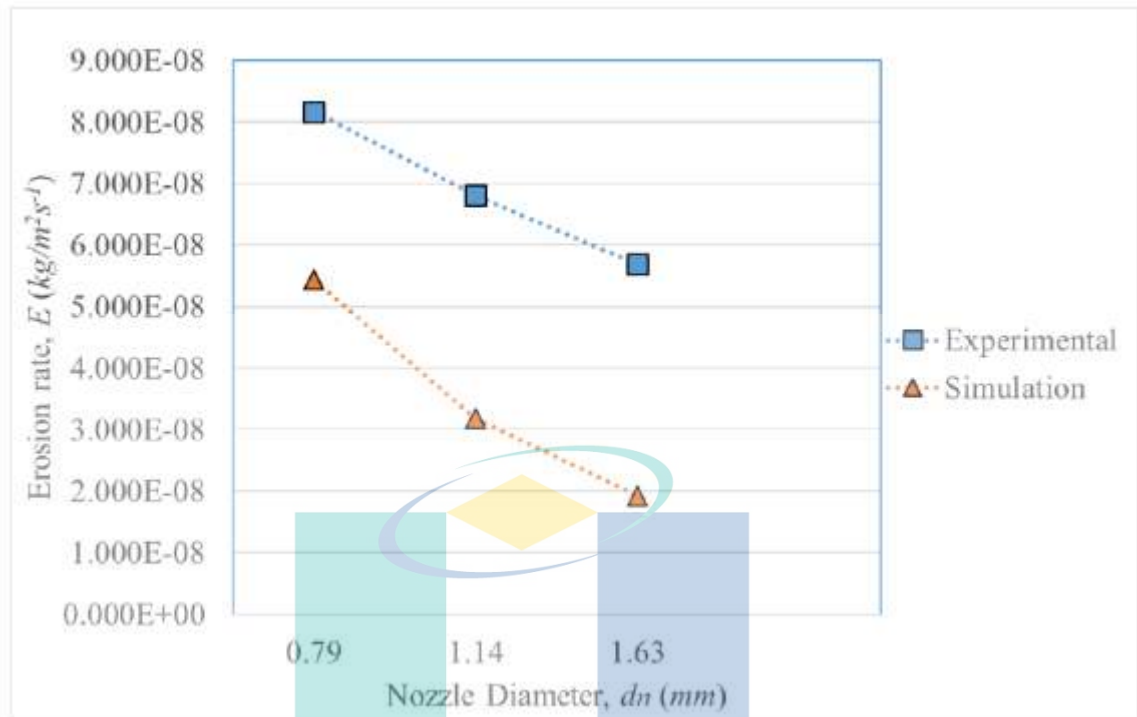


Figure 4.22 Effect of Nozzle diameter on nozzle erosion.

Table 4.5 Erosion Rate and Error comparison between Experimental Model and Simulated Erosion of AWJ Nozzle at different nozzle diameter

Experimental model		Simulation	
Nozzle Diameter, $d_n$ (mm)	Erosion Rate, $E$ ( $\text{kg/m}^2\text{s}^{-1}$ )	Erosion Rate, $E$ ( $\text{kg/m}^2\text{s}^{-1}$ )	Error (unitless)
0.79	8.171E-08	5.434E-08	-2.737E-08
1.14	6.802E-08	3.180E-08	-3.622E-08
1.63	5.688E-08	1.919E-08	-3.769E-08

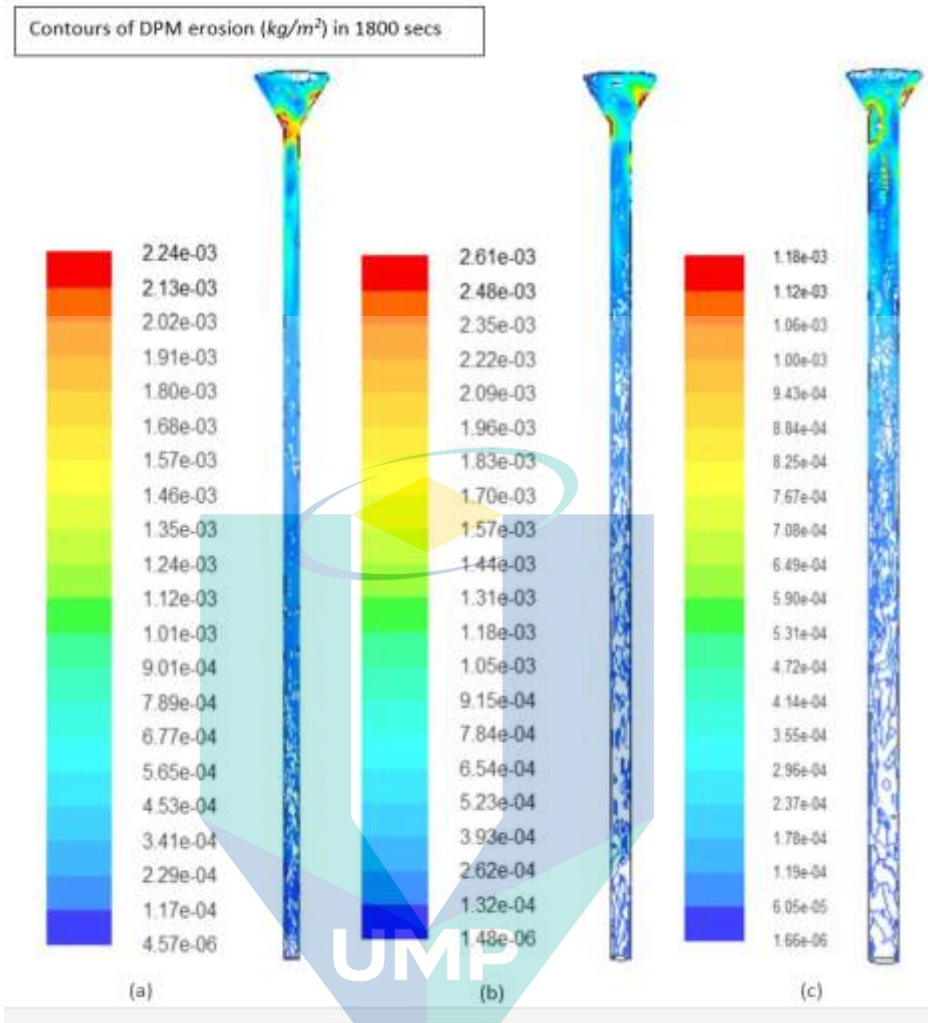


Figure 4.23 Contours of erosion for different nozzle diameters (a) 0.79 mm (b) 1.14 mm (c) 1.63 mm

Figure 4.23 shows the contours of erosion for different nozzle diameters. It was observed that the smaller the diameter of the nozzle, the higher erosion rate was found along the length of the nozzle. As the nozzle becomes larger in diameter, the erosion pattern began to decrease. The erosion profile also shows that the erosion activities are higher at the inlet and began to show less erosion throughout the length of the nozzle.

#### 4.7 Abrasive Flow Rate

Figure 4.24 shows the effect of abrasive flow rate on the nozzle's erosion. It is observed that the trends show a steady linear increase in erosion profile with the increasing abrasive flow rates. In a study investigating the outlet degradation of nozzle

as increasing the abrasive flow rate shows that the trend of erosion pattern remains the same for different flow rates set (Nanduri et al., 2002). Further investigation that the increase of abrasive concentration only affects the abrasive flow rate without manipulating the flow rate of the water itself. This came to the assumption that the velocity of the abrasives decreases as the abrasive flow rates increases. It can be concluded that the converging abrasives cancel out the slightly reduced stream velocity. The high waterjet velocity therefore is not affected due to solely the concentration of abrasives mixed into the nozzle.

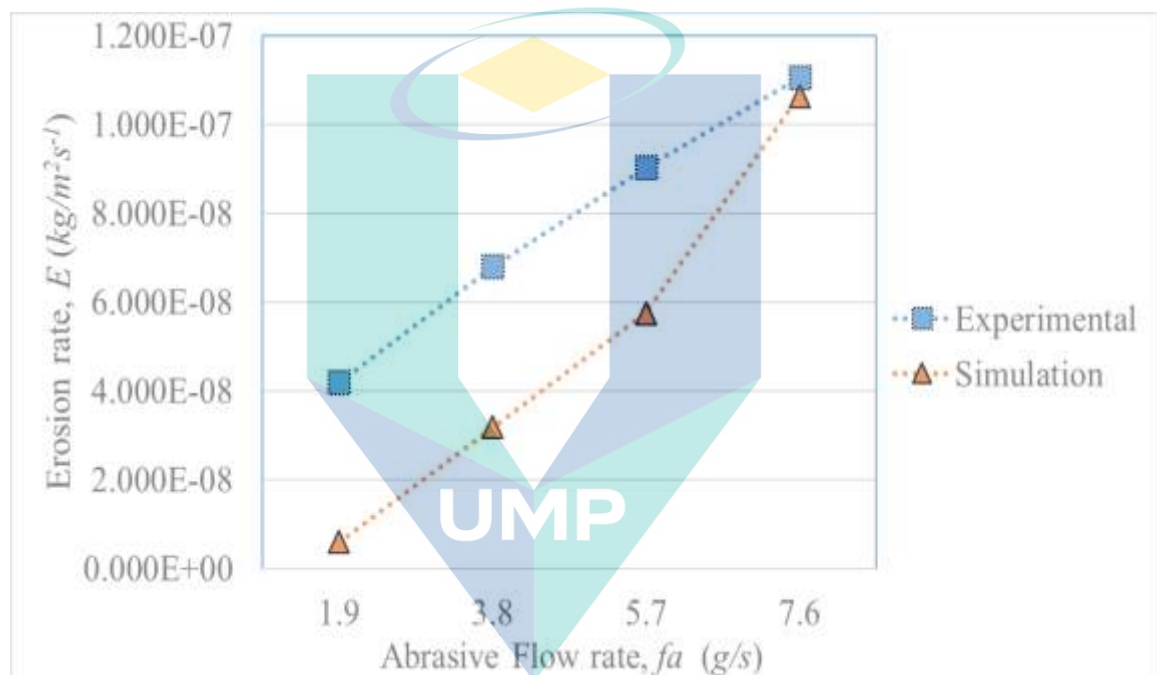


Figure 4.24 Effect of abrasive flow rate on nozzle erosion.

Table 4.6 Erosion Rate and Error of Experimental and Simulated Erosion Model in Different Abrasive Flow Rates

Experimental model		Simulation	
Abrasive flow rate, $f_a$ (g/s)	Erosion Rate, $E$ ( $\text{kg/m}^2\text{s}^{-1}$ )	Erosion Rate, $E$ ( $\text{kg/m}^2\text{s}^{-1}$ )	Error (unitless)
1.9	4.187E-08	6.022E-09	-3.585E-08
3.8	6.802E-08	3.180E-08	-3.622E-08
5.7	9.034E-08	5.745E-08	-3.289E-08
7.6	1.105E-07	1.063E-07	-4.176E-09

In Table 4.6 shows the effect of different abrasive flow rate showed a considerable accuracy and consistent trend between the experimental and simulation rate of erosion. Erosion profile showed that increased abrasive flow rates increase the wear rate without changing the wear pattern. The simulated erosion rate suddenly spiked to close with the experimental erosion rate where it is expected to then decrease. This is due to the simulation picks up accumulating abrasives at the inlet where it begins to increase its average erosion rate. Nanduri et al. (2002) also supported by enough water pressure that could carry the capacity of the abrasives through the nozzle. also supported the statement suggesting that increasing the abrasive flow rate will reduce the overall velocity of the abrasives slightly but the concentration effect will still overcome the effect of the slightly reduced slurry velocity.

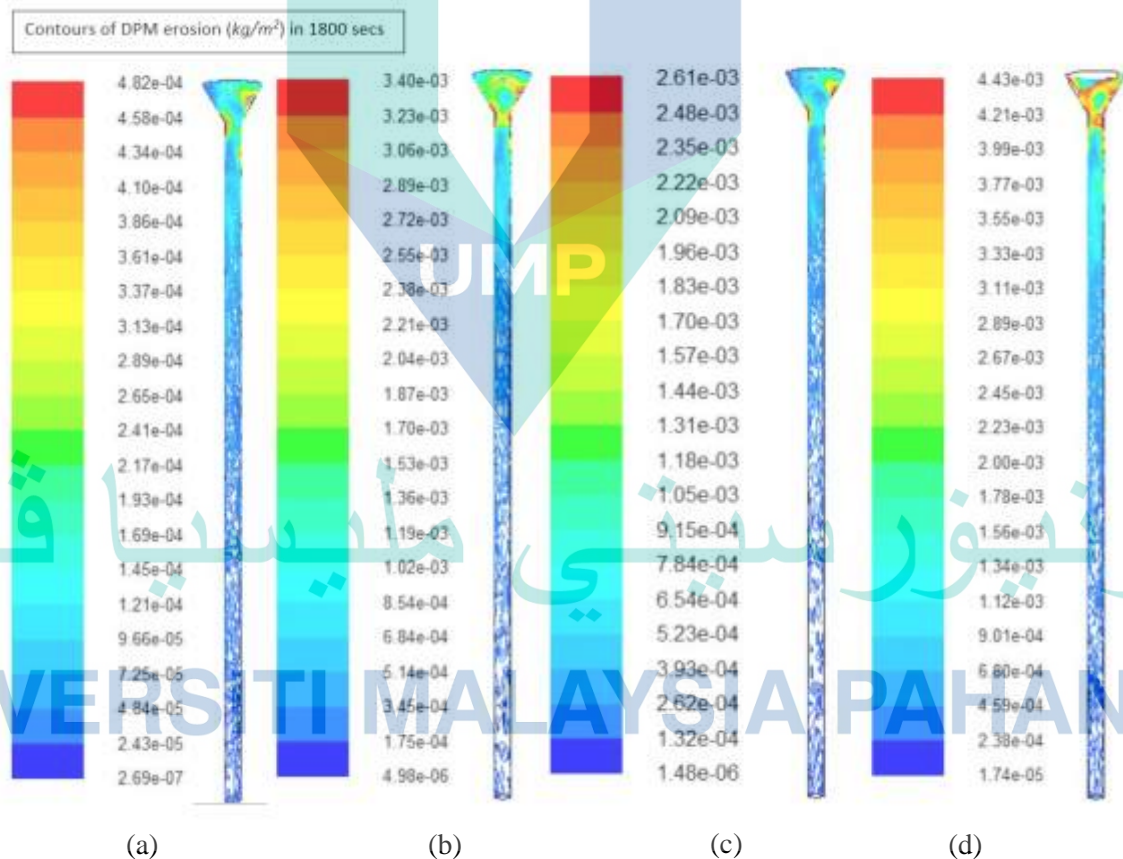


Figure 4.25 Contours of erosion for different abrasive flow rate (a)1.9 g/s (b)3.8 g/s (c)5.7 g/s (d)7.6 g/s.

Figure 4.25 shows the contours of erosion for the different abrasive flow rate where it can be observed that the contours have a large erosion activity at the focusing section of the inlet. The erosion begins to dissipate as it is progressing along the nozzle. Observed in the contours of erosion for the highest abrasives flow rate which is 7.6 g/s, the contours relatively show the larger erosion activities as compared to others. Although Nanduri et al.(2002) stated that there should be a decrease of erosion rate if the abrasives flow rate is increased to a certain level because a great influx of particles within the nozzle will lead it to become congested and would much drop the movement of the particle. The lack of kinetic energy will then decrease the erosion activity. However, the erosion rate in the simulation still shows an increase of erosion activity as the abrasives flow rates gets higher. The reason would probably be because the simulation lacks the capability to simulate the reduction of kinetic energy when the nozzle become congested of abrasives particles. The other possible reasons are because the abrasives flow rate from the simulation have not yet reached the value that is assumed to be where the erosion activity decreases.

To discuss the effect of the particle motion, attention has been focused on the probability distributions of particle-wall incidence speed and incidence angle in the whole elbows (Chen et al., 2015). It is found in the study of abrasives erosion to pipe elbow that there are much more particles impacting on the wall at lower velocities. The probability of particle incidence speed within 2–3 m/s is more than twice as much as that of when the particles are moving at a higher velocity. To the contrary, the probability of higher particle incidence, due to the increasing rebounds, more inter-particle collisions, greater developed turbulence and more particles were introduced. The former two weakens the energy of particles, lowering the incidence speed, and the last deviated particles from mainstream direction to impact on the wall at more variable angles which leads to the increased erosion rate.

#### **4.8 Orifice Diameter**

In Figure 4.26, The erosion rate profile shows consistent trend between simulation and experimental. Apparently, the trends also have similarity to the nozzle diameter effect. The increase of erosion is mainly due to the increasing the ratio,  $R_o$ ,

increasing the size of the diameter, increases the water flow rate value and decreases abrasive flow rate concentration. The transfer between momentum efficiency improves and velocity of abrasives increases (Anand & Katz, 2003; Nanduri et al., 2002; V. N. Pi & Tuan, 2009). It is also expected that increasing the orifice diameter will lead to less efficiency (Nanduri et al., 2002). Although the experimental erosion rate had a stable increase, the simulation was suddenly dropped as to supporting the statement above. A five-percentage accuracy when it is at a 0.28 mm of diameter, but it went to seventy-two percentage of difference when it reaches 0.38 mm. If the fusing diameter increases, the fusing efficiency will decrease which will result in lowering the flow energy density where when associated with abrasives impingement of target material will lead to lower cutting quality (Mohamed Hashish, 1989).

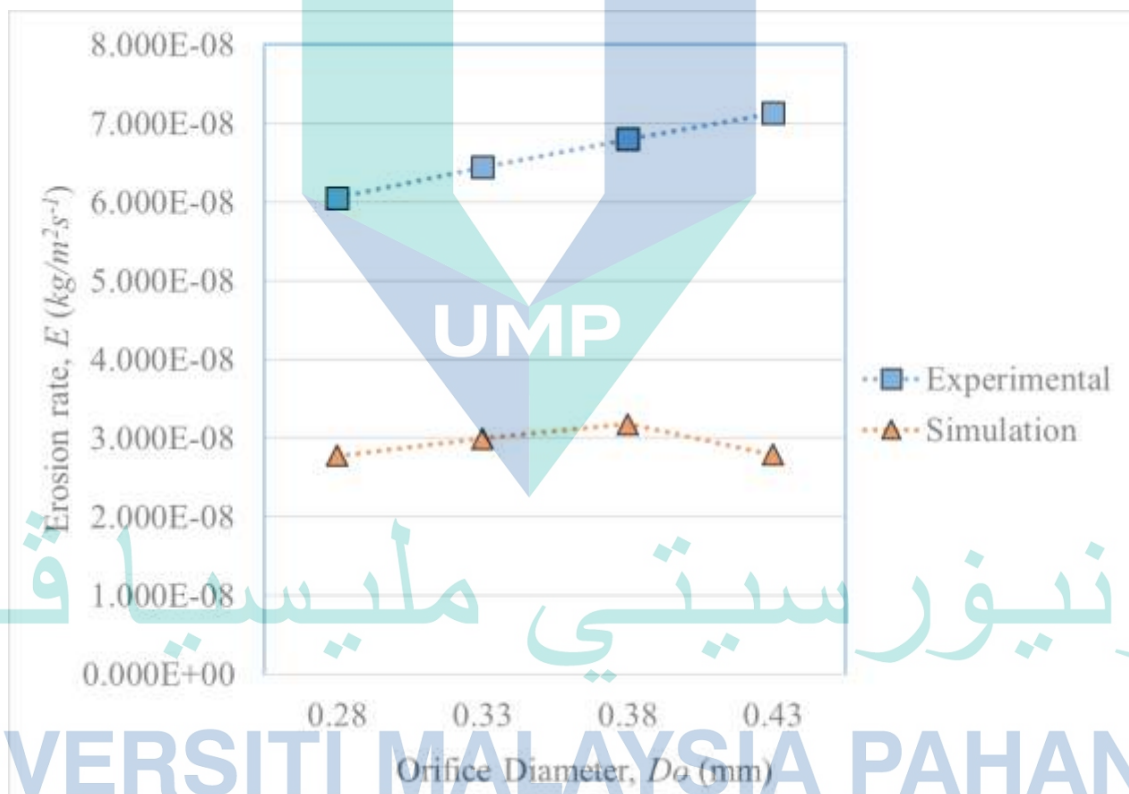


Figure 4.26 Effect of orifice diameter on nozzle erosion.

Table 4.7 Erosion Rate and Error between Experimental and Simulated Erosion Model in Different Diameters of Orifice Parameters

Experimental model		Simulation	
Orifice Diameter, $D_o$ (mm)	Erosion Rate, $E$ ( $\text{kg/m}^2\text{s}^{-1}$ )	Erosion rate, $E$ ( $\text{kg/m}^2\text{s}^{-1}$ )	Error (unitless)
0.28	6.057E-08	2.778E-08	-2.783E-09
0.33	6.447E-08	2.992E-08	-1.955E-08
0.38	6.802E-08	3.180E-08	-3.622E-08
0.43	7.129E-08	2.79E-08	-4.342E-08

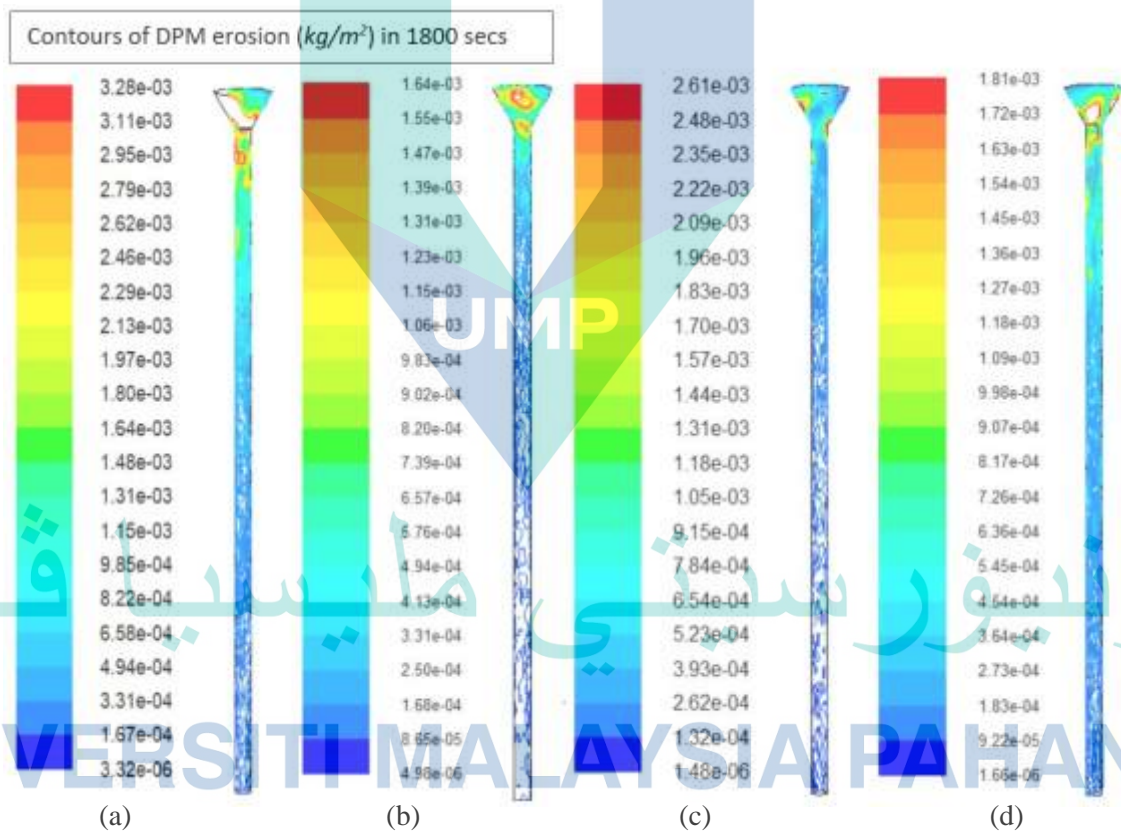


Figure 4.27 Contours of erosion for different nozzle orifice diameter (a) 0.28mm (b) 0.33mm (c) 0.38mm and (d) 0.43mm.

Generally, maintaining the ratio of orifice to nozzle diameter of approximately 0.3 to 0.4 and maintain other process factors constant produced the most superior fusing and cutting environment. The distribution of abrasives particle in nozzle tubes under different parameters of fusing environment was recently investigated using micro based

impact method (Hlaváč, Hlaváčová, Geryk, & Plančár, 2015). Three different fusing parameters of ratio orifice to nozzle inner diameter of 0.22, 0.30, and 0.42 were produced by varying the ranges of orifice to nozzle diameter.

It was observed that the ratio of 0.42 produced the most effective distribution of abrasives particle in the ranges tested. The simulation tested the parameters in the ratio of 0.48, 0.33, and 0.23 were to be well correlated with past study. The erosion rate observed in the simulation here are therefore consistent with expectation. Efficient particle distribution of fusing environment also produces better cutting kerf width quality and but unfortunately increase in nozzle wear erosion.

The same observation was also monitored when investigating the effect of inlet angle. The erosion profile of the 0.79 mm nozzle has shown a very well shape of wavy pattern which conforms with past study. This suggested that there are inefficient exchanges of momentum between water and abrasives producing an excessively choking environment inside the nozzle. Whereas a larger nozzle diameter which was indicated for 1.63 mm diameter nozzle have an area to expansive which produces a low-quality momentum exchanges between water and abrasives. However, reduced erosion rate were shown in both parameters tested. Study suggest that the nozzle with 1.14 mm diameter and a ratio of 0.33 to orifice and nozzle inlet diameter in typical fusing setting produces the most minor nozzle erosion rate. When the ratio of 0.48 was tested, there were indication that there were higher concentration of wear impingement at the outlet portion of the nozzle that produces higher erosion rate. It can be concluded that as the diameter of the orifice increases there were distinctively lower erosion rate

#### 4.9 Water Pressure

Figure 4.28 presents the effect of water pressure on the experimental and the simulated nozzle erosion rate. The erosion rate were observed to rise with the increasing water pressure which is due to increase in pressure which produces in higher fractalization of the abrasive particles thus reduces their capability in degrading the nozzle (M Nanduri et al., 2002). However, just like in the simulation, there is no significance in reduction of erosion rate even at the outlet of the nozzle. The simulation shows small decrease as it reaches the 310 MPa but increased only slightly at 359 MPa.

The experimental nozzle rate however starts to have slight reduction when it reaches 359 MPa.

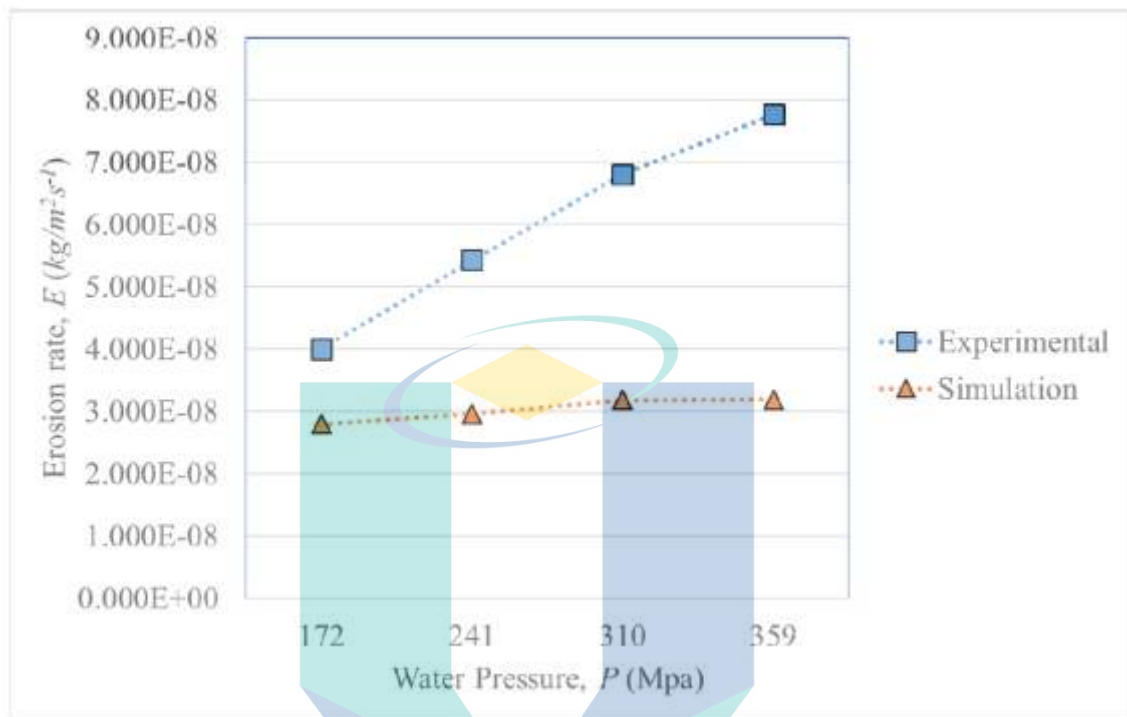


Figure 4.28 Effect of water pressure on nozzle erosion

Table 4.8 Erosion Rate and Accuracy between Experimental And Simulated Erosion Model in Different Parameters of Water Pressure

Experimental model		Simulation	
Water Pressure, P (Mpa)	Erosion Rate, E (kg/m²s⁻¹)	Erosion rate, E (kg/m²s⁻¹)	Error (unitless)
172	4.003E-08	2.795E-08	-5.075E-09
241	5.423E-08	2.958E-08	-2.044E-08
310	6.802E-08	3.180E-08	-3.622E-08
359	7.762E-08	3.886E-08	-4.876E-08

In Table 4.8, the accuracy of the erosion rate between the simulation experimental model can be seen. The simulation has a considerable accuracy of 53 to 30 percent. A comprehensive work on the study of pressure effects in AWJM has found that the increasing the pressure will increases the waterjet rate of momentum which in

turn increases the abrasive particle velocity (M Hashish, 1994). At higher pressure, the simulated erosion model begins to diverge from the experimental results. Findings from previous work stated that the rate of change of particle fragmentation with pressure declines as pressure increases. The simulation still is not capable to capture the particle fragmentation as it hits the wall which leads to the lower erosion rate on the simulation.

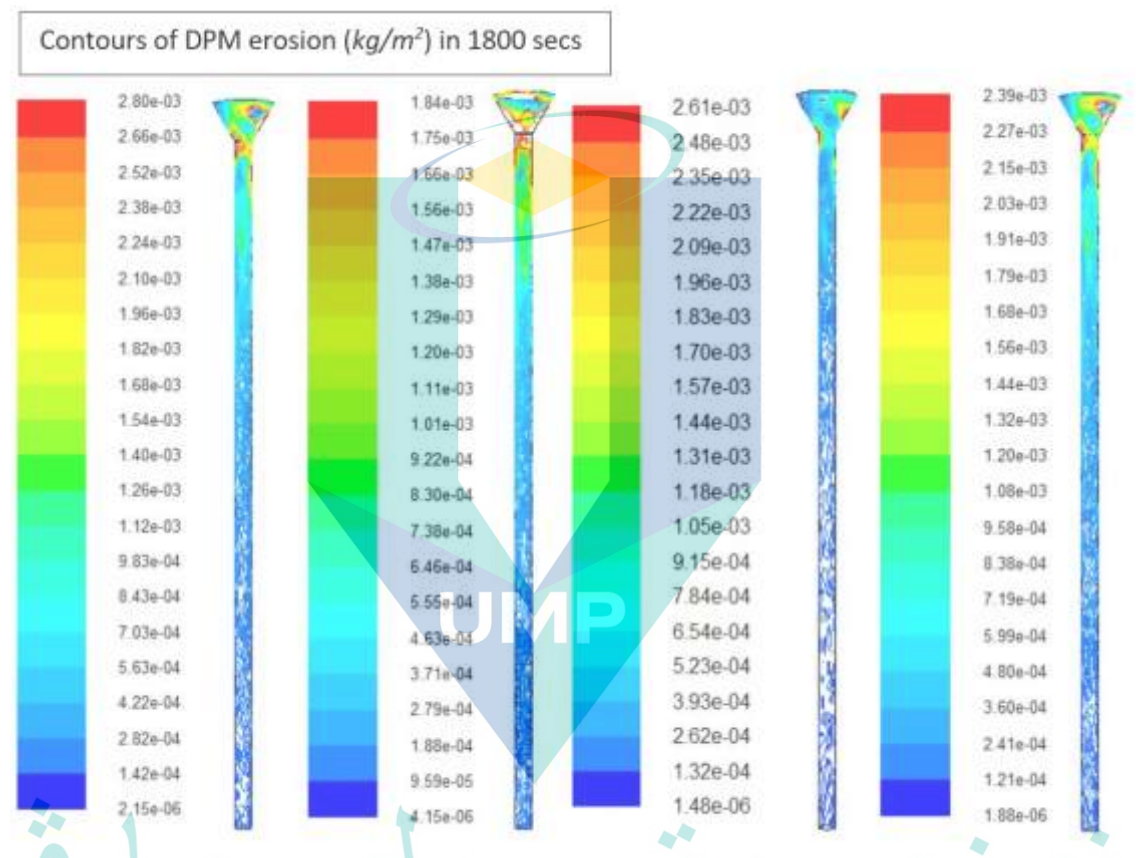


Figure 4.29 Contours of erosion for different water pressure (a) 172 MPa (b) 241 MPa (c) 310 MPa and (d) 359 MPa

The trajectory of the particle depends on the drag force thus preventing the particle to interact with the wall as the pressure increases. For the experimental results, when the pressure increase, the fragmentations of abrasives particle became higher and this results a higher velocities. Another reasons that contributes the lower erosion rate is that in particle-wall interaction of the simulation. There are particles that were terminated because the maximum allowed number of time steps was exceeded thus may causes the nozzle wall to have less particle interaction. The particles can also be aborted during numerical processing because of trajectories that fail to complete due to numerical or round-off reasons. This can be improved by redoing the calculation with

modified lengths scale or different initial conditions however there are no optimal procedures to ensure the simulation quality will increase.

Figure 4.29 shows the contours of erosion for different size of nozzle orifice whereby it can be seen that there are similar patterns of erosion in each of the different water pressure simulation. There is no obvious difference of erosion patterns for each of the simulations. The erosion pattern from the inlet to the outlet also follows the trend in which it has a high erosion activity at the beginning of the inlet and begins to dissipate as it approaches the outlet.

#### 4.10 Summary of Nozzle Erosion Simulation of Different Parameters of Geometrical and Working Condition.

Table 4.9 shows the summary of nozzle erosion simulation results of different parameters of geometrical and working conditions. Observed in the nozzle length parameters, the erosion rate decreases as the nozzle length increases in size. From  $9.723E^{-08}$   $\text{kg/m}^2\text{s}^{-1}$  to  $3.907E^{-08}$   $\text{kg/m}^2\text{s}^{-1}$  where the simulation results also decreases but from  $4.078E^{-08}$   $\text{kg/m}^2\text{s}^{-1}$  to  $2.315E^{-08}$   $\text{kg/m}^2\text{s}^{-1}$ . As for the nozzle diameter, the erosion rate decreases as the nozzle diameter increases in size. The experimental results shows decrease in erosion rate from  $8.171E^{-08}$   $\text{kg/m}^2\text{s}^{-1}$  to  $5.688E^{-08}$   $\text{kg/m}^2\text{s}^{-1}$  whereas the simulation shows  $5.343E^{-08}$   $\text{kg/m}^2\text{s}^{-1}$  to  $1.919E^{-08}$   $\text{kg/m}^2\text{s}^{-1}$ . Whereas for the orifice diameter, as the diameter of the orifice increase in size, the erosion rate were also increased. The experimental results shows an increase from  $6.057E^{-08}$   $\text{kg/m}^2\text{s}^{-1}$  to  $7.129E^{-08}$   $\text{kg/m}^2\text{s}^{-1}$  whereby the simulated results are from  $2.778E^{-08}$   $\text{kg/m}^2\text{s}^{-1}$  to  $2.787E^{-08}$   $\text{kg/m}^2\text{s}^{-1}$ .

In term of water pressure, as the pressure increases, the erosion rate also increases. The experimental results shows increase from  $4.003E^{-08}$   $\text{kg/m}^2\text{s}^{-1}$  to  $7.762E^{-08}$  where the simulations results were  $2.795E^{-08}$   $\text{kg/m}^2\text{s}^{-1}$  to  $3.886E^{-08}$   $\text{kg/m}^2\text{s}^{-1}$ . Whereas for the abrasive flow rate, the erosion rate also increased linearly. The experimental results shows increase from  $4.187E^{-08}$   $\text{kg/m}^2\text{s}^{-1}$  to  $1.105E^{-07}$   $\text{kg/m}^2\text{s}^{-1}$ . Similarly, the simulation shows linear increase from  $-3.585E^{-08}$   $\text{kg/m}^2\text{s}^{-1}$  to  $-1.063E^{-07}$   $\text{kg/m}^2\text{s}^{-1}$ .

Overall, the accuracy of the errors is around the range of  $6.022E^{-09}$   $\text{kg/m}^2\text{s}^{-1}$  to  $1.063E^{-07}$   $\text{kg/m}^2\text{s}^{-1}$  where there is consistency throughout the different parameters of simulation. The trends of the simulated erosion rates were also consistent with the

experimental results however the erosion rates appear to be mostly smaller values as compared to the experimental results.

Table 4.9 Summary of Nozzle Erosion Simulation of Different Parameters of Geometrical and Working Conditions

(a) Nozzle length				(b) Nozzle Diameter			
Experimental		Simulation		Experimental		Simulation	
Nozzle length (mm)	Erosion Rate, $E$ ( $\text{kg}/\text{m}^2\text{s}^{-1}$ )	Erosion rate, $E$ ( $\text{kg}/\text{m}^2\text{s}^{-1}$ )	Error (unitless)	Nozzle Diameter (mm)	Erosion Rate, $E$ ( $\text{kg}/\text{m}^2\text{s}^{-1}$ )	Erosion rate, $E$ ( $\text{kg}/\text{m}^2\text{s}^{-1}$ )	Error (unitless)
32.5	9.723E-08	4.078E-08	-5.645E-08	0.79	8.171E-08	5.434E-08	-2.737E-08
50.8	6.802E-08	3.180E-08	-3.622E-08	1.14	6.802E-08	3.180E-08	-3.622E-08
76.2	4.918E-08	2.621E-08	-2.297E-08	1.63	5.688E-08	1.919E-08	-3.769E-08
101.6	3.907E-08	2.315E-08	-1.591E-08				

(c) Orifice Diameter				(d) Water Pressure			
Experimental		Simulation		Experimental		Simulation	
Orifice Diameter (mm)	Erosion Rate, $E$ ( $\text{kg}/\text{m}^2\text{s}^{-1}$ )	Erosion rate, $E$ ( $\text{kg}/\text{m}^2\text{s}^{-1}$ )	Error (unitless)	Water Pressure (Mpa)	Erosion Rate, $E$ ( $\text{kg}/\text{m}^2\text{s}^{-1}$ )	Erosion rate, $E$ ( $\text{kg}/\text{m}^2\text{s}^{-1}$ )	Error (unitless)
0.28	6.057E-08	2.778E-08	-2.783E-09	172	4.003E-08	2.795E-08	-5.075E-09
0.33	6.447E-08	2.992E-08	-1.955E-08	241	5.423E-08	2.958E-08	-2.044E-08
0.38	6.802E-08	3.180E-08	-3.622E-08	310	6.802E-08	3.180E-08	-3.622E-08
0.43	7.129E-08	2.79E-08	-4.342E-08	359	7.762E-08	3.886E-08	-4.876E-08

(e) Abrasive Flow Rate			
Experimental		Simulation	
Abrasive Flow Rate (g/s)	Actual Erosion Rate ( $\text{kg}/\text{m}^2\text{s}$ )	Erosion rate ( $\text{kg}/\text{m}^2\text{s}$ )	Error (unitless)
1.9	4.187E-08	6.022E-09	-3.585E-08
3.8	6.802E-08	3.180E-08	-3.622E-08
5.7	9.034E-08	5.745E-08	-3.289E-08
7.6	1.105E-07	1.063E-07	-4.176E-09

## CHAPTER 5

### CONCLUSION

#### 5.1 Conclusion

The thesis has demonstrated simulation of AWJM nozzle erosion using ANSYS FLUENT software and utilize the features already available in the program. The simulation results were compared with experimental results to determine methods with the fastest processing time, high quality of convergence and accuracy of simulated nozzle erosion.

The Quadrilateral mesh assembly methods and the Realizable  $K-\varepsilon$  turbulence model were chosen as the most suitable methods for nozzle erosion simulation. The processing time, quality of convergence and accuracy of the simulated and experimental results were evaluated. In terms of the processing time, it was found that the Quadrilateral mesh methods had the most efficient processing time as compared to Cut-cell and Tetrahedral. The average time for Quadrilateral processing time was around 72 hours, Cut-cell was 92 hours and Tetrahedral was 168 hours. In term of the quality of convergence, it was found that the Quadrilateral mesh showed greater convergence whilst the other mesh methods were prevalent to diverged. Choosing quadrilateral mesh not just help improve the accuracy but decreases processing time and convergence quality. The turbulence model was also determined by comparing the nozzle erosion accuracy using the Standard  $k-\varepsilon$  and Realizable turbulence model. The Standard  $k-\varepsilon$  turbulence model was selected as it shows a more accurate and consistent result as compared to the Realizable turbulence Model.

The pre-determined mesh methods and turbulence model factor were then used to evaluate the simulated erosion profile with a worn-out nozzle used in the industry. The erosion profile was then compared against the simulation and it was found that the results shows minimal difference and were consistent showing the wavy erosion profile. There were also concerns with unknown parameters that were used from the worn-out

nozzle obtained from the industries and from past experimental parameters. However, the results are agreeable and give lots of potential for future modifications

The parameters of geometrical and working conditions were also simulated against the experimental results of nozzle erosion. It is acknowledgeable that all simulations showed considerable consistency in trends. Errors found to be around the range of  $6.022E^{-09}$  kg/m<sup>2</sup>s<sup>-1</sup> to  $1.063E^{-07}$  kg/m<sup>2</sup>s<sup>-1</sup> where there is consistency throughout the different parameters of simulation. Although the erosion rates appear to be mostly smaller values as compared to the experimental results, however it can be considered acceptable as it is within tolerable decimal.

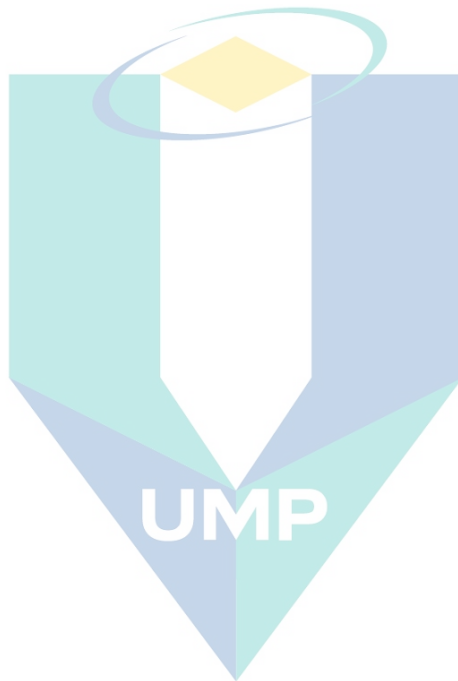
## 5.2 Recommendation

There are many interesting aspects for the continued research of nozzle erosion in AWJ machine. The following are recommendations for future works and research;

- i. Conduct a real time nozzle erosion simulation in order to predict nozzle erosion during the machining process. This could be done by using sensors that can detect important data from the machine and make evaluation of the nozzle's life using the prediction model. Achieving this can improve the quality of machined products caused by increased kerf width caused by worn out nozzle.
- ii. Use a real time erosion prediction that will allow the AWJ machine to obtain data and adjust the machining parameters automatically such as abrasive flow rate and water pressure to further increase product quality.
- iii. One of the drawbacks of the AWJ machine is that it can only cut product of certain thickness depending on the AWJ water jet pressure and the type of materials. Therefore, using simulation can help to create various design concepts of a new nozzle or a different AWJ system.
- iv. Utilize the User Define Function (UDF) in ANSYS software to convert mathematical models for erosion into programming language. This will give a wider data of nozzle prediction and will allow researcher to determine which is better for nozzle prediction.
- v. Study the effect of other geometry conditions and machining parameters such as the abrasive and nozzle material, mixing angle, inlet and outlet mixing nozzle shapes, type of slurry used or additional liquid/material added to the mixing of

water and abrasives, particle diameter, particle shape, target material and impact material properties.

- vi. Reduce processing time by utilizing current hardware such as using Solid State Disk in computers instead of the hard disk drive that is highly affordable in the current market.



اونيورسيتي مليسيا قهغ

UNIVERSITI MALAYSIA PAHANG

## REFERENCES

- Abdolkarimi, V., & Mohammadikhah, R. (2013). CFD modeling of particulates erosive effect on a commercial scale pipeline bend. *ISRN Chemical Engineering*, 2013.
- Al-Baghdadi, M. A., Resan, K. K., & Al-Waily, M. (2017). CFD investigation of the erosion severity in 3D flow elbow during crude oil contaminated sand transportation. *Engineering and Technology Journal*, 35(9 Part (A) Engineering), 930–935.
- Al-Khayat, R. H., Al-Baghdadi, M. A. R. S., Neama, R. A., & Al-Waily, M. (2018). Optimization CFD study of erosion in 3D elbow during transportation of crude oil contaminated with sand particles. *International Journal of Engineering & Technology*, 7(3), 1420–1428.
- Aldaş, K., & Yapıcı, R. (2014). Investigation of effects of scale and surface roughness on efficiency of water jet pumps using CFD. *Engineering Applications of Computational Fluid Mechanics*, 8(1), 14–25.
- Anand, U., & Katz, J. (2003). Prevention of nozzle wear in abrasive water suspension jets (AWSJ) using porous lubricated nozzles. *Journal of Tribology*, 125(1), 168–180.
- Anantharamaiah, N., Tafreshi, H. V., & Pourdeyhimi, B. (2006). A study on hydroentangling waterjets and their impact forces. *Experiments in Fluids*, 41(1), 103.
- Arabnejad, H., Mansouri, A., Shirazi, S. A., & McLaury, B. S. (2015a). Development of mechanistic erosion equation for solid particles. *Wear*, 332, 1044–1050.
- Arabnejad, H., Mansouri, A., Shirazi, S. A., & McLaury, B. S. (2015b). *Evaluation of solid particle erosion equations and models for oil and gas industry applications*. In *SPE Annual Technical Conference and Exhibition*. Society of Petroleum Engineers.
- Arabnejad, H., Mansouri, A., Shirazi, S. A., & McLaury, B. S. (2017). Abrasion erosion modeling in particulate flow. *Wear*, 376–377. doi:10.1016/j.wear.2017.01.042
- Aslam Noon, A., & Kim, M. H. (2017). Erosion wear on Francis turbine components due to sediment flow. *Wear*, 378–379. doi:10.1016/j.wear.2017.02.040
- Azhari, A., Schindler, C., Godard, C., Gibmeier, J., & Kerscher, E. (2016). Effect of multiple passes treatment in waterjet peening on fatigue performance. *Applied Surface Science*, 388, 468–474.
- Baggaley, N., & Potts, J. (2017). Sensitivity of the PESERA soil erosion model to terrain and soil inputs. *Geoderma Regional*, 11, 104–112.

- Baisheng, N. I. E., Hui, W., Lei, L. I., Jufeng, Z., Hua, Y., Zhen, L. I. U., ... Hailong, L. (2011). Numerical investigation of the flow field inside and outside high-pressure abrasive waterjet nozzle. *Procedia Engineering*, 26, 48–55. doi:http://dx.doi.org/10.1016/j.proeng.2011.11.2138
- Banakermani, M. R., Naderan, H., & Saffar-Avval, M. (2018). An investigation of erosion prediction for 15° to 90° elbows by numerical simulation of gas-solid flow. *Powder Technology*, 334, 9–26.
- Barkley, D., Song, B., Mukund, V., Lemoult, G., Avila, M., & Hof, B. (2015). The rise of fully turbulent flow. *Nature*, 526(7574), 550.
- Barton, N., Lewis, M., & Emmerson, P. (2016). *CFD erosion prediction in gas-liquid-sand flow*. In *SPE International Oilfield Corrosion Conference and Exhibition*. Society of Petroleum Engineers.
- Ben-Ami, Y., Uzi, A., & Levy, A. (2016). Modelling the particles impingement angle to produce maximum erosion. *Powder Technology*, 301, 1032–1043.
- Benzley, S. E., Perry, E., Merkley, K., Clark, B., & Sjaardama, G. (1995). A comparison of all hexagonal and all tetrahedral finite element meshes for elastic and elasto-plastic analysis. In *Proceedings, 4th International Meshing Roundtable* (Vol. 17, pp. 179–191). Sandia National Laboratories Albuquerque, NM.
- Bhowmik, S., & Ray, A. (2017). Abrasive water jet machining of composite materials. In *Advanced Manufacturing Technologies* (pp. 77–97). Springer.
- Bitter, J. G. A. (1963). A study of erosion phenomena part I. *Wear*, 6(1), 5–21. doi:10.1016/0043-1648(63)90003-6
- Blazek, J. (2015). *Computational Fluid Dynamics: Principles and Applications: Third Edition*. *Computational Fluid Dynamics: Principles and Applications: Third Edition*. doi:10.1016/C2013-0-19038-1
- Borrelli, P., Lugato, E., Montanarella, L., & Panagos, P. (2017). A new assessment of soil loss due to wind erosion in European agricultural soils using a quantitative spatially distributed modelling approach. *Land Degradation & Development*, 28(1), 335–344.
- Brauer, J. (1993). *What every engineer should know about finite element analysis*. CRC Press.
- Brennen, C. E. (2005). *Fundamentals of multiphase flow*. Cambridge university press.
- Cengel, Y. A. (2010). *Fluid mechanics*. Tata McGraw-Hill Education.
- Chappell, A., & Webb, N. P. (2016). Using albedo to reform wind erosion modelling, mapping and monitoring. *Aeolian Research*, 23, 63–78.

- Chappell, A., Webb, N. P., Guerschman, J. P., Thomas, D. T., Mata, G., Handcock, R. N., ... Butler, H. J. (2018). Improving ground cover monitoring for wind erosion assessment using MODIS BRDF parameters. *Remote Sensing of Environment*, 204, 756–768.
- Chappell, A., Webb, N. P., Leys, J. F., Waters, C. M., Orgill, S., & Eyres, M. J. (2019). Minimising soil organic carbon erosion by wind is critical for land degradation neutrality. *Environmental Science & Policy*, 93, 43–52.
- Chen, J., Wang, Y., Li, X., He, R., Han, S., & Chen, Y. (2015). Reprint of “Erosion prediction of liquid-particle two-phase flow in pipeline elbows via CFD–DEM coupling method”. *Powder Technology*, 282, 25–31.
- Chen, Xianghui, McLaury, B. S., & Shirazi, S. A. (2006). Numerical and experimental investigation of the relative erosion severity between plugged tees and elbows in dilute gas/solid two-phase flow. *Wear*, 261(7–8), 715–729. doi:http://dx.doi.org/10.1016/j.wear.2006.01.022
- Chen, Xiaochen, Deng, S., Guan, J., & Hua, W. (2017). Experiment and simulation research on abrasive water jet nozzle wear behavior and anti-wear structural improvement. *Journal of the Brazilian Society of Mechanical Sciences and Engineering*, 1–11.
- Cignoni, P., Constanza, D., Montani, C., Rocchini, C., & Scopigno, R. (2000). *Simplification of tetrahedral meshes with accurate error evaluation*. In *Proceedings of the conference on Visualization '00* (pp. 85–92). IEEE Computer Society Press.
- Clark, H. M., & Wong, K. K. (1995). Impact angle, particle energy and mass loss in erosion by dilute slurries. *Wear*, 186, 454–464.
- Darihaki, F., Hajidavalloo, E., Ghasemzadeh, A., & Safian, G. A. (2017). Erosion prediction for slurry flow in choke geometry. *Wear*, 372, 42–53.
- Deepak, D., Anjaiiah, D., Karanth, K. V., & Sharma, N. Y. (2012). CFD simulation of flow in an abrasive water suspension jet: the effect of inlet operating pressure and volume fraction on skin friction and exit kinetic energy. *Advances in Mechanical Engineering*, 4, 186430.
- Desale, G. R., Gandhi, B. K., & Jain, S. C. (2008). Slurry erosion of ductile materials under normal impact condition. *Wear*, 264(3–4), 322–330. doi:http://dx.doi.org/10.1016/j.wear.2007.03.022
- Dosanjh, S., & Humphrey, J. A. C. (1985). The influence of turbulence on erosion by a particle-laden fluid jet. *Wear*, 102(4), 309–330.
- Duarte, C. A. R., de Souza, F. J., & dos Santos, V. F. (2015). Numerical investigation of mass loading effects on elbow erosion. *Powder Technology*, 283, 593–606.
- Edelsbrunner, H., & Edelsbrunner, H. (2009). Tetrahedron meshes. *Geometry and Topology for Mesh Generation*, 111–135. doi:10.1017/cbo9780511530067.007

- Elkholy, A. (1983). Prediction of abrasion wear for slurry pump materials. *Wear*, 84(1), 39–49. doi:http://dx.doi.org/10.1016/0043-1648(83)90117-5
- ElTobgy, M. S., Ng, E., & Elbestawi, M. A. (2005). Finite element modeling of erosive wear. *International Journal of Machine Tools and Manufacture*, 45(11), 1337–1346. doi:http://dx.doi.org/10.1016/j.ijmactools.2005.01.007
- Finnie, I. (1960). Erosion of surfaces by solid particles. *Wear*, 3(2), 87–103. doi:http://dx.doi.org/10.1016/0043-1648(60)90055-7
- Flemmer, R. L. C., & Banks, C. L. (1986). On the drag coefficient of a sphere. *Powder Technology*, 48(3), 217–221.
- Foldyna, J., Heiniger, K., Mettler, S., Sitek, L., & Scucka, J. (2007). Enhancing of water jet effects by pulsations. *Manufacturing Engineering/ Vyrobné Inžinierstvo*, 6(4), 30–33.
- Gandhi, B. K., Singh, S. N., & Seshadri, V. (1999). Study of the parametric dependence of erosion wear for the parallel flow of solid–liquid mixtures. *Tribology International*, 32(5), 275–282. doi:http://dx.doi.org/10.1016/S0301-679X(99)00047-X
- Gandhi, M. B., Vuthaluru, R., Vuthaluru, H., French, D., & Shah, K. (2012). CFD based prediction of erosion rate in large scale wall-fired boiler. *Applied Thermal Engineering*, 42, 90–100. doi:http://dx.doi.org/10.1016/j.applthermaleng.2012.03.015
- Gosman, A. D., Lekakou, C., Politis, S., Issa, R. I., & Looney, M. K. (1992). Multidimensional modeling of turbulent two-phase flows in stirred vessels. *AIChE Journal*, 38(12), 1946–1956. doi:10.1002/aic.690381210
- Gou, W., Zhang, H., Li, H., Liu, F., & Lian, J. (2018). Effects of silica sand on synergistic erosion caused by cavitation, abrasion, and corrosion. *Wear*, 412–413. doi:10.1016/j.wear.2018.07.023
- Guide, A. F. U. (2016). Release 17.0. *Ansys Inc.*
- Gupta, R., Singh, S. N., & Sehadri, V. (1995). Prediction of uneven wear in a slurry pipeline on the basis of measurements in a pot tester. *Wear*, 184(2), 169–178. doi:http://dx.doi.org/10.1016/0043-1648(94)06566-7
- Hadavi, V., Moreno, C. E., & Papini, M. (2016). Numerical and experimental analysis of particle fracture during solid particle erosion, Part II: Effect of incident angle, velocity and abrasive size. *Wear*, 356, 146–157.
- Hadžiahmetović, H., Hodžić, N., Kahrimanović, D., & Džaferović, E. (2014). COMPUTATIONAL FLUID DYNAMICS (CFD) BASED EROSION PREDICTION MODEL IN ELBOWS. *Tehnicki Vjesnik/Technical Gazette*, 21(2).
- Haider, A., & Levenspiel, O. (1989). Drag coefficient and terminal velocity of spherical and nonspherical particles. *Powder Technology*, 58(1), 63–70.

- Hashish, M. (1994a). Observations of wear of abrasive-waterjet nozzle materials. *Journal of Tribology*, 116(3), 439–444.
- Hashish, M. (1994b). Observations of Wear of Abrasive-Waterjet Nozzle Materials. *Journal of Tribology*, 116(3), 439–444. doi:10.1115/1.2928861
- Hashish, Mohamed. (1984). A Modeling Study of Metal Cutting With Abrasive Waterjets. *Journal of Engineering Materials and Technology*, 106(1), 88–100. doi:10.1115/1.3225682
- Hashish, Mohamed. (1989). Pressure effects in abrasive-waterjet(AWJ) machining. *ASME, Transactions, Journal of Engineering Materials and Technology*, 111, 221–228.
- Hashish, Mohamed. (2009). Trends and Cost Analysis of AWJ Operation at 600MPa Pressure. *Journal of Pressure Vessel Technology*, 131(2), 21410.
- Hernandez, M., Nearing, M. A., Weltz, M. A., Spaeth, K. E., Armendariz, G., Pierson, F. B., ... Green, C. (2016). Rangeland Hydrology and Erosion Model Tutorial Guide: Desert Southwest Grassland, Limy Slopes 12-16” PZ Ecological Site. United States Department of Agriculture. *Agricultural Research Service, Southwest Watershed Research Center, Tucson, Arizona, General Technical Report*.
- Hlaváč, L. M., Hlaváčová, I. M., Geryk, V., & Plančár, Š. (2015). Investigation of the taper of kerfs cut in steels by AWJ. *The International Journal of Advanced Manufacturing Technology*, 77(9–12), 1811–1818.
- Hu, G., Zhu, W., Yu, T., & Yuan, J. (2008). Numerical simulation and experimental study of liquid-solid two-phase flow in nozzle of DIA jet. *Communications in Computer and Information Science*, 15, 92–100. doi:10.1109/INDIN.2008.4618377
- Huang, C., Chiovelli, S., Minev, P., Luo, J., & Nandakumar, K. (2008). A comprehensive phenomenological model for erosion of materials in jet flow. *Powder Technology*, 187(3), 273–279. doi:http://dx.doi.org/10.1016/j.powtec.2008.03.003
- Huang, C., Minev, P., Luo, J., & Nandakumar, K. (2010). A phenomenological model for erosion of material in a horizontal slurry pipeline flow. *Wear*, 269(3–4), 190–196. doi:http://dx.doi.org/10.1016/j.wear.2010.03.002
- Hughes, T. J. R. (1987). The finite element method Prentice-Hall. *Englewood Cliffs, NJ*.
- Humphrey, J. A. C. (1990). Fundamentals of fluid motion in erosion by solid particle impact. *International Journal of Heat and Fluid Flow*, 11(3), 170–195. doi:10.1016/0142-727X(90)90036-B
- Hutchings, I. M. (1981). A model for the erosion of metals by spherical particles at normal incidence. *Wear*, 70(3), 269–281. doi:http://dx.doi.org/10.1016/0043-1648(81)90347-1

- Hutchings, I. M., & Winter, R. E. (1974). Particle erosion of ductile metals: a mechanism of material removal. *Wear*, 27(1), 121–128.
- Jafari, M., Mansoori, Z., Saffar Avval, M., Ahmadi, G., & Ebadi, A. (2014). Modeling and numerical investigation of erosion rate for turbulent two-phase gas–solid flow in horizontal pipes. *Powder Technology*, 267, 362–370. doi:http://dx.doi.org/10.1016/j.powtec.2014.08.004
- Jegaraj, J. J. R., & Babu, N. R. (2016). Condition Monitoring of Orifice in Abrasive Waterjet Cutting System Using High Pressure Sensor. *Procedia Manufacturing*, 5, 578–593.
- Junkar, M., Jurisevic, B., Fajdiga, M., & Grah, M. (2006). Finite element analysis of single-particle impact in abrasive water jet machining. *International Journal of Impact Engineering*, 32(7), 1095–1112. doi:http://doi.org/10.1016/j.ijimpeng.2004.09.006
- Kamarudin, N. H., Rao, A. K. P., & Azhari, A. (2016). *CFD Based Erosion Modelling of Abrasive Waterjet Nozzle using Discrete Phase Method*. In *IOP Conference Series: Materials Science and Engineering* (Vol. 114, p. 12016). IOP Publishing.
- Karabelas, A. J. (1978). An experimental study of pipe erosion by turbulent slurry flow. *Proc. HT5*, 47–61.
- Kim, S.-E., & Boysan, F. (1999). Application of CFD to environmental flows. *Journal of Wind Engineering and Industrial Aerodynamics*, 81(1), 145–158.
- Kinnell, P. I. A. (2018). Determining soil erodibilities for the USLE-MM rainfall erosion model. *Catena*, 163, 424–426.
- Klavon, K., Fox, G., Guertault, L., Langendoen, E., Enlow, H., Miller, R., & Khanal, A. (2017). Evaluating a process-based model for use in streambank stabilization: insights on the Bank Stability and Toe Erosion Model (BSTEM). *Earth Surface Processes and Landforms*, 42(1), 191–213.
- Kovacevic, R. (1992). Monitoring the depth of abrasive waterjet penetration. *International Journal of Machine Tools and Manufacture*, 32(5), 725–736. doi:10.1016/0890-6955(92)90026-D
- Lauder, B. E., & Shima, N. (1989). Second-moment closure for the near-wall sublayer-Development and application. *AIAA Journal*, 27(10), 1319–1325.
- Lebar, A., & Junkar, M. (2004). Simulation of abrasive water jet cutting process: Part 1. Unit event approach. *Modelling and Simulation in Materials Science and Engineering*, 12(6), 1159–1170. doi:10.1088/0965-0393/12/6/010
- Lee, J. F., Lamar, M., Mudrow, M. S., Weissinger, M. J., & Shanbhag, D. (2018, December 4). Turbulent flow spiral multi-zone precursor vaporizer. Google Patents.
- Lewis, R. W. (n.d.). Fundamentals of the FEM for heat and fluid flow.

- Li, M.-J., Tang, S.-Z., Wang, F., Zhao, Q.-X., & Tao, W.-Q. (2017). Gas-side fouling, erosion and corrosion of heat exchangers for middle/low temperature waste heat utilization: a review on simulation and experiment. *Applied Thermal Engineering*, 126, 737–761.
- Li, Y., Kirkpatrick, A., Mitchell, C., & Willson, B. (2004). Characteristic and computational fluid dynamics modeling of high-pressure gas jet injection. *Journal of Engineering for Gas Turbines and Power*, 126(1), 192–197. doi:10.1115/1.1635398
- Lin, N., Arabnejad, H., Shirazi, S. A., McLaury, B. S., & Lan, H. (2018). Experimental study of particle size, shape and particle flow rate on Erosion of stainless steel. *Powder Technology*, 336, 70–79.
- Lin, N., Lan, H., Xu, Y., Dong, S., & Barber, G. (2015). Effect of the gas–solid two-phase flow velocity on elbow erosion. *Journal of Natural Gas Science and Engineering*, 26, 581–586.
- Liu, H.-T. P., Cutler, V., Raghavan, C., Miles, P., Schubert, E., & Webers, N. (2018). Advanced Abrasive Waterjet for Multimode Machining. *Abrasive Technology: Characteristics and Applications*, 39.
- Liu, H., Wang, J., Brown, R. J., & Kelson, N. (2003). Computational fluid dynamics (CFD) simulation of ultrahigh velocity abrasive waterjet. *Key Engineering Materials*, (2), 477–482.
- Liu, H., Wang, J., Kelson, N., & Brown, R. (2003). CFD simulation and mathematical models of the abrasive waterjet characteristics.
- Liu, J., BaKeDaShi, W., Li, Z., Xu, Y., Ji, W., Zhang, C., ... Zhang, R. (2017). Effect of flow velocity on erosion–corrosion of 90-degree horizontal elbow. *Wear*, 376, 516–525.
- Long, G., Liu, S., Xu, G., Wong, S.-W., Chen, H., & Xiao, B. (2018). A perforation-erosion model for hydraulic-fracturing applications. *SPE Production & Operations*, 33(04), 770–783.
- López-Vicente, M., Quijano, L., Palazón, L., Gaspar, L., & Izquierdo, A. N. (2015). Assessment of soil redistribution at catchment scale by coupling a soil erosion model and a sediment connectivity index (Central Spanish Pre-Pyrenees). *Cuadernos de Investigación Geográfica/Geographical Research Letters*, (41), 127–147.
- Lyczkowski, R. W., & Bouillard, J. X. (2002). State-of-the-art review of erosion modeling in fluid/solids systems. *Progress in Energy and Combustion Science*, 28(6), 543–602. doi:10.1016/S0360-1285(02)00022-9
- Magoulès, F. (2011). *Computational fluid dynamics. Computational Fluid Dynamics*. doi:10.1007/978-3-319-76234-0\_3

- Maniadaki, K., Antoniadis, A., & Bilalis, N. (2011). Effect of impact angle and velocity in crater circularity in abrasive water jet machining by means of multi-particle impact simulation. *International Journal of Machining and Machinability of Materials*, 10(1–2), 34–47.
- Maniadaki, K., Kestis, T., Bilalis, N., & Antoniadis, A. (2007a). A finite element-based model for pure waterjet process simulation. *The International Journal of Advanced Manufacturing Technology*, 31(9–10), 933–940.
- Maniadaki, K., Kestis, T., Bilalis, N., & Antoniadis, A. (2007b). A finite element-based model for pure waterjet process simulation. *International Journal of Advanced Manufacturing Technology*, 31(9–10), 933–940. doi:10.1007/s00170-005-0274-8
- Mansouri, A, Arabnejad, H., Shirazi, S. A., & McLaury, B. S. (2015). A combined CFD/experimental methodology for erosion prediction. *Wear*, 332, 1090–1097.
- Mansouri, Amir, Arabnejad, H., Karimi, S., Shirazi, S. A., & McLaury, B. S. (2015). Improved CFD modeling and validation of erosion damage due to fine sand particles. *Wear*, 338, 339–350.
- Manu, R., & Babu, N. R. (2009). An erosion-based model for abrasive waterjet turning of ductile materials. *Wear*, 266(11–12), 1091–1097. doi:10.1016/j.wear.2009.02.008
- Marzen, M., Iserloh, T., de Lima, J. L. M. P., Fister, W., & Ries, J. B. (2017). Impact of severe rain storms on soil erosion: Experimental evaluation of wind-driven rain and its implications for natural hazard management. *Science of the Total Environment*, 590, 502–513.
- Messa, G. V., Ferrarese, G., & Malavasi, S. (2015). A mixed Euler-Euler/Euler-Lagrange approach to erosion prediction. *Wear*, 342–343. doi:10.1016/j.wear.2015.08.015
- Mezősi, G., Blanka, V., Bata, T., Kovács, F., & Meyer, B. C. (2015). Estimation of regional differences in wind erosion sensitivity in Hungary. *Natural Hazards and Earth System Sciences*, 15, 97–107.
- Miller, P. L. (2018, September 18). Abrasive entrainment waterjet cutting. Google Patents.
- Momber, A. W., & Kovacevic, R. (2012). *Principles of abrasive water jet machining*. Springer Science & Business Media.
- Morrison, G., Chen, Y., Steck, D., Chen, Y., Bai, C., & Patil, A. (2017). *Effect of Gas Presence on Erosive Wear of Split-Vane Electrical Submersible Pump*. In *Proceedings of the 46th Turbomachinery & 33rd Pump Symposia, Houston, Texas, USA*.
- Morsi, Sa., & Alexander, A. J. (1972). An investigation of particle trajectories in two-phase flow systems. *Journal of Fluid Mechanics*, 55(02), 193–208.

- Mostofa, M. G., Kil, K. Y., & Hwan, A. J. (2010). Computational fluid analysis of abrasive waterjet cutting head. *Journal of Mechanical Science and Technology*, 24(1), 249–252.
- Nanduri, M, Taggart, D. G., & Kim, T. J. (1996). 'A New High Velocity Micro-Particle Impact Technique Applied to Abrasive Waterjet Cutting Head Design. In *Proceedings of the VIII International Congress on Experimental Mechanics* (pp. 433–434).
- Nanduri, M, Taggart, D. G., Kim, T. J., Haney, C., & Skeele, F. P. (1997). 'Effect of the Inlet Taper Angle on AWJ Nozzle Wear. In *Proceedings of the 9th American Water Jet Conference* (pp. 223–238).
- Nanduri, Madhusarathi, Taggart, D. G., & Kim, T. J. (2002). The effects of system and geometric parameters on abrasive water jet nozzle wear. *International Journal of Machine Tools and Manufacture*, 42(5), 615–623. doi:http://dx.doi.org/10.1016/S0890-6955(01)00147-X
- Nearing, M. A., Lane, L. J., & Lopes, V. L. (2017). Modeling soil erosion. In *Soil erosion research methods* (pp. 127–158). Routledge.
- Ness, E., & Zibbell, R. (1996). Abrasion and erosion of hard materials related to wear in the abrasive waterjet. *Wear*, 196(1–2), 120–125.
- Ng, E. Y.-K., & Guannan, D. (2015). The stability of 30- $\mu$ m-diameter water jet for jet-guided laser machining. *The International Journal of Advanced Manufacturing Technology*, 78(5–8), 939–946.
- Njobuenwu, D. O., & Fairweather, M. (2012). Modelling of pipe bend erosion by dilute particle suspensions. *Computers & Chemical Engineering*, 42, 235–247. doi:http://dx.doi.org/10.1016/j.compchemeng.2012.02.006
- Noon, A. A., & Kim, M.-H. (2017). Erosion wear on Francis turbine components due to sediment flow. *Wear*, 378, 126–135.
- Ochieng, A., & Onyango, M. S. (2008). Drag models, solids concentration and velocity distribution in a stirred tank. *Powder Technology*, 181(1), 1–8.
- Oka, Y. I., Ohnogi, H., Hosokawa, T., & Matsumura, M. (1997). The impact angle dependence of erosion damage caused by solid particle impact. *Wear*, 203, 573–579. doi:http://dx.doi.org/10.1016/S0043-1648(96)07430-3
- Olsen, J. J., Hemmingsen, C. S., Bergmann, L., Nielsen, K. K., Glimberg, S. L., & Walther, J. H. (2017). Characterization and erosion modeling of a nozzle-based inflow-control device. *SPE Drilling & Completion*, 32(04), 224–233.
- Pandya, D. A., Dennis, B. H., & Russell, R. D. (2017). A computational fluid dynamics based artificial neural network model to predict solid particle erosion. *Wear*, 378, 198–210.

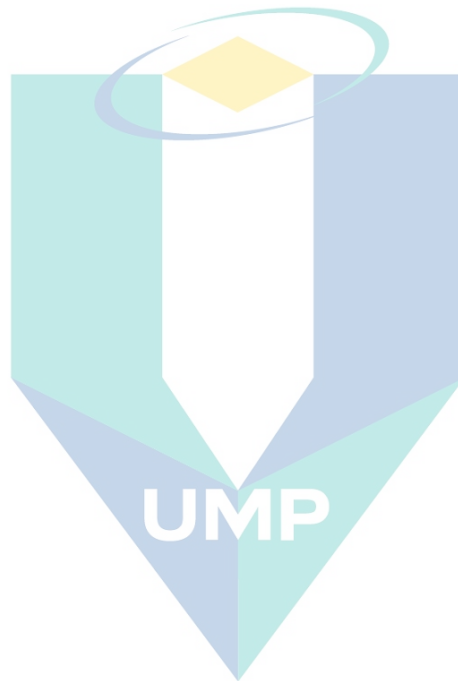
- Parsi, M., Agrawal, M., Srinivasan, V., Vieira, R. E., Torres, C. F., McLaury, B. S., & Shirazi, S. A. (2015). CFD simulation of sand particle erosion in gas-dominant multiphase flow. *Journal of Natural Gas Science and Engineering*, 27, 706–718.
- Parsi, M., Al-Sarkhi, A., Kara, M., Sharma, P., McLaury, B. S., & Shirazi, S. A. (2017). A new dimensionless number for solid particle erosion in natural gas elbows. *Wear*, 390, 80–83.
- Parsi, M., Kara, M., Agrawal, M., Kesana, N., Jatale, A., Sharma, P., & Shirazi, S. (2017). CFD simulation of sand particle erosion under multiphase flow conditions. *Wear*, 376, 1176–1184.
- Parsi, M., Kara, M., Sharma, P., McLaury, B. S., & Shirazi, S. A. (2016). *Comparative study of different erosion model predictions for single-phase and multiphase flow conditions*. In *Offshore Technology Conference*. Offshore Technology Conference.
- Parsi, M., Najmi, K., Najafifard, F., Hassani, S., McLaury, B. S., & Shirazi, S. A. (2014). A comprehensive review of solid particle erosion modeling for oil and gas wells and pipelines applications. *Journal of Natural Gas Science and Engineering*, 21, 850–873. doi:10.1016/j.jngse.2014.10.001
- Parsi, M., Vieira, R. E., Kesana, N., McLaury, B. S., & Shirazi, S. A. (2015). Ultrasonic measurements of sand particle erosion in gas dominant multiphase churn flow in vertical pipes. *Wear*, 328, 401–413.
- Parvaz, F., Hosseini, S. H., Elsayed, K., & Ahmadi, G. (2018). Numerical investigation of effects of inner cone on flow field, performance and erosion rate of cyclone separators. *Separation and Purification Technology*, 201, 223–237.
- Peng, W., & Cao, X. (2016a). Numerical prediction of erosion distributions and solid particle trajectories in elbows for gas–solid flow. *Journal of Natural Gas Science and Engineering*, 30, 455–470.
- Peng, W., & Cao, X. (2016b). Numerical simulation of solid particle erosion in pipe bends for liquid–solid flow. *Powder Technology*, 294, 266–279.
- Pereira, G. C., de Souza, F. J., & de Moro Martins, D. A. (2014). Numerical prediction of the erosion due to particles in elbows. *Powder Technology*, 261, 105–117. doi:http://dx.doi.org/10.1016/j.powtec.2014.04.033
- Pi, H., Sharratt, B., Feng, G., & Lei, J. (2017). Evaluation of two empirical wind erosion models in arid and semi-arid regions of China and the USA. *Environmental Modelling & Software*, 91, 28–46.
- Pi, V. N., & Tuan, N. Q. (2009). *A study on nozzle wear modeling in abrasive waterjet cutting*. In *Advanced Materials Research* (Vol. 76, pp. 345–350). Trans Tech Publ.
- Pierre, C., Kergoat, L., Hiernaux, P., Baron, C., Bergametti, G., Rajot, J., ... Marticorena, B. (2018). Impact of agropastoral management on wind erosion in Sahelian croplands. *Land Degradation & Development*, 29(3), 800–811.

- Poirier, D. R., & Geiger, G. H. (2016). *Transport phenomena in materials processing*. Springer.
- Powell, M. (2009). Optimization of UHP Waterjet Cutting Head, The Orifice. *Flow International, While the Date of the Publication Is Unknown, It Is Believed to Be Prior to Aug, 19, 19*.
- Prisco, U., & D'Onofrio, M. C. (2008). Three-dimensional CFD simulation of two-phase flow inside the abrasive water jet cutting head. *International Journal for Computational Methods in Engineering Science and Mechanics*, 9(5), 300–319.
- Priyadarshana, P. J. A., Weaver, D. S., Syrnyk, P., & Goodson, D. (2018, July 3). Ultrasonic flow metering with laminar to turbulent transition flow control. Google Patents.
- Rezazadeh, M., Irannejad, P., & Shao, Y. (2016). An Assessment of Wind Erosion Schemes in Dust Emission Simulations over the Middle East. *Environmental Erosion Research Journal*, 6(3), 14–32.
- Schlichting, H., Gersten, K., Krause, E., Oertel, H., & Mayes, K. (1960). *Boundary-layer theory* (Vol. 7). Springer.
- Schubauer, G. B., & Tchen, C. M. (2015). *Turbulent flow*. Princeton University Press.
- Sedrez, Thiana A, Shirazi, S. A., Rajkumar, Y. R., Sambath, K., & Subramani, H. J. (2019). Experiments and CFD simulations of erosion of a 90° elbow in liquid-dominated liquid-solid and dispersed-bubble-solid flows. *Wear*, 426, 570–580.
- Sedrez, Thiana Alexandra, Decker, R. K., da Silva, M. K., Noriler, D., & Meier, H. F. (2017). Experiments and CFD-based erosion modeling for gas-solids flow in cyclones. *Powder Technology*, 311, 120–131.
- Seehanam, W., Pianthong, K., Sittiwong, W., Milton, B. E., & Takayama, K. (2012). Investigation on the generation process of impact-driven high-speed liquid jets using a CFD technique. *Shock Waves*, 22(5), 465–475.
- Shabarchin, O., & Tesfamariam, S. (2016). Internal corrosion hazard assessment of oil & gas pipelines using Bayesian belief network model. *Journal of Loss Prevention in the Process Industries*, 40, 479–495.
- Sheikholeslami, M., Jafaryar, M., & Li, Z. (2018). Nanofluid turbulent convective flow in a circular duct with helical turbulators considering CuO nanoparticles. *International Journal of Heat and Mass Transfer*, 124, 980–989.
- Shih, T. H., Liou, W. W., Shabbir, A., Yang, Z., & Zhu, J. (1994). A New ke Eddy Viscosity Model for High Reynolds Number Turbulent Flows—Model Development and Validation. *Institute for Computational Mechanics in Propulsion and Center of Modeling of Turbulence and Transition*.

- Shirazi, S. A., McLaury, B. S., & Arabnejad, H. (2016). *A semi-mechanistic model for predicting sand erosion threshold velocities in gas and multiphase flow production*. In *SPE Annual Technical Conference and Exhibition*. Society of Petroleum Engineers.
- Shitole, P. P., Gawande, S. H., Desale, G. R., & Nandre, B. D. (2015). Effect of impacting particle kinetic energy on slurry erosion wear. *Journal of Bio-and Tribo-Corrosion*, 1(4), 29.
- Simon Ka-Keung, L., Humphrey, J. A. C., & Levy, A. V. (1981). Erosive wear of ductile metals by a particle-laden high velocity liquid jet. *Wear*, 73(2), 295–309. doi:http://dx.doi.org/10.1016/0043-1648(81)90297-0
- Sinclair, G. B., Beisheim, J. R., & Sezer, S. (2006). *Practical convergence-divergence checks for stresses from FEA*. In *Proceedings of the 2006 international ANSYS conference* (p. 50).
- Sittiwong, W., Seehanam, W., Pianthong, K., & Matthujak, A. (2010). *Effect of Stand-Off Distance on Impact Pressure of High Speed Water Jets*. In *AIP Conference Proceedings* (Vol. 1225, pp. 864–873). AIP.
- Syazwani, H., Mebrahitom, G., & Azmir, A. (2016). *A review on nozzle wear in abrasive water jet machining application*. In *IOP Conference Series: Materials Science and Engineering* (Vol. 114, p. 12020). IOP Publishing.
- Tafreshi, H. V., & Pourdeyhimi, B. (2003). The effects of nozzle geometry on waterjet breakup at high Reynolds numbers. *Experiments in Fluids*, 35(4), 364–371.
- Taylor, R. L., & Zienkiewicz, O. C. (1989). *The finite element method*. McGraw-Hill.
- Touré, A., Marticorena, B., Siour, G., Pierre, C., Bouet, C., Bergametti, G., ... Couvreur, F. (2018). *Wind erosion and dust emission in the Sahel: a regional modelling approach to evaluate the impact of climate and land-use*.
- Tsai, W., Humphrey, J. A. C., Cornet, I., & Levy, A. V. (1981). Experimental measurement of accelerated erosion in a slurry pot tester. *Wear*, 68(3), 289–303. doi:http://dx.doi.org/10.1016/0043-1648(81)90178-2
- Uzi, A., & Levy, A. (2018). Energy absorption by the particle and the surface during impact. *Wear*, 404, 92–110.
- Van Pelt, R. S., Hushmurodov, S. X., Baumhardt, R. L., Chappell, A., Nearing, M. A., Polyakov, V. O., & Strack, J. E. (2017). The reduction of partitioned wind and water erosion by conservation agriculture. *Catena*, 148, 160–167.
- Verma, S., Mishra, S. K., & Moulick, S. K. (2015). CFD analysis of nozzle in abrasive water.
- Vieira, R E, Sajeev, S., Shirazi, S. A., McLaury, B. S., & Kouba, G. (2015). *Experiments and modelling of sand erosion in gas-liquid cylindrical cyclone separators under gas production and low-liquid loading conditions*. In *17th International Conference on Multiphase Production Technology*. BHR Group.

- Vieira, Ronald E, Mansouri, A., McLaury, B. S., & Shirazi, S. A. (2016). Experimental and computational study of erosion in elbows due to sand particles in air flow. *Powder Technology*, 288, 339–353.
- Wang, S., Zhang, S., Wu, Y., & Yang, F. (2017). Exploring kerf cut by abrasive waterjet. *The International Journal of Advanced Manufacturing Technology*, 93(5–8), 2013–2020.
- Webb, N. P., Herrick, J. E., Van Zee, J. W., Courtright, E. M., Hugenholtz, C. H., Zobeck, T. M., ... Boyd, R. (2016). The National Wind Erosion Research Network: Building a standardized long-term data resource for aeolian research, modeling and land management. *Aeolian Research*, 22, 23–36.
- Xie, J., & Rittel, D. (2017). A two-dimensional model for metallic surface roughness resulting from pure waterjet peening. *International Journal of Engineering Science*, 120, 189–198.
- Yakhot, V., & Orszag, S. A. (1986). Renormalization group analysis of turbulence. I. Basic theory. *Journal of Scientific Computing*, 1(1), 3–51.
- Zahedi, P., Karimi, S., Mahdavi, M., McLaury, B. S., & Shirazi, S. A. (2016). *Parametric analysis of erosion in 90 degree and long radius bends*. In *ASME 2016 Fluids Engineering Division Summer Meeting collocated with the ASME 2016 Heat Transfer Summer Conference and the ASME 2016 14th International Conference on Nanochannels, Microchannels, and Minichannels*. American Society of Mechanical Engineers Digital Collection.
- Zahedi, P., Parvande, S., Asgharpour, A., McLaury, B. S., Shirazi, S. A., & McKinney, B. A. (2018). Random forest regression prediction of solid particle Erosion in elbows. *Powder Technology*, 338, 983–992.
- Zamani, M., Seddighi, S., & Nazif, H. R. (2017). Erosion of natural gas elbows due to rotating particles in turbulent gas-solid flow. *Journal of Natural Gas Science and Engineering*, 40, 91–113.
- Zhang, J., Kang, J., Fan, J., & Gao, J. (2016). Study on erosion wear of fracturing pipeline under the action of multiphase flow in oil & gas industry. *Journal of Natural Gas Science and Engineering*, 32, 334–346.
- Zhang, Y., Reuterfors, E. P., McLaury, B. S., Shirazi, S. A., & Rybicki, E. F. (2007). Comparison of computed and measured particle velocities and erosion in water and air flows. *Wear*, 263(1–6), 330–338. doi:<http://dx.doi.org/10.1016/j.wear.2006.12.048>
- Zhang, Yongjie, Bajaj, C., & Xu, G. (2009). Surface smoothing and quality improvement of quadrilateral/hexahedral meshes with geometric flow. *International Journal for Numerical Methods in Biomedical Engineering*, 25(1), 1–18.
- Zheng, C., Liu, Y., Chen, C., Qin, J., Ji, R., & Cai, B. (2017). Numerical study of impact erosion of multiple solid particle. *Applied Surface Science*, 423, 176–184.

- Zheng, C., Liu, Y., Wang, H., Zhu, H., Liu, Z., Cai, B., & Shen, Y. (2016). Numerical study on improving the erosion life of ball seat for oil and gas reservoir fracturing. *Engineering Failure Analysis*, 60, 188–198.
- Zhu, C., Qiu, N., Cao, H., Rao, S., & Hu, S. (2016). Paleogeothermal reconstruction and thermal evolution modeling of source rocks in the Puguang gas field, northeastern Sichuan Basin. *Journal of Earth Science*, 27(5), 796–806.
- Zhu, H., Han, Q., Wang, J., He, S., & Wang, D. (2015). Numerical investigation of the process and flow erosion of flushing oil tank with nitrogen. *Powder Technology*, 275, 12–24.



اونيورسيتي ملايسيا قهغ

UNIVERSITI MALAYSIA PAHANG

**APPENDIX A**  
**SAMPLE CALCULATION FOR PERCENTAGE OF ACCURACY**  
**CALCULATION**

The Percentage of accuracy was calculated using the following formula;

$$\text{Accuracy, \%} = \frac{E_{\text{simulation}} - E_{\text{experimental}}}{E_{\text{experimental}}} \quad \text{A.1}$$

Taking the value for the erosion rate of a 32.5 mm nozzle length where the experimental model is  $9.723E-08 \text{ kg/m}^2\text{s}^{-1}$  and for Quadrilateral mesh method erosion rate is  $4.078E-08 \text{ kg/m}^2\text{s}^{-1}$ . Therefore;

$$\begin{aligned} \text{Accuracy, \%} &= \frac{9.723E-08 - 4.078E-08}{9.723E-08} \\ &= -0.58 \approx -58\% \end{aligned}$$

The error was calculated using the following formula;

$$\begin{aligned} \text{Error (unitless)} &= E_{\text{experimental}} - E_{\text{simulation}} \\ &= 6.802E-08 - 3.180E-08 \\ &= -3.622E-08 \end{aligned}$$

اونيورسيتي ملايسيا قهغ

UNIVERSITI MALAYSIA PAHANG

**APPENDIX B**  
**SAMPLE CALCULATION TO OBTAIN THEORETICAL AND WATERJET VELOCITY**

Below shows the calculation to obtain the theoretical waterjet velocity,  $V_{th}$  as in Equation 2.3. The followings are the parameter values that is set in the typical simulation;

Table 5.1 Parameters used in Typical Simulation

Parameters	Typical Values
Operating pressure, $P$ [MPa]	470
Water density, $\rho$ [kg/m <sup>3</sup> ]	997
Pump Plunger Pressure, $L$ [MPa]	310
Discharge Coefficients, $C_d$	0.85
Constant, $n$	0.1368

Insert the values into equation 2.3 and equation 2.6;

$$V_{th} = \sqrt{\frac{2(470)}{997}}$$

$$= 970.10 \text{ m/s}$$

$$\varphi = \sqrt{\frac{310}{470(1 - 0.1368)} \left[ \left(1 + \frac{470}{310}\right)^{1-0.1368} - 1 \right]} = 0.96$$

**UNIVERSITI MALAYSIA PAHANG**

Therefore inserting the values to Equation 2.7 to find the Waterjet Velocity,  $V_j$  ;

$$V_j = C_d \varphi V_{th}$$

$$= (0.85)(0.96)(970.10)$$

$$= 791.60 \text{ m/s}$$

**APPENDIX C**  
**SAMPLE OF SCALED RESIDUALS VERSUS ITERATIONS**

Below show the scaled residuals versus iterations that is used to evaluate the convergence of the simulations.

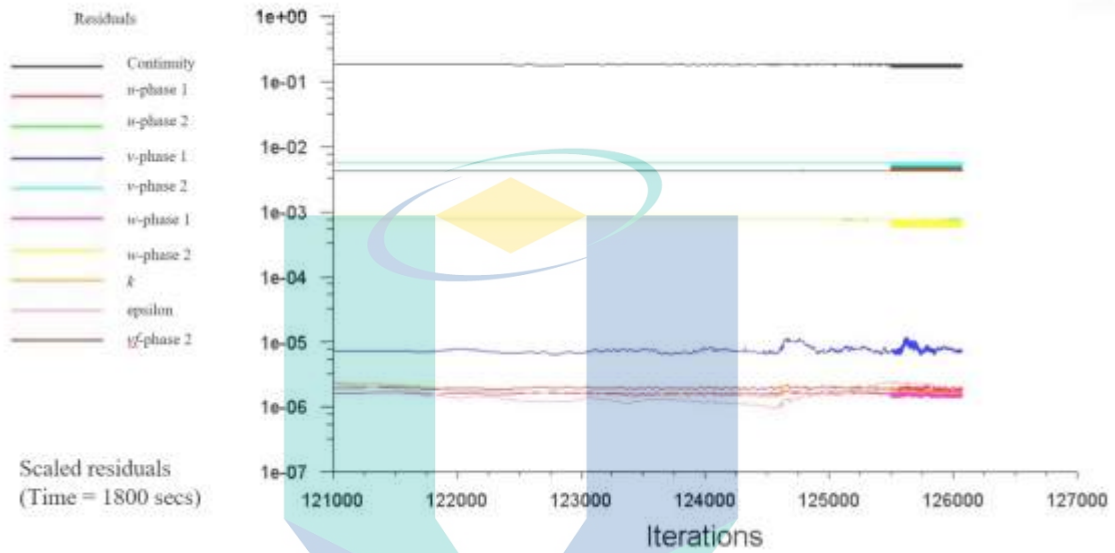


Figure 5.1 Residuals monitor for cut-cell mesh simulation

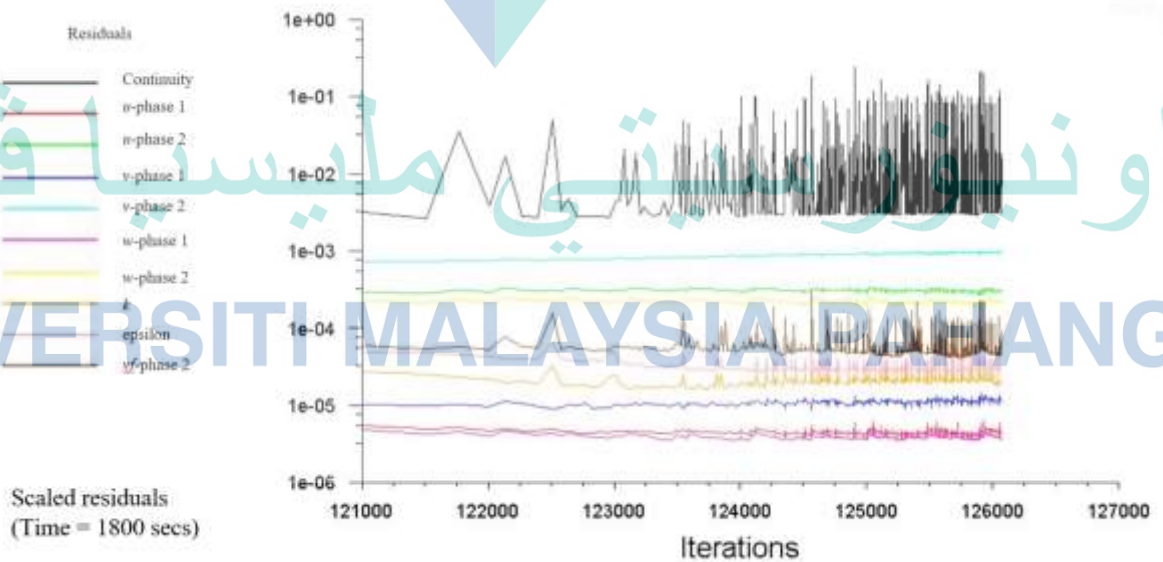


Figure 5.2 Residuals monitoring for tetrahedral mesh simulation

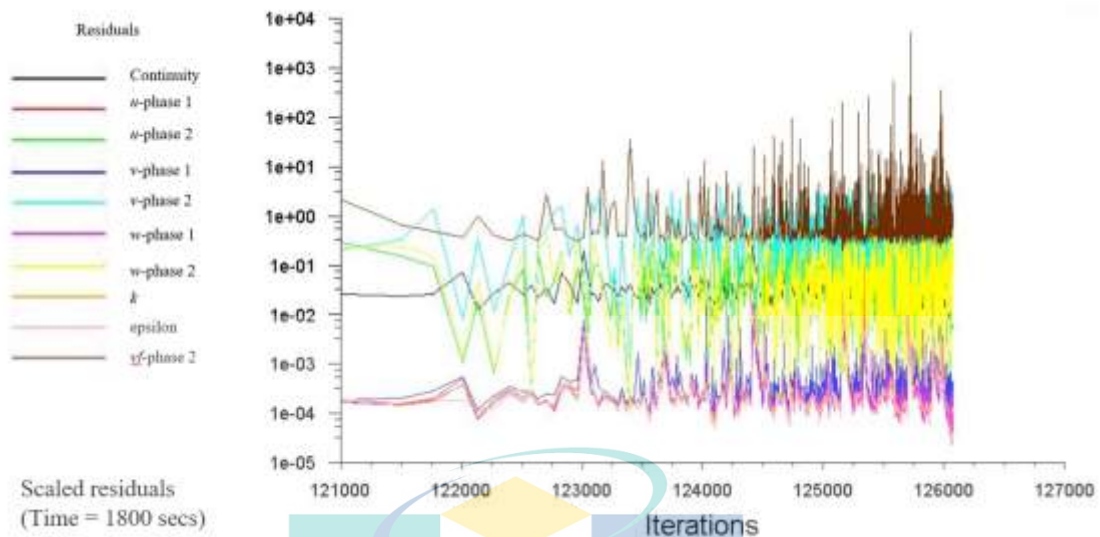
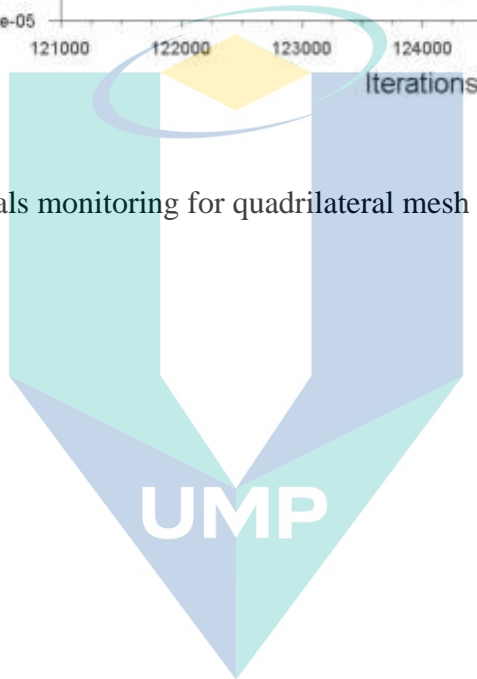


Figure 5.3 Residuals monitoring for quadrilateral mesh simulation



اونيورسيتي مليسيا قهغ  
 UNIVERSITI MALAYSIA PAHANG

**APPENDIX D**  
**SAMPLE CALCULATION TO OBTAIN PERCENTAGE INTENSITY**

Below shows the calculation to obtain the percentage intensity is set in the typical simulation. The Reynolds number were determined by inserting the value of water jet velocity,  $V_j$  obtained in APPENDIX C into Equation 2.10;

$$Re_{Dh} = \frac{(997)(791.60)(0.005)}{8.9E^{-4}}$$
$$= 4419174.12$$

Where the size of diameter,  $D_h$  is 0.005 mm, the flow velocity,  $u$  is equivalent to the water jet velocity,  $V_j = 791.60$  m/s, and the dynamic viscosity of water,  $\mu = 8.9E^{-4}$  kg m<sup>-1</sup> s<sup>-1</sup>. Thereby the inserting the value obtained into equation 2.9;

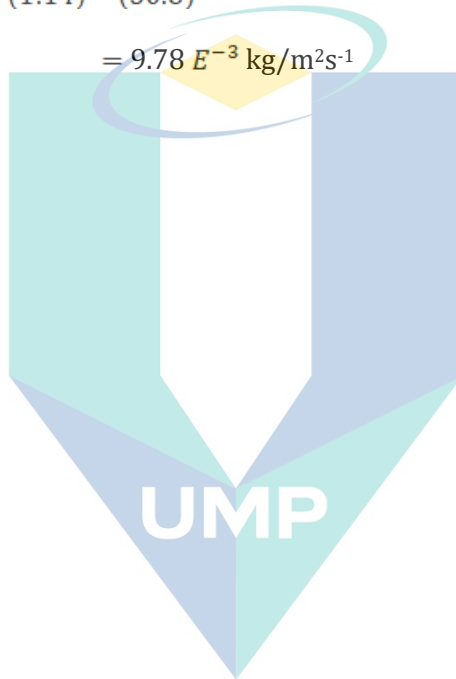
$$I = 0.16(4419174.12)^{-1/8}$$
$$= 0.0236 \approx 2.3\%$$

**UNIVERSITI MALAYSIA PAHANG**

**APPENDIX E**  
**SAMPLE CALCULATION TO OBTAIN PERCENTAGE INTENSITY**

The erosion rate was obtained by inserting the values of parameters specified in Table 3.1. The sample calculation below shows the calculation by inserting the typical values in the simulation.

$$E = (8.07 E^{-4}) \frac{(310)^{0.9} (0.38)^{0.38} (3.8)^{0.7}}{(1.14)^{0.7} (50.8)^{0.8}} \quad 5.1$$
$$= 9.78 E^{-3} \text{ kg/m}^2\text{s}^{-1}$$



اونيورسيتي مليسيا قهغ  
UNIVERSITI MALAYSIA PAHANG